

UNCLASSIFIED

AD NUMBER

AD455565

LIMITATION CHANGES

TO:

Approved for public release; distribution is unlimited. Document partially illegible.

FROM:

Distribution authorized to U.S. Gov't. agencies and their contractors;  
Administrative/Operational Use; NOV 1964. Other requests shall be referred to Army Electronics Laboratory, Fort Monmouth, NJ 07703.

AUTHORITY

usaec ltr 15 jan 1967

THIS PAGE IS UNCLASSIFIED

**Best  
Available  
Copy**

UNCLASSIFIED

AD 4 5 5 5 6 5

DEFENSE DOCUMENTATION CENTER

FOR

SCIENTIFIC AND TECHNICAL INFORMATION

CAMERON STATION ALEXANDRIA, VIRGINIA  
CAMERON STATION ALEXANDRIA, VIRGINIA



UNCLASSIFIED

NOTICE: When government or other drawings, specifications or other data are used for any purpose other than in connection with a definitely related government procurement operation, the U. S. Government thereby incurs no responsibility, nor any obligation whatsoever; and the fact that the Government may have formulated, furnished, or in any way supplied the said drawings, specifications, or other data is not to be regarded by implication or otherwise as in any manner licensing the holder or any other person or corporation, or conveying any rights or permission to manufacture, use or sell any patented invention that may in any way be related thereto.

455565

CATALOGED BY DDC

455565  
AD W6  
AS

Report No: 8

Final Report

1 July 1962 to 30 September 1964

RESEARCH ON DIELECTRICS FOR MICROWAVE ELECTRON DEVICES

Prepared for:

ARMY ELECTRONICS LABORATORIES  
FT MONMOUTH, NEW JERSEY 07703

CONTRACT NO: DA-36-039-SE-90856  
TASK NO: OST 7776-11-017-38 00

STANFORD RESEARCH INSTITUTE

MENLO PARK, CALIFORNIA



**DDC AVAILABILITY NOTICE**

**Qualified requesters may obtain copies  
of this report from DDC.**



November 1964

Report No. 9

Final Report

1 July 1962 to 30 September 1964

## RESEARCH ON DIELECTRICS FOR MICROWAVE ELECTRON DEVICES

Prepared for:

U. S. ARMY ELECTRONICS LABORATORIES  
FORT MONMOUTH, NEW JERSEY 07703

CONTRACT NO. DA-36-039-SC-90856  
TASK NO. OST 7776-11-017-38-00

By: L. FEINSTEIN J. BORDEAUX D. PETERS C. PELTZER

SRI Project PMU-4160

Approved: A. E. GORUM, DIRECTOR  
MATERIAL SCIENCES DIVISION

Object of the Research: To investigate and identify the factors that contribute to the behavior and failure of dielectric materials used in microwave electron devices.

This research is a part of Project DEFENDER, sponsored by the Advanced Research Projects Agency, Department of Defense, under Order No. 318-62 and Project Code No. 7300, and is conducted under the technical guidance of the U.S. Army Electronics Laboratories, Fort Monmouth, N.J. 07703.

Copy No. 127

## CONTENTS

LIST OF ILLUSTRATIONS.....	v
LIST OF TABLES.....	vii
PURPOSE.....	ix
ABSTRACT.....	xi
CONFERENCES, MEETINGS, AND PUBLICATIONS.....	xiii
 FACTUAL DATA.....	 1
I.    Experiments on Growth of Aluminum Oxide.....	1
A.    Current Work.....	1
B.    Summary of Film Work.....	3
II.   Preparation of Sintered Alumina.....	11
III.  Ionization of Gas in Voids in Windows.....	13
A.    Design of Test Cavity.....	18
IV.   Electrical Measurements on Sapphire.....	21
A.    Discussion.....	21
B.    Sample Preparation.....	23
C.    Experimental Apparatus.....	25
D.    Electrical Conductivity of Single Crystal $Al_2O_3$ .....	28
E.    Electrical Conductivity of Specimens, A, B, C, D....	30
F.    Thermoelectric Power.....	33
G.    Mass Transport Experiment.....	36
H. $Al_2O_3$ Optical Absorption.....	41
I.    Electrical Properties of Sapphire.....	46
V.    Electron Bombardment Studies of Sapphire.....	55
VI.   Studies of Defects in Alumina.....	67
VII.  Theoretical Treatment.....	73
A.    Mixed Ionic and Electronic Conductivity.....	74
B.    Electronic Energy Levels.....	78
C.    Internal Fields in Dielectrics.....	82



OVERALL CONCLUSIONS.....	93
RECOMMENDATIONS FOR FUTURE WORK.....	95
KEY TECHNICAL PERSONNEL.....	97
REFERENCES.....	99

## LIST OF ILLUSTRATIONS

---

Figure 1	Electron Beam Source Heater and Substrate Furnace Mounted in Ultrahigh Vacuum System.....	2
Figure 2	Schematic of Electron Beam Evaporation Unit.....	2
Figure 3	Complete View of Vacuum Station.....	4
Figure 4	Perspective Drawing of Ultrahigh Vacuum System.....	5
Figure 5(a)	Multi-Source Carousel System.....	6
Figure 5(b)	Multi-Source Carousel System.....	6
Figure 6	Schematic Drawing of Multiple Deposition System.....	7
Figure 7	Schematic Drawing of Reaction System.....	8
Figure 8	Schematic Drawing of Hot Press Assembly.....	11
Figure 9	Dimensions of Test Cavity.....	16
Figure 10	Void Test Setup.....	16
Figure 11	Breakdown Test Setup.....	17
Figure 12	Energy Band Model for Ideal Polycrystalline Material....	22
Figure 13	Model of Grain Boundary.....	22
Figure 14	Cross Section of Specimens.....	24
Figure 15	Experimental Apparatus.....	25
Figure 16	Experimental Apparatus (Schematic Diagram).....	26
Figure 17	Resistance vs. Temperature.....	27
Figure 18	Electrical Conductivity of Sapphire as a Function of Temperature.....	29
Figure 19	Temperature Dependence of Electrical Conductivity.....	31
Figure 20	Band Model.....	32
Figure 21	Physical Model.....	32
Figure 22	Thermoelectric Apparatus.....	34

Figure 23	Thermoelectric Power-Sapphire.....	35
Figure 24	Stack of Sapphire Discs for Conductivity Experiment....	38
Figure 25	Sample Holder with Sapphire Stack Mounted in Position..	38
Figure 26	Al <sub>2</sub> O <sub>3</sub> Absorption T = 20°C.....	43
Figure 27	Al <sub>2</sub> O <sub>3</sub> Absorption T = 300°C.....	43
Figure 28	Al <sub>2</sub> O <sub>3</sub> Absorption T = 500°C.....	44
Figure 29	Al <sub>2</sub> O <sub>3</sub> Absorption T = 700°C.....	44
Figure 30	Al <sub>2</sub> O <sub>3</sub> Absorption T = 900°C.....	45
Figure 31	Al <sub>2</sub> O <sub>3</sub> Band Gap vs. Temperature.....	45
Figure 32	Schematic Diagram of Experimental Apparatus.....	52
Figure 33	Conductivity vs. Temperature.....	53
Figure 34	Schematic of Induced Conductivity Test.....	56
Figure 35	Electron Bombardment Induced Conductivity Test Setup...	57
Figure 36	Current at Front and Rear Faces of Sapphire Specimen vs. Applied Positive Voltage for Bombarding Current of App. 10 <sup>-6</sup> amp.....	58
Figure 37	Current at Front Face of Sapphire Specimen vs. Applied Negative Voltage for Bombarding Currents of App. 10 <sup>-8</sup> , 10 <sup>-7</sup> , 10 <sup>-6</sup> amp.....	59
Figure 38	Current on Front and Rear Faces under Pulsed Bombardment (Low Bombarding Current), Accelerating Voltage 1000 V.....	60
Figure 39	Current on Front and Rear Faces under Pulsed Bombardment (High Bombarding Current), Accelerating Voltage 6000 V.....	60
Figure 40	Proposed Charge Distribution in Specimen.....	61
Figure 41	Sapphire Crystal Bent to Introduce Slip Bands.....	67
Figure 42(a)	Etched Section of Bent Specimen.....	68
Figure 42(b)	Etched Section of Bend Specimen.....	68

Figure 43	New Breakdown Test Fixture.....	69
Figure 44	Breakdown Data for Bent and Unbent Sapphire Specimens,.....	71
Figure 45	Breakdown Data for Heat-Cycled and Uncycled Sapphire Specimens.....	72
Figure 46	Electronic Energy Levels for $\alpha$ -Al <sub>2</sub> O <sub>3</sub> .....	79

#### LIST OF TABLES

---

Table I	Semiconductor Theory Computations.....	47
Table II	Localized Level Computations.....	49

## PURPOSE

The purpose of this research was to study the properties of dielectrics used in microwave devices, with special emphasis on materials used for microwave windows. It was concerned with study and understanding of the factors that influence the properties of the dielectric material. The first material to be studied was aluminum oxide, which was investigated to determine the relationship between its properties and its structures as influenced by impurities, defects, additional phases, and particle bombardment. Among the important problems to be considered was the mechanism of breakdown of the dielectric as a function of these parameters.

The approach undertaken in this program was that of preparation of high purity films of the dielectric having known compositions and structures. It was anticipated that this attack on the problem, when correlated with the analytical study of the material, would allow identification of the contribution of the various factors to the behavior of the materials studied.

## ABSTRACT

This report reviews the results of twenty-seven months' study of the transport and breakdown properties of aluminum oxide and of methods of growth of this dielectric from the vapor phase in an evacuated system.

An ultrahigh vacuum system capable of reaching pressures of  $10^{-9}$ - $10^{-10}$  torr was completed. Growth of aluminum oxide films ranging in thickness from 1000 Å to 5000 Å by five different methods was achieved in an interim vacuum system operating in the  $10^{-6}$  to  $10^{-7}$  torr range. Alpha aluminum oxide films were grown by thermal evaporation in the ultrahigh vacuum system.

Data from experiments on transport in single crystal sapphire indicate that electron or hole conduction is primarily due to the effect of impurities or defects and, therefore, indicates either an impurity band or hopping process or a polaron conduction mechanism. The degree of ionic conductivity is still uncertain, particularly at high temperatures ( $1600^{\circ}\text{C}$ ). The effect of the glassy phase that exists in commercial polycrystalline aluminas is to form a barrier to conduction across the boundary between the aluminum oxide crystals and the glassy phase.

The data from electron bombardment and breakdown studies indicate that particle bombardment, in addition to creating defects if particle energy is sufficiently high, can also lead to formation of separated charge regions in the material. These regions can act as sources of internal fields within the dielectric. Defects within the material introduced by bending sapphire single crystals have a pronounced effect on decreasing the breakdown strength of specimens.

Analytic studies indicate a need for developing a method of describing the relation between imperfection states in a dielectric and the inhomogeneous internal fields within the material. These fields must be accounted for in describing the factors that control breakdown in dielectrics.

The study on the effect of ionization of gas in alumina ceramics has been completed. Experiments conducted indicated that microwave fields in the order of 132,000 v/cm peak and 4000 v/cm average at 3000 mc do not cause breakdown in aluminum oxide ceramics with 0.020-in.-diameter voids.

CONFERENCES, MEETINGS AND PUBLICATIONS  
(for period 30 June 1964 to 30 Sept. 1964)

Mr. L. Feinstein attended the Summer Institute on Quantum Chemistry and Solid State Physics at the University of Uppsala, Sweden from mid-July to August 24, 1964.

Dr. John J. Bordeaux attended the Eleventh National Vacuum Symposium held in Chicago, Illinois, 30 September 1964 through 1 October 1964.

A paper, "Studies of Dielectrics for use in Microwave Devices," was presented at the Tube Techniques Conference in September 1964.

A paper on the barrier effect, entitled "Alumina Polyphase Heterojunction," was cleared for presentation at the American Ceramic Society meeting in October 1964.

A paper, "On the High Temperature Electrical Conductivity of Alumina," was submitted for clearance for publication.



## FACTUAL DATA

### I Experiments on Growth of Aluminum Oxide

#### A. Current Work

##### 1. Ultrahigh Vacuum System

Problems in the mechanical and electrical operation of the ultrahigh vacuum system were remedied. A new can of heavier material was placed into operation and several runs at ultrahigh vacuum were made, with no difficulties.

A special electron beam evaporation system designed by the Applied Physics Laboratory of the Institute was installed in the ultrahigh vacuum system together with the substrate heater. The electron beam unit was designed so as not to require water cooling. Evaporations of alumina have been carried out with the system at ultrahigh vacuum and yielded alpha alumina. A detailed description of the procedure is given in the next section of this report.

##### 2. Thermal Evaporation in Ultrahigh Vacuum

During the last quarter, equipment for carrying out thermal evaporation in the ultrahigh vacuum system was assembled and two evaporations were made. The equipment used in these evaporations was the standard substrate heater furnace used in all of the deposition experiments and described in Quarterly Report No. 3; also used as mentioned in Section A,1 above was a newly designed electron-beam-heated evaporation source. A photograph of these two pieces of equipment mounted in the ultrahigh vacuum chamber is shown in Fig. 1; a schematic drawing of the evaporation unit is shown in Fig. 2. After achieving ultrahigh vacuum conditions, i.e., in the  $10^{-8}$  torr range or better, the procedure for deposition was as follows:

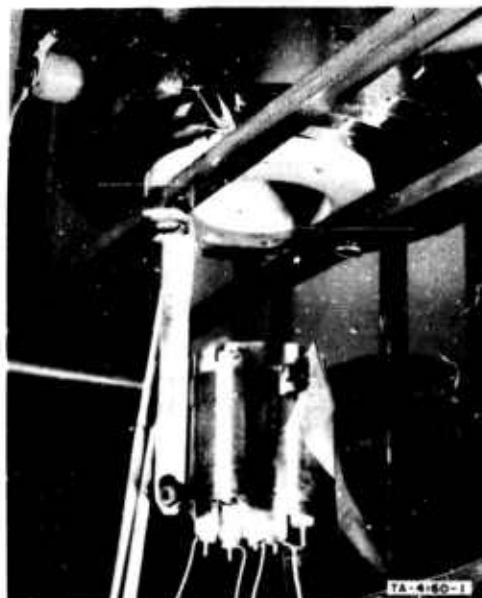


FIG. 1 ELECTRON BEAM SOURCE  
HEATER AND SUBSTRATE  
FURNACE MOUNTED IN  
ULTRAHIGH VACUUM SYSTEM

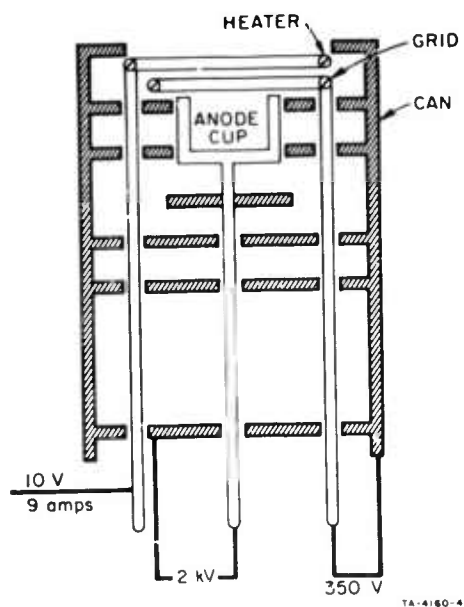


FIG. 2 SCHEMATIC OF ELECTRON  
BEAM EVAPORATION UNIT

- a. Heat substrate to a temperature of about 500°C
- b. Turn on high voltage and heat source to evaporation temperature by predetermined current-voltage settings
- c. Evaporate for required time
- d. Turn off source heater
- e. Increase substrate temperature to 1000°C for 5 minutes
- f. Turn off substrate heater.

In both evaporation runs, alumina was found to be the deposit and was not contaminated within the limits of the electron diffraction detections. In the first experiment, a short occurred in the source heating unit after 10 minutes and the run was stopped. The deposit obtained in this run was too thin for a structural evaluation beyond the identification of alumina. In the second experiment, the deposit was carried out for one hour, and the deposit was estimated to be in excess of 5000 Å. Electron diffraction analysis indicates the deposit to be extremely fine crystallites of alpha alumina.

## B. Summary of Film Work

### 1. Ultrahigh Vacuum System

An ultrahigh vacuum system capable of achieving vacuums in the  $10^{-9}$  to  $10^{-10}$  torr range was assembled. Repeated runs from atmosphere to ultrahigh vacuum were completed and the vacuum system was shown to be operational. The features of this system are:

- a. bake out of the ultrahigh vacuum chamber and its contents at 800 to 900°C, to aid in attaining  $10^{-10}$  torr in a very short time, and to remove all relatively volatile contaminants and residues.
- b. instrumentation, including a mass spectrometer, for analyzing and rate-controlling the desired reactions.

At the present time, it is possible that the mass spectrometer may not be able to withstand minimum bakeout conditions. A picture of the system is shown in Fig. 3 and a perspective drawing is shown in Fig. 4.

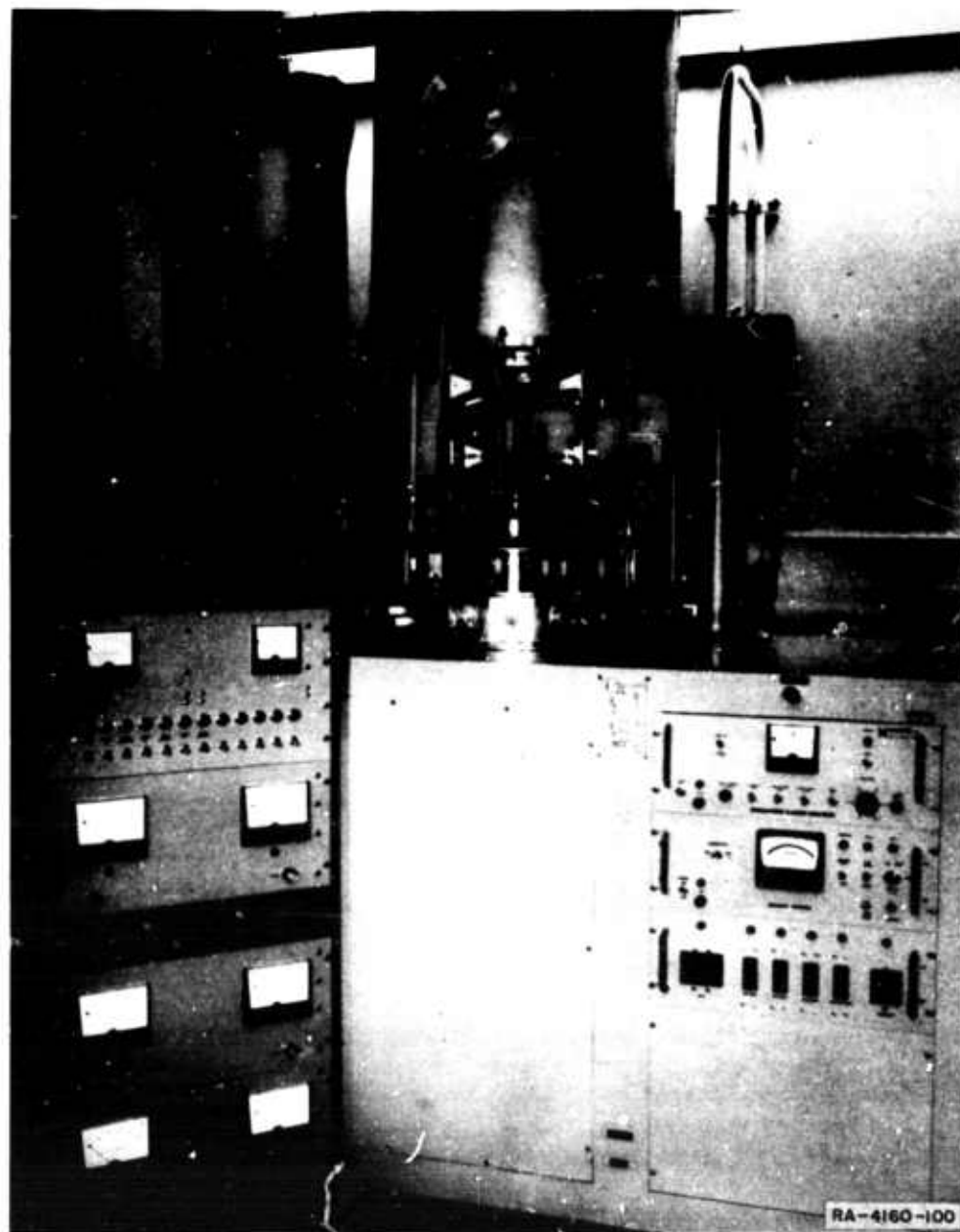


FIG. 3 COMPLETE VIEW OF VACUUM STATION

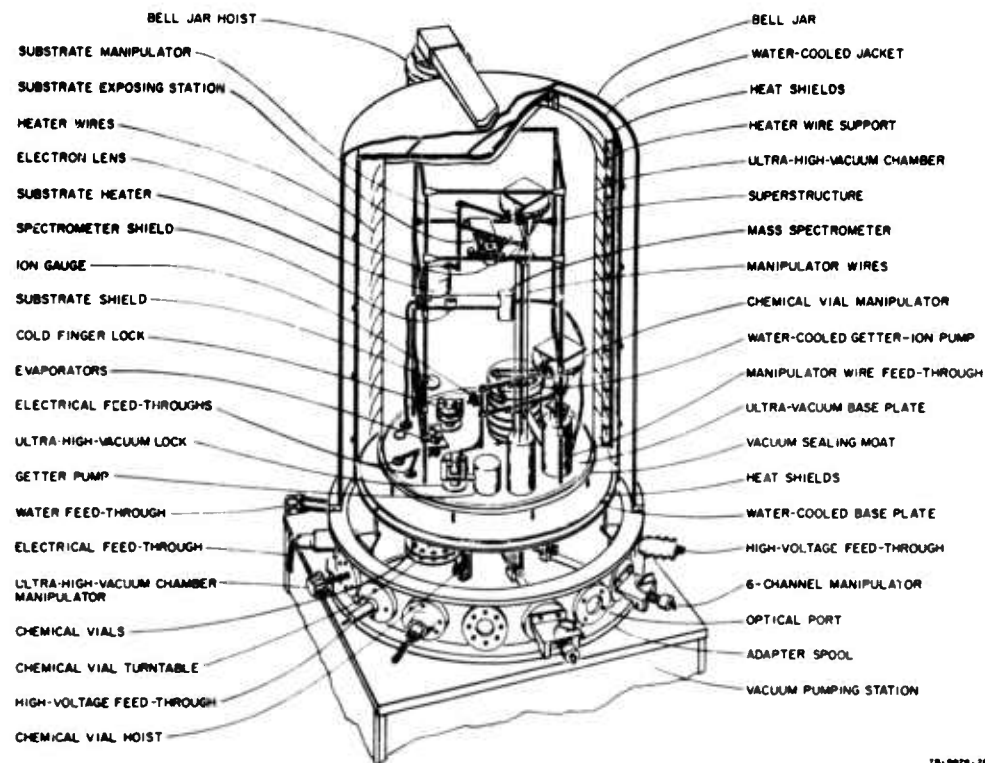


FIG. 4 PERSPECTIVE DRAWING OF ULTRAHIGH VACUUM SYSTEM

Much of the work during the past two years was spent in assembling and becoming familiar with the operation of the various components of the system and in trouble-shooting minor problems. It is believed that the system is now in good operating condition for either thermal evaporation or for adapting to property measurements.

## 2. Interim Experimental High Vacuum Equipment

It was recognized that experiments to be ultimately performed in the ultrahigh vacuum system should be first tested in a high vacuum environment. A system capable of achieving  $1 \times 10^{-7}$  torr in vacuum was available and experiments in making deposits of alumina in five different ways were carried out. A carousel arrangement was built that would allow a series of reactive deposition experiments to be carried out, and was also so constructed that an electron beam heated evaporation could be done. Figures 5(a) and (b) show photographs and Fig. 6 a drawing of the system.

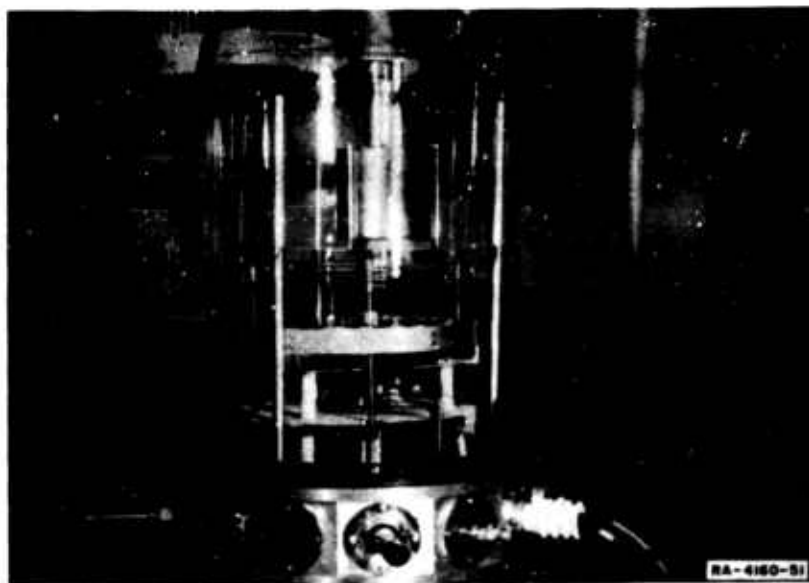


FIG. 5(a) MULTI-SOURCE CAROUSEL SYSTEM

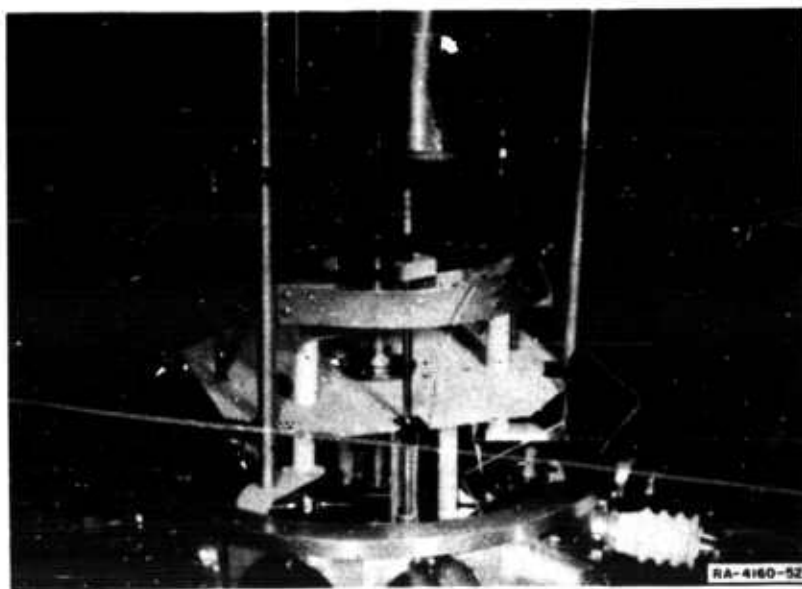
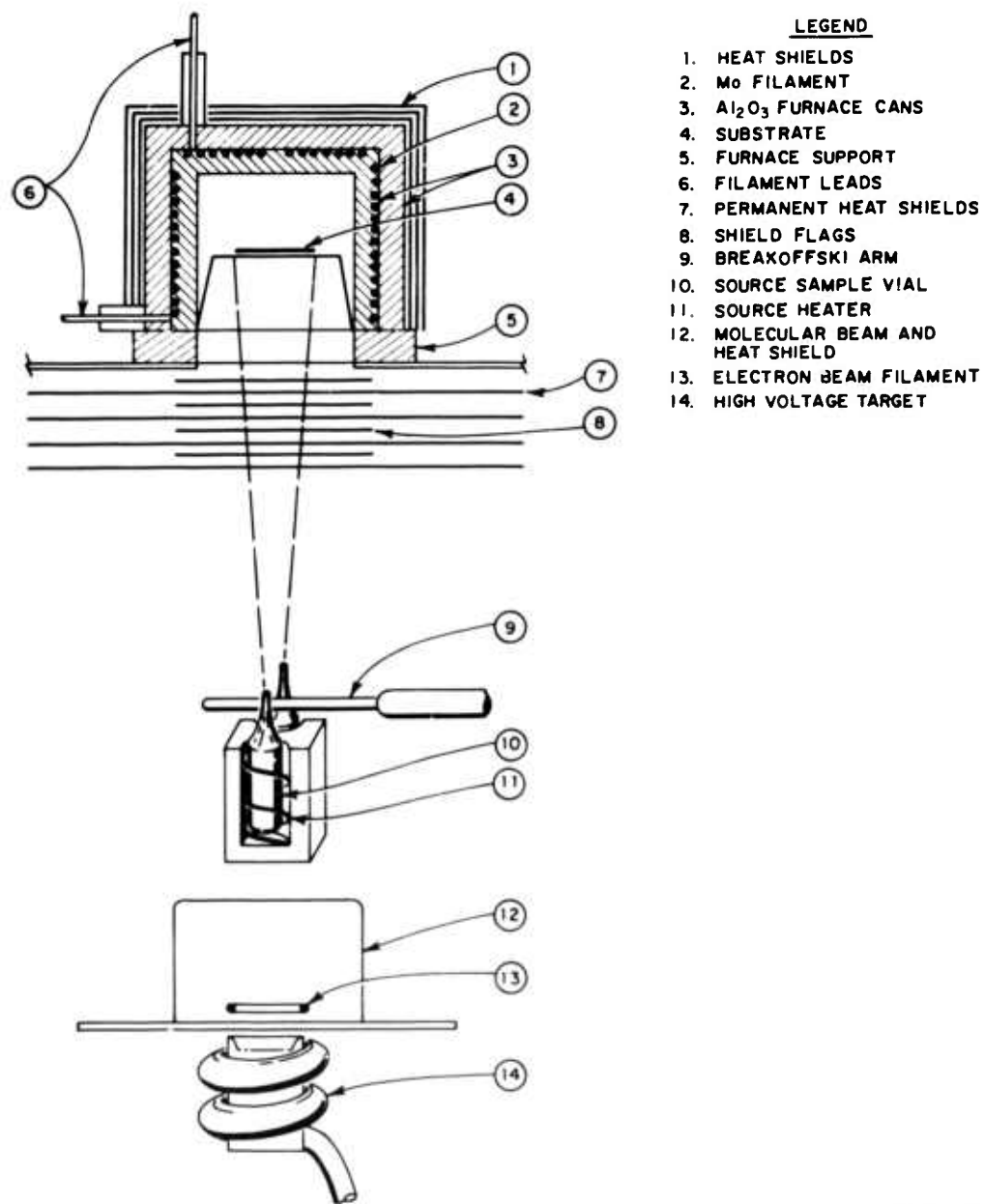


FIG. 5(b) MULTI-SOURCE CAROUSEL SYSTEM



RB-4160-54

FIG. 6 SCHEMATIC DRAWING OF MULTIPLE DEPOSITION SYSTEM

In addition, a hot filament evaporation system was installed for evaporating aluminum and a gas inlet tube was introduced for admitting oxygen into the chamber. Figure 7 schematically shows this system.

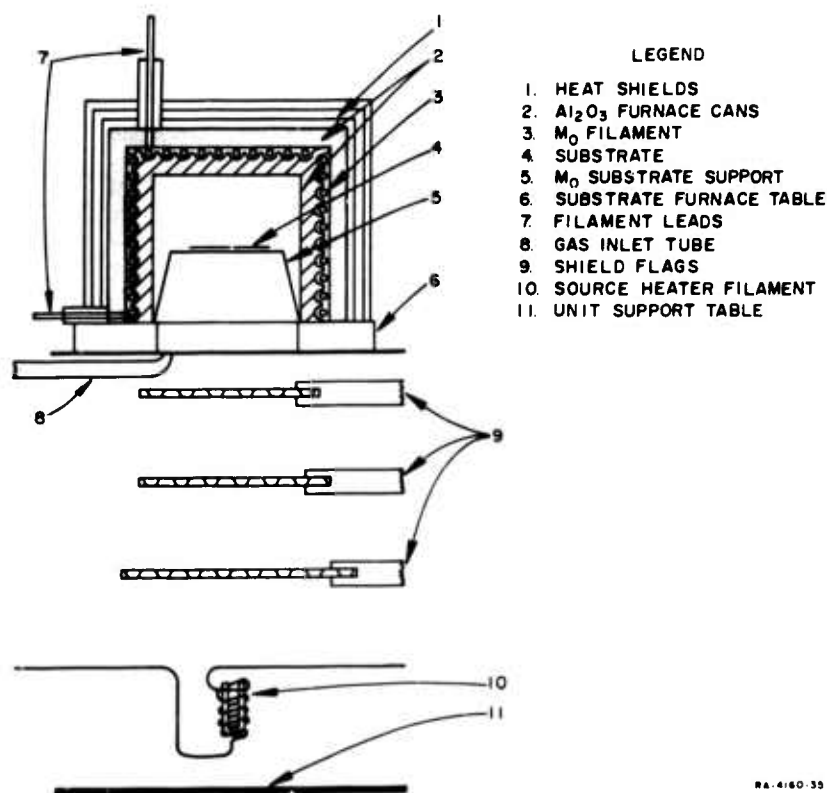


FIG. 7 SCHEMATIC DRAWING OF REACTION SYSTEM

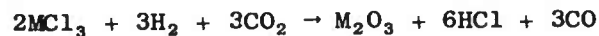
### 3. Deposition Techniques

Deposition of aluminum oxide was accomplished by five methods. All produced alpha alumina, but in some cases, a post treatment was required. Three of the methods used were essentially based on the same technique, that is, they involved the hydrolysis of aluminum chloride.

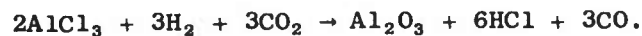
The methods, in detail, are as follows:

#### a. Volatile Metal Halide-Hydrogen-Carbon Dioxide Reaction

Reaction between a volatile metal halide, hydrogen, and carbon dioxide forms the metal oxide at a heated surface. This reaction is written in its general form as:



and, specifically for alumina formation:





The reaction was known to proceed at a reasonable rate at atmospheric or slightly positive pressures and with the substrate temperature at 1000°C. It was shown that thin films of alpha alumina could be produced under vacuum conditions with this method. The source of hydrogen for the reaction was titanium hydride, which is reported to contain excess hydrogen. Upon heating to 400°C, approximately 80% of the hydrogen is lost. Carbon dioxide for the reaction was obtained by thermally decomposing magnesium carbonate to form magnesium oxide and CO<sub>2</sub>.

b. Reactive Deposition with NH<sub>4</sub>NO<sub>3</sub>

The general procedure was the same as that above; the reactants were vaporized and allowed to react at the hot substrate surface. The result was formation of alpha alumina.

c. Reactive Deposition with H<sub>2</sub>O

Again the general procedure was the same; however, the source of the water vapor was Mg(ClO<sub>3</sub>)<sub>2</sub> that was saturated with water. Upon heating in vacuum, the water vapor is quantitatively released. In this case, the result was again an alpha alumina deposit.

d. Alumina Formation in an Oxygen Environment

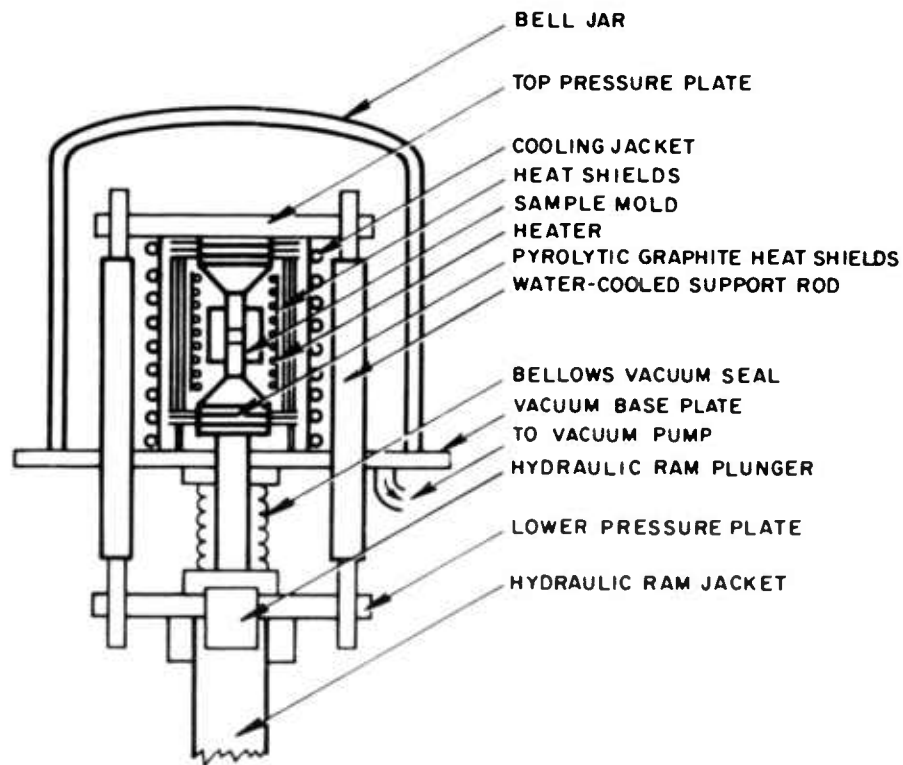
A thin film of aluminum metal was evaporated on a previously oxidized substrate. With the substrate at a temperature of about 650°C, pure oxygen was introduced into the system. By alternately evacuating the system, evaporating a thin film of aluminum, and admitting oxygen, a thick film of alumina was produced. This was shown to be alpha alumina after a post treatment of heating to 1000°C.

e. Thermal Evaporation of Alumina

Thermal evaporation of alumina was carried out by electron beam heating of the source material, both in the high vacuum interim system and in the ultrahigh vacuum system. In both systems, the material deposited and post-treated by heating to 1000°C was alpha alumina.

## II Preparation of Sintered Alumina

The equipment for preparing sintered alumina bodies will consist of a vacuum hot pressing system. The component parts are being fabricated and assembled. The vacuum system is a standard oil diffusion pumped, liquid nitrogen trapped unit being assembled from components by Institute personnel. The hot press is a modification of a standard pressing assembly; an over-all drawing of the press is shown in Fig. 8.



TA-4160-3

FIG. 8 SCHEMATIC DRAWING OF HOT PRESS ASSEMBLY

### III Ionization of Gas in Voids in Windows

A part of the investigation of breakdown of microwave ceramics was a study of the concept that residual gas in pores of ceramics could be ionized by high r.f. fields and that this ionization could lead to breakdown of the ceramics. This effect has been reported in the literature for frequencies in the range of  $10^5$  cps, <sup>1,2,3,4</sup> but not for microwave frequencies. Therefore, it was decided to investigate this phenomenon at a frequency at which many power microwave tubes operated: 3000 mc.

In a commercial gas-tight ceramic, the pores that are formed during the sintering operation are small gas-tight pockets that may range in size from the order of microns to a few thousandths of an inch. The gas content of these pores is probably air, or perhaps air with an excess of products from the sintering operation. For the purposes of estimate, the assumption of air is considered satisfactory. The shape of the pores is also variable but for simplicity a spherical shape was assumed as a model. The ceramic may then be considered as a homogeneous material of dielectric constant  $\epsilon_1$  with spherical impurities of dielectric constant  $\epsilon_2$ . When an external field  $E_0$  is applied across the dielectric, the field within the impurity sphere is

$$E_2 = \frac{3\epsilon_1}{2\epsilon_1 + \epsilon_2} E_0$$

Using aluminum oxide as the homogeneous dielectric,  $\epsilon_1 = 9$  and air  $\epsilon_2 = 1$  as the spherical impurity  $E_2$  is  $1.42 E_0$ .

The pressure within the void may be estimated by using the gas law,  $PV = RT$ , and assuming that the pores are sealed off at the sintering temperature,

$$P_2 = \frac{P_1 T_2}{T_1 K}$$

where  $T_1$  is the sintering temperature  $^{\circ}K$ ,  $T_2$  is room temperature  $^{\circ}K$ ,  $P_1$  is atmospheric pressure,  $P_2$  is gas pressure in the void, and  $K$  is the

volume contraction of the alumina. The sintering temperature is taken as 2000° Kelvin and volume contraction as 0.80. This leads to a pressure within the voids of 139 torr.

Referring to the work of Brown,<sup>5</sup> Rose and Brown,<sup>6</sup> Gould and Roberts,<sup>7</sup> and Francis,<sup>8</sup> the process of ionization of air in the voids is assumed to be essentially due to inelastic collisions between free electrons and the air, where the free electrons gain their energy from the r.f. fields across the ceramic. The loss mechanisms controlling the density of electrons available for ionization are assumed to be diffusion to the void walls and attachment. Therefore, for ionization to occur, the mean free path of the electrons must be less than the cross-section of the void. The mean free path of an electron is a function of the density of the gas in which it is situated as well as the electron temperature, which is determined by the energy state of the electron. Using as a rough approximation:

$$(\text{mfp})_e = 4\sqrt{2} (\text{mfp of gas})^9$$

the mean free path of an electron at room temperature and 139 torr is  $3 \times 10^{-4}$  cm, which is probably correct within an order of magnitude. Therefore, if the voids are greater in size than this value for the mean free path, collisions leading to ionization of the residual gas in the voids could occur.

Gould and Roberts<sup>7</sup> developed certain parameters for breakdown of air in microwave cavities as a result of their experiments. One parameter is  $p\lambda$  (mm Hg-cm) where  $\lambda$  is the wavelength of the applied field in cm, and  $p\lambda$  indicates the degree of energy modulation of an electron by an applied r.f. field. For  $p\lambda$  greater than 5000, energy modulation becomes 100%. Another parameter is p.d., which corresponds to the pressure-gap parameter used in defining Paschin's relations for d.c. breakdown of a gas. This latter parameter takes into account the diffusion length of the gas.

As a result of their investigations, Gould and Roberts published a series of curves that would indicate the probability of ionization under

given conditions as a function of the parameters cited above. From the curves, it is difficult to predict the precise breakdown or ionization field for voids smaller than 0.5 mm at pressures in the range of 140 torr. However, for a sphere having a diameter of 0.5 mm (0.020-in.), the ionizing field is found to be 4600 v/cm for CW conditions. For pulsed conditions this field will be modified to some extent.

It was decided, therefore, since it was not possible to predict ionization of gas in voids on a reliable basis, to conduct a series of experiments to determine whether ionization of gas in voids was indeed a likely cause of breakdown of ceramics. The method of test consisted of applying an r.f. field to a reentrant cavity in which were located ceramic disks with a known percentage of voids of specified diameter.

The specimens to be tested consisted of four different groups having voids in the order of 0.020-in., 0.010-in., 0.005-in. diameter, and normally prepared material. The specimens were prepared by adding spheres of a volatile material such as naphthalene to the ceramic mix before pressing and sintering. In each case 10% by volume of the mix consisted of the naphthalene spheres.

The cavity was designed<sup>10,11</sup> to fit into a pressurized s band waveguide that was filled with sulfur hexafluoride at about 50 psi. Pressurized gas was used to suppress any possibility of multipactor during the experiment and to extend the power range of the system. Figure 9 is a schematic diagram of the test cavity and Fig. 10 is a schematic diagram of the testing setup. The power source was a 2J26 magnetron operating at 3000 mc with a peak power output of 250 kw pulsed. The cavity was tuned to this frequency and the Q was found to be 300 with specimen in place. The voltage standing wave ratio was 3 and R/Q was found to be 115.6.<sup>12,13</sup>

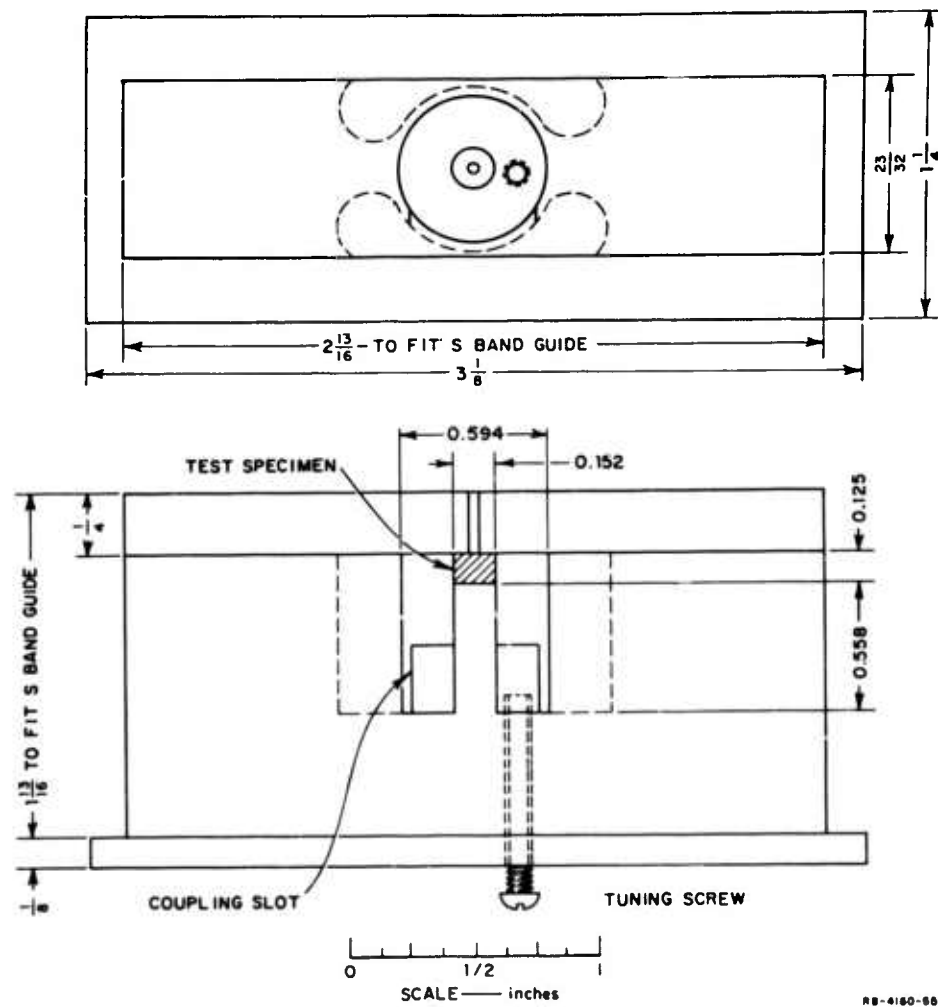


FIG. 9 DIMENSIONS OF TEST CAVITY

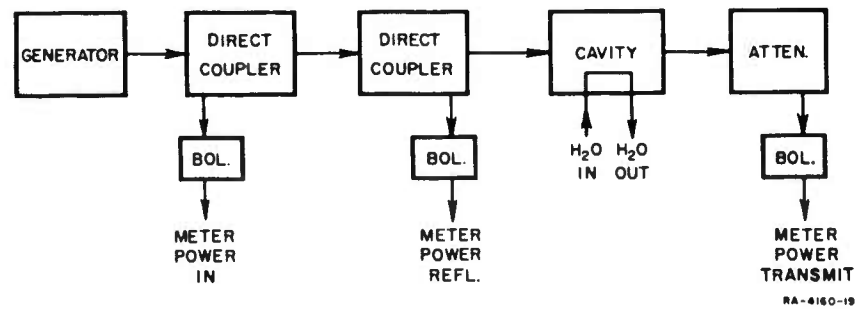


FIG. 10 VOID TEST SETUP

In performing the actual breakdown tests, two sources of difficulty were found: arcing across the specimen surface, and arcing between the post of the reentrant cavity and the specimen. The former difficulty was met by coating specimens with silicone coating and the latter by using a silver paste to ensure intimate contact between post and specimen. Figure 11 is a photograph of the test setup. The arcing was evidenced by distortion or breakup of the output from the tube as observed on an oscilloscope.

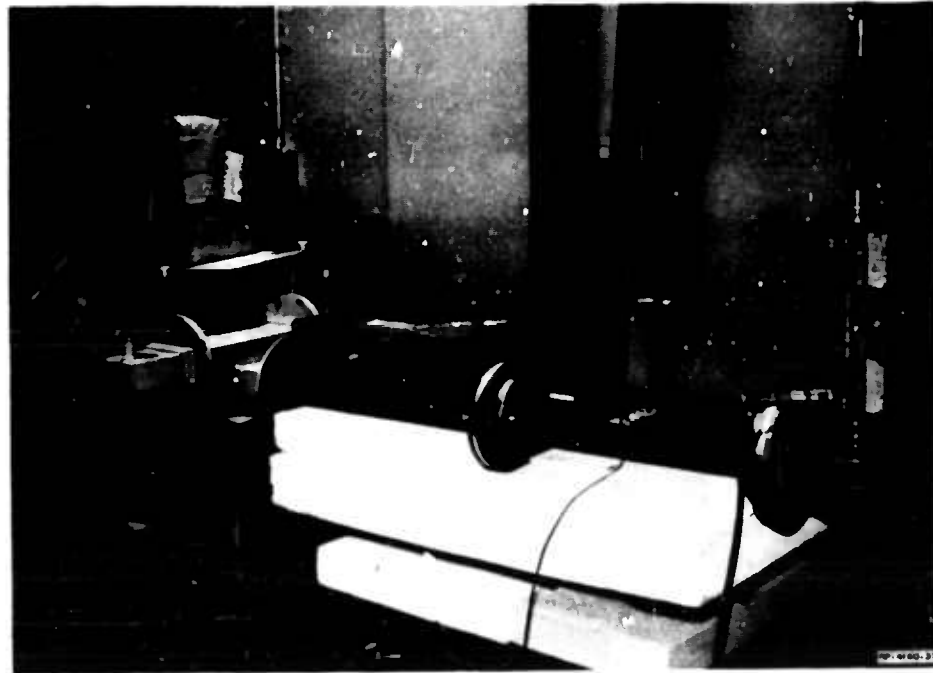


FIG. 11 BREAKDOWN TEST SETUP

When the difficulties in testing were overcome, the testing of the specimens was performed. Due to the vswr of 3 to 1, peak powers in the order of 164 kw and average powers in the order of 132 w were delivered to the specimens. The four different groups were tested and no breakdown of any of the specimens was observed. Taking into account the parameters of the system, peak fields of 132,000 v/cm and average fields of 4,050 v/cm were developed across the specimens without breakdown.

These levels of field may be compared with those found in windows of the 100 mw peak power and 400 kw average power tubes used at Eitel McCullough, Inc., San Carlos, California, or at the Stanford Linear Accelerator Center. In these tubes, peak fields are 56,000 v/cm and average fields are 250 v/cm at 2700 mc.

It may therefore be said that at this time ionization of gas in voids in windows is not indicated as a source of window breakdown for existing power levels of microwave tubes, since test fields were far in excess of those developed in actual tubes and no breakdown due to ionization of gas was observed.

#### A. Design for Test Cavity

A reentrant cavity was chosen for breakdown testing because the fields developed across the specimen, which is in line with the center post, can be calculated with a high degree of certainty when the cavity is treated as a coaxial line with a dielectric placed in part of the center conductor. The thickness of the specimen was 0.125-in. and its diameter was selected as 0.152-in. The post diameter was selected to be 0.170-in. to ensure that fields within the specimen would be essentially parallel. The characteristic impedance of the cavity was selected as 75 ohms. The calculations for the cavity are based on the approach of Marcuvitz<sup>12</sup> for the susceptance of the capacitive gap terminating a coaxial line and with a ratio of cavity diameter to center post diameter of 3.59.

The capacity of the dielectric is:

$$C'_d = \frac{\epsilon_0 K' A}{1} = 1.175 \text{ picofarads}$$

where  $\epsilon_0$  = dielectric constant of free space

$K'$  = dielectric constant of specimen

$A$  = area of specimen

$1$  = thickness of specimen.

The susceptance of the capacitive gap is



$$\frac{B}{Y_0} = \frac{4b'}{\lambda} = \ln \left[ \frac{a'}{b'} \left( \frac{\pi b'}{4 l} + \ln \frac{(a' b')}{1} \right) \right] = 0.115$$

where  $Y_0$  = susceptance of capacitive gap

$b'$  = radius of post

$a'$  = radius of cavity

$\lambda$  = freespace wavelength at operating frequency.

The characteristic impedance is given by

$$Z_0 = 60 \ln \left( \frac{a'}{b'} \right) = 75 \text{ ohms.}$$

The capacitance of the gap is

$$C_0 = \frac{B}{2\pi f_0} = \frac{0.115 Y_0}{2\pi f_0} = 0.0813 \text{ picofarads.}$$

The capacitive reactance at the gap is

$$X_c = \frac{1}{2\pi f_0 (C_0 + C'_d)} = 42.3 \text{ ohms.}$$

Then, at resonance,  $X_L = X_c$  and  $X_L = Z_0 \tan \beta l'$  where  $X_L$  = inductive reactance of post

$$\beta = 2\pi/\lambda = \text{propagation constant of the line (post)}$$

$$l' = \text{length of post (line)} = 0.683 \text{ inch.}$$

Subtracting the length of the specimen, the length of the post is 0.558 inch.

The  $R/Q$  for the cavity was found to be 115.6 and the  $Q$  was found to be 300 when the specimen was in place. The effective resistance of the specimen may be computed to a first order from

$$R_s = \frac{1}{\sqrt{\epsilon'}} \left( \frac{R}{Q} \right) Q_s$$

where  $R_s$  is effective resistance of the specimen,  $Q_s$  is  $Q$  of cavity with specimen in place, and  $\epsilon'$  is the dielectric constant of the specimen.

$R_s$  was found to be 11,000 ohms.

The ratio of power delivered to the specimen to the power generated by the tube (magnetron) is

$$\frac{P}{P_{\max}} = \frac{4s}{(s+1)^2} = 0.75$$

where  $s$  is the standing wave ratio. The voltage across the cavity gap with the dielectric specimen in place is then computed from

$$V = \sqrt{PR_s}.$$

From this the peak and average voltages and fields were determined.

#### IV Electrical Measurements on Sapphire

##### A. Discussion

The atomic picture of a grain boundary is not known in detail, since, in most cases, the boundary is extremely complicated. In the case of aluminum oxide (polycrystalline) the boundary is formed at an elevated temperature with a sintering compound. Such a boundary introduces perturbations in the lattice potential. These perturbations will modify the wave function of the conduction electrons and macroscopically change the conductivity of the material. Figure 12 represents a theoretical energy level diagram for a polycrystalline material. This model excludes impurities which may act as donors, acceptors, or traps. The bottom of the conduction band is not a straight line because the individual crystals are randomly oriented. The random orientation with respect to the direction makes the location of the fermi level, within a given crystal, a function of  $x$ . When these crystals are in contact with each other, the fermi level must be at the same level throughout the bulk material. This results in a stepping of the conduction band energy levels as a function of  $x$ , as shown in Fig. 12.

Figure 13 is a model of a grain boundary which might exist in a real polycrystalline material such as aluminum oxide because the boundary is formed with an additive material. Since the impurity content is high, the step height (or junction) may be quite large compared with the ideal model in Fig. 12. The points  $P_1$  and/or  $P_2$  may be above the bottom of the  $Al_2O_3$  conduction band or below the top of the  $Al_2O_3$  valence band, depending upon the impurities in the additive, the impurities in the crystals of  $Al_2O_3$ , and the additive itself. In the former case a barrier to electron flow would exist, if point  $P_1$  was several  $KT$  above the top of the  $Al_2O_3$  conduction band.

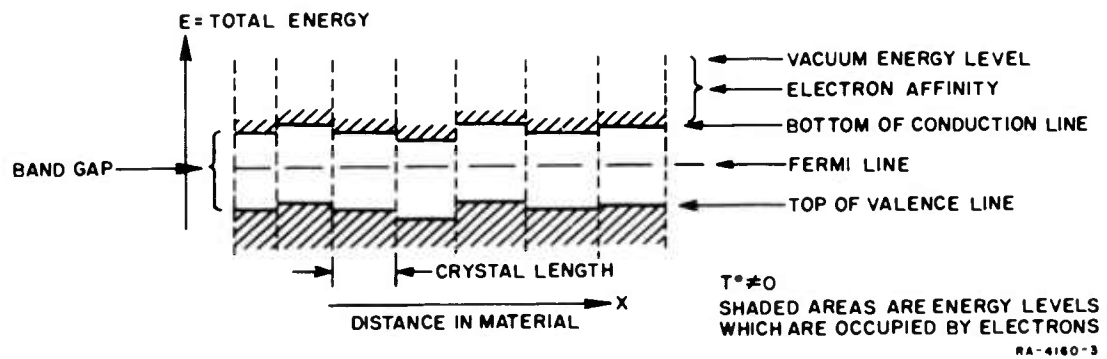


FIG. 12 ENERGY BAND MODEL FOR IDEAL POLYCRYSTALLINE MATERIAL

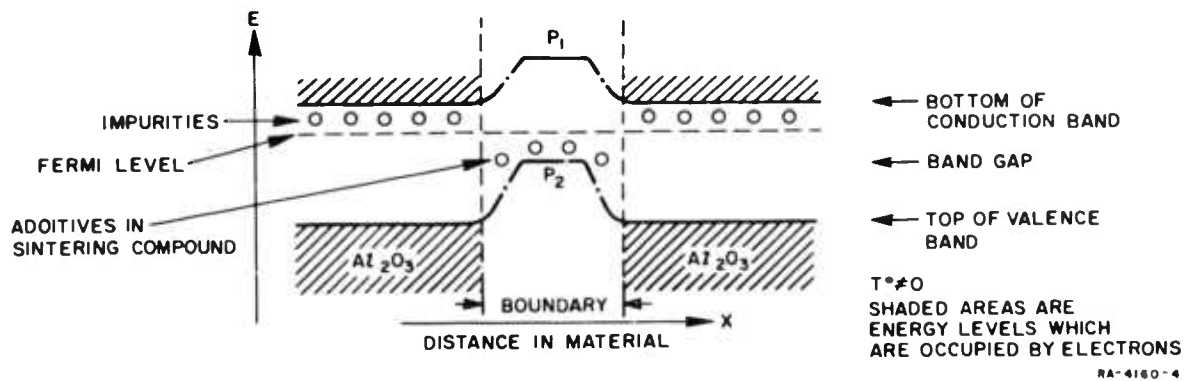


FIG. 13 MODEL OF GRAIN BOUNDARY

Measurements made on aluminum oxide and sapphire<sup>14,15</sup> involve both impurity and grain boundary effects; thus, little is known about their individual effects on transport processes. If more were known about grain boundaries it might be possible to modify the conduction and breakdown parameters of aluminum oxide, for example, lower leakage current and higher breakdown fields.

The approach taken here is to form a single, large area, grain boundary between two oriented sapphire crystals. By this method, comparison measurements may be made between sapphire samples without a grain boundary and sapphire samples with a grain boundary. Measurements on conductivity versus temperature, current versus voltage, and voltage breakdown will be made on the comparison samples. From these data it will be possible to improve our knowledge of the physical picture of grain boundaries in aluminum oxide.

## B. Sample Preparation

### 1. Specimens

Figure 14 shows the four basic specimens A, B, C, and D. All single crystal specimens were cut from the same boule and have their c-axis perpendicular to the crystal face.

#### a. Specimen A

Specimen A consisted of two sapphire crystals sintered together at 1750°C in air for three hours, using a sintering compound composed of 50% CaCO<sub>3</sub> and 50% SiO<sub>2</sub>. This compound corresponds to the industrial compound used to make 97.6% polycrystalline alumina. Three "A" specimens were made at different times and measured for conductivity as a function of temperature. All specimens in this experiment had the same temperature history; that is, although specimen C was not a sintered configuration, it was still fired at 1750°C. Specimens which were not fired were also measured for conductivity. Specimen A therefore represents a planar model of a situation that exists in three dimensions in polycrystalline alumina.

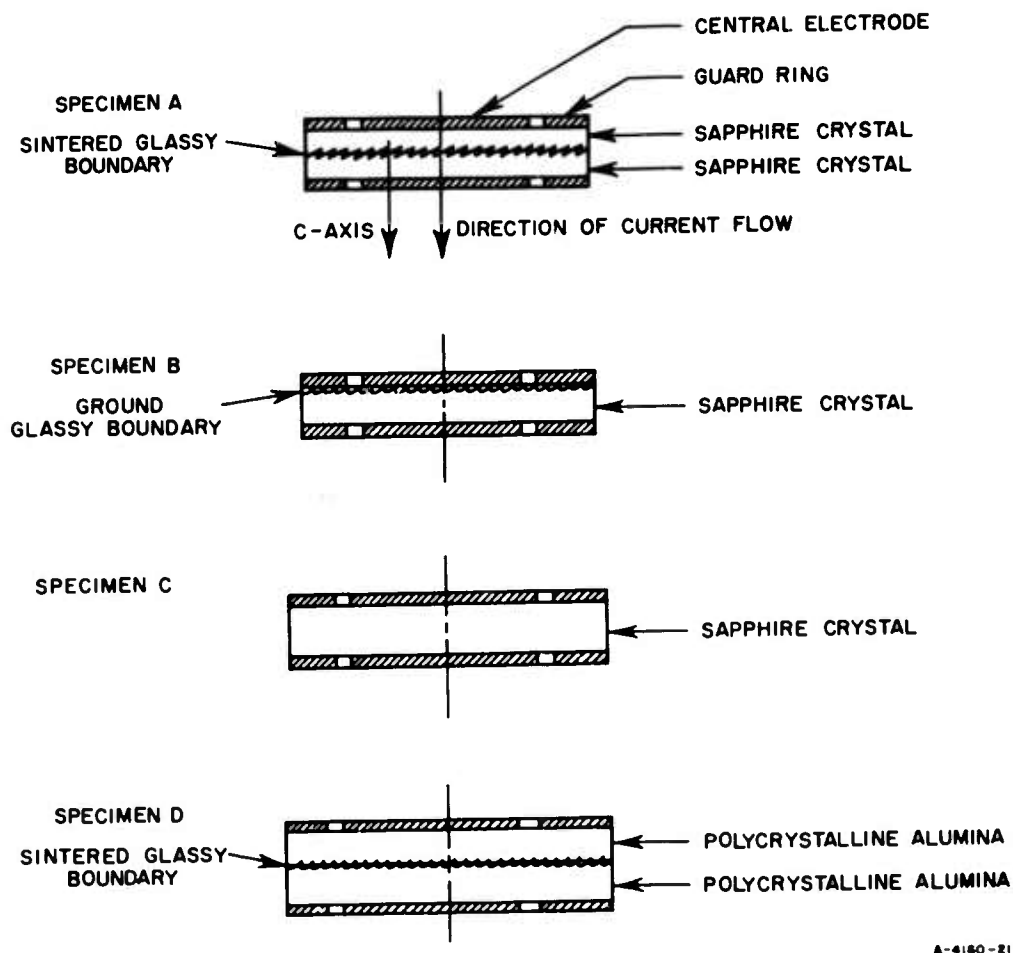


FIG. 14 CROSS SECTION OF SPECIMENS

b. Specimen B

Specimen B was made the same as A and was measured as an A-type specimen. After being measured for conductivity it was split into two pieces by being fractured through the glass boundary. The glass boundary was ground off until it was believed to be completely removed from the underlying sapphire disc. Specimen B therefore represents a planar model which enables one to determine the effects of the glass on the sapphire crystal.

c. Specimen C

Specimen C was a single disc of sapphire.

d. Specimen D

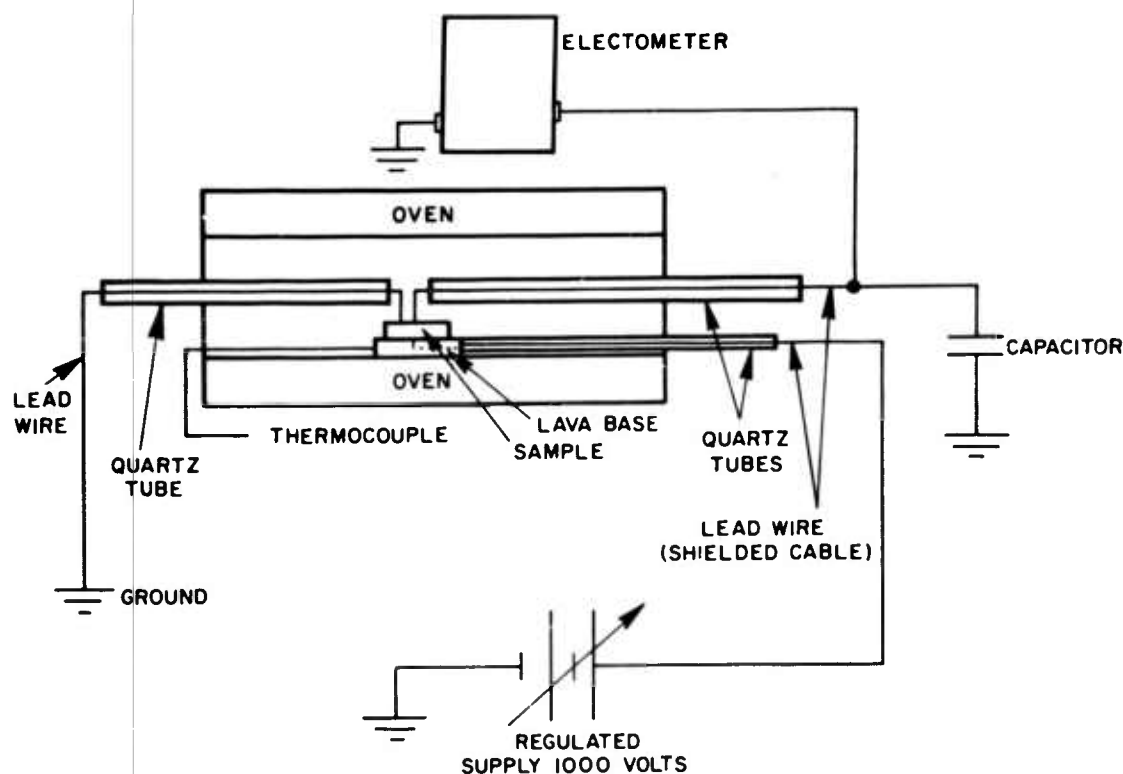
Specimen D consisted of two discs of polycrystalline alumina sintered together (as was specimen A), with the same sintering compound and temperature.

C. Experimental Apparatus

The apparatus to be used for measurements involving elevated temperatures is shown in Fig. 15. Figure 16 is a schematic of the electrical circuit. The oven is capable of reaching  $1100^{\circ}\text{C}$  as recorded with the chromel-alumel thermocouple. The quartz tubes reduce leakage paths to ground and provide mechanical supports for the platinum leads within the furnace. Contact between the platinum leads and the sample is made by mechanical pressure, exerted through the quartz tubes, on the platinum wires. The lead to the electrometer is carefully isolated from the surrounding circuitry. The capacitor (1 microfarad, 100 volts) bypasses alternating currents to ground. The maximum background noise current is  $2 \times 10^{-13}$  amp, which is at least an order of magnitude less than the sapphire currents to be measured.



FIG. 15 EXPERIMENTAL APPARATUS



RA-4160-7

FIG. 16 EXPERIMENTAL APPARATUS (Schematic Diagram)

### 1. Sapphire Electrodes

The electrodes on the sapphire are in the form of a central disc with a surrounding ring. The ring is a guard ring which eliminates measurements of leakage currents on the sapphire surface.

The electrodes on the sapphire samples were platinum and gold. Platinum and gold paint were painted on the sapphire samples after they had been washed and rinsed in trichloroethylene and alcohol. The sample was then fired at 800°C in air for 1/2 hour, thereby removing the binder and producing an adherent metallic film. It is essential that the wet film be placed in the oven at room temperature or flaking of the film will occur. In order to form a guard ring the film was scribed in a circle with a diamond pencil, resulting in a central circular disc surrounded by a ring. The films resist attack by aqua regia and are highly adherent. Figure 17 shows the temperature limit of both gold and platinum films fired in air as measured in our laboratory.



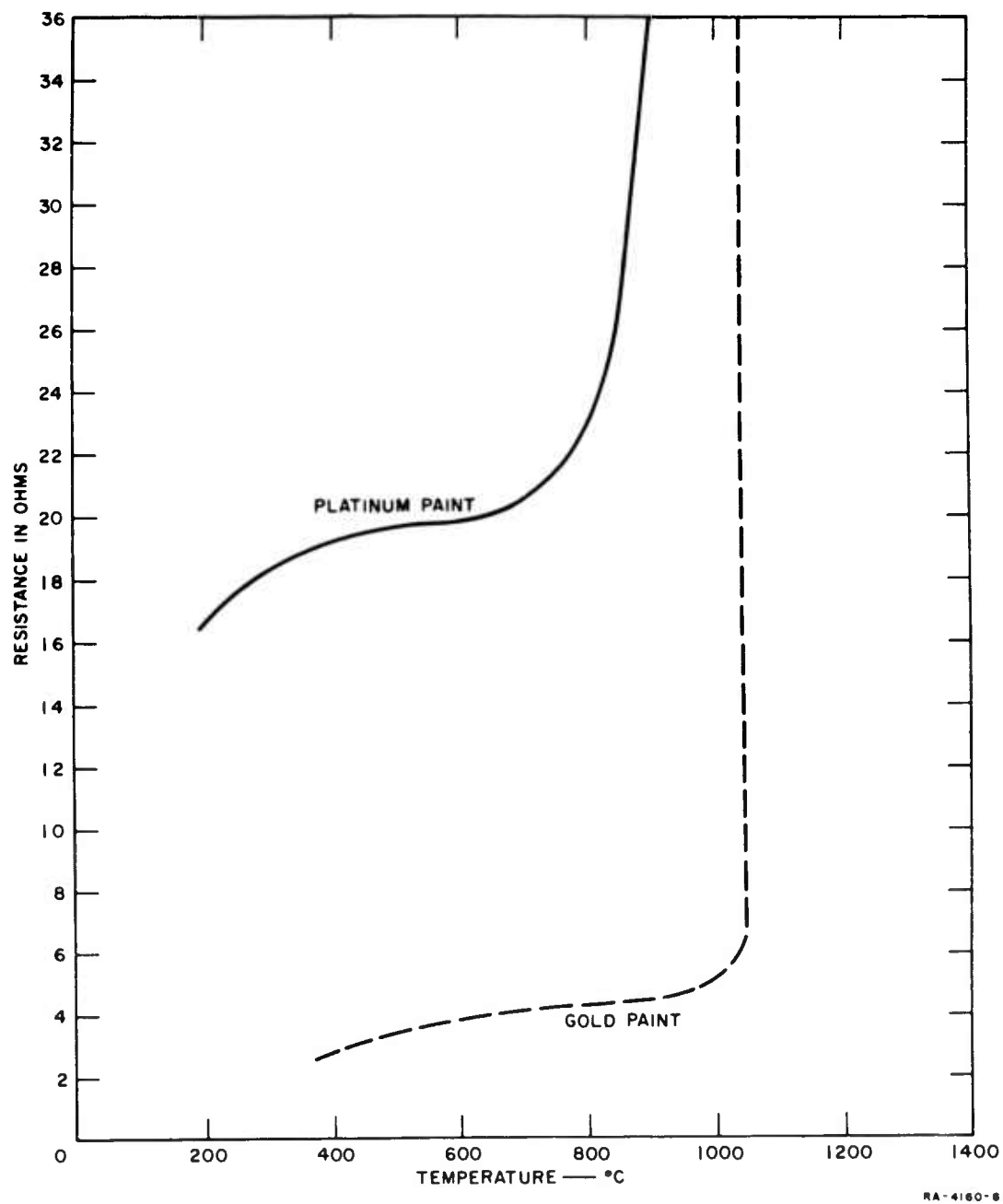


FIG. 17 RESISTANCE vs. TEMPERATURE

## 2. Lead Wires

Platinum wires, 0.005-in. and 0.010-in. in diameter, were attached to the electrodes on the sapphire samples by brazing techniques. The platinum-coated sapphire sample, platinum lead wire, and gold braze material were cleaned in trichloroethylene and rinsed in methanol. The sample was placed in the air furnace with the gold braze material between the platinum film and the platinum wire. The temperature of the oven was briefly raised to 1080°C. The strength of the resulting braze was limited by the film adherence to the sapphire sample. The gold braze method is satisfactory for applications where only moderate mechanical stresses are involved.

### D. Electrical Conductivity of Single Crystal Al<sub>2</sub>O<sub>3</sub>

The purpose of this portion of the experiment was to measure the electrical conductivity of single crystal Al<sub>2</sub>O<sub>3</sub> as a function of temperature. Figure 18 shows the results of the measurements. The vertical lines on the curve represent spread in data. Four specimens were measured. The activation energy may be determined from the slope of the conductivity versus temperature curve. The theoretical expression for the number of free carriers per unit volume for an insulator is<sup>18</sup>

$$n_c = (2 N_D)^{1/2} \left( 2\pi \frac{m^x kT}{h^2} \right)^{3/4} \exp(-\Delta E/KT) \quad (1)$$

where  $n_c$  is the number of carriers per unit volume,  $N_D$  is the number of donor atoms per unit volume,  $m^x$  is the effective mass of the carrier,  $k$  is Boltzmann's constant,  $h$  is Planck's constant,  $T$  is the absolute temperature and  $\Delta E$  is the energy difference between the bottom of the conduction band and the energy level of the donors. The conductivity is

$$\sigma = n_c e \mu \quad (2)$$

where  $\sigma$  is the conductivity,  $e$  is the carrier charge, and  $\mu$  is the mobility. From Eqs. (1) and (2) and the data of Fig. 18, the activation energy  $\Delta E$  may be determined. The result is

$$\Delta E = 2.34 \text{ electron-volts}$$

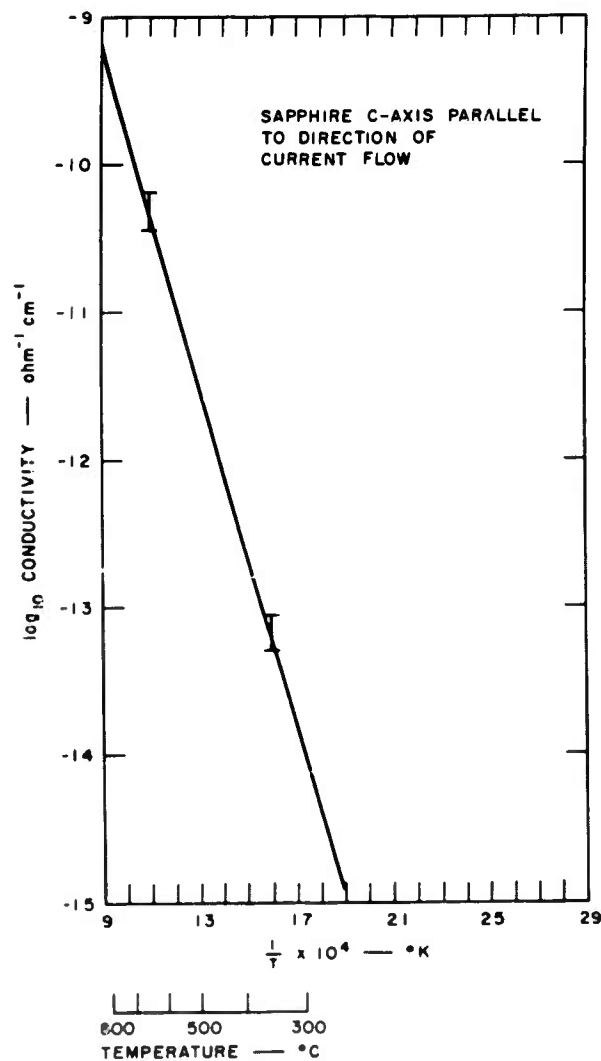


FIG. 18 ELECTRICAL CONDUCTIVITY OF SAPPHIRE  
AS A FUNCTION OF TEMPERATURE

The value of 2.34 electron-volts is extremely small for sapphire compared with values obtained at high temperatures (1700°C).<sup>14</sup> This value is most likely due to impurity conduction. The sapphire specimens contained  $10^{18}$  iron atoms/cm<sup>3</sup>.<sup>17</sup> If it is assumed that each iron atom is located 2.34 electron-volts below the bottom of the conduction band, an estimate of the mobility ( $\mu$ ) may be made by using equations (1) and (2) and the conductivity data. The resulting value of mobility is

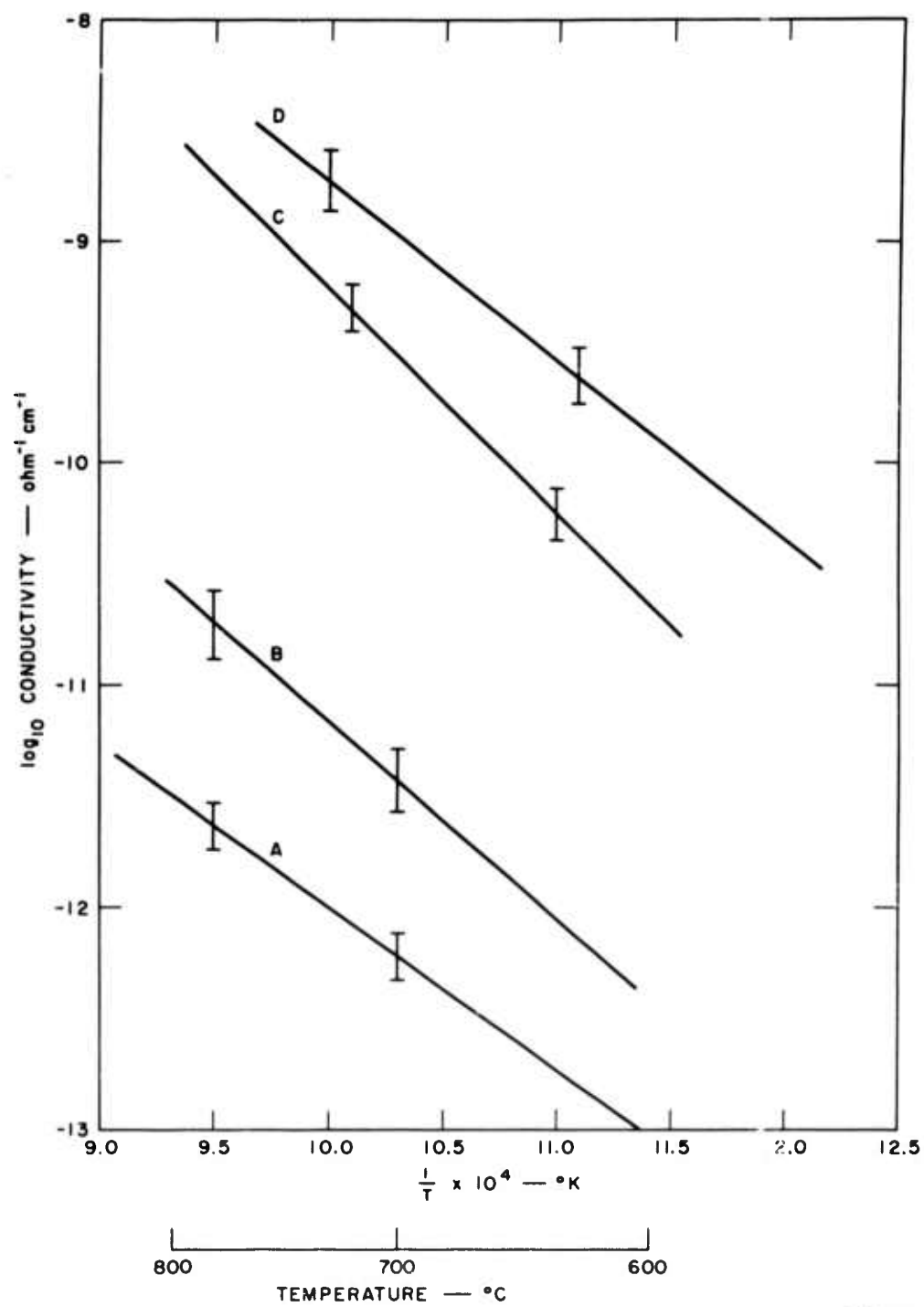
$$\mu = 0.1 \text{ cm}^2/\text{volt-sec.}$$

This is a reasonable value of mobility for sapphire. The mobility of the sapphire specimens can be expected to be low because the crystal structure is poor and the impurity content is high. The mobility would be low also because it is a conductivity or drift mobility, not a Hall mobility, and therefore includes trapping effects.

#### E. Electrical Conductivity of Specimens A, B, C, D

Figure 19 shows the results of the measurements on the four specimens. The conductivity values for specimens C and D are in good agreement with measurements made by other investigators.<sup>15,16</sup> The conductivity values shown for specimen A are in some doubt, since the corresponding currents were near the values measured without a sample in the system. The short vertical lines represent the spread in data or error.

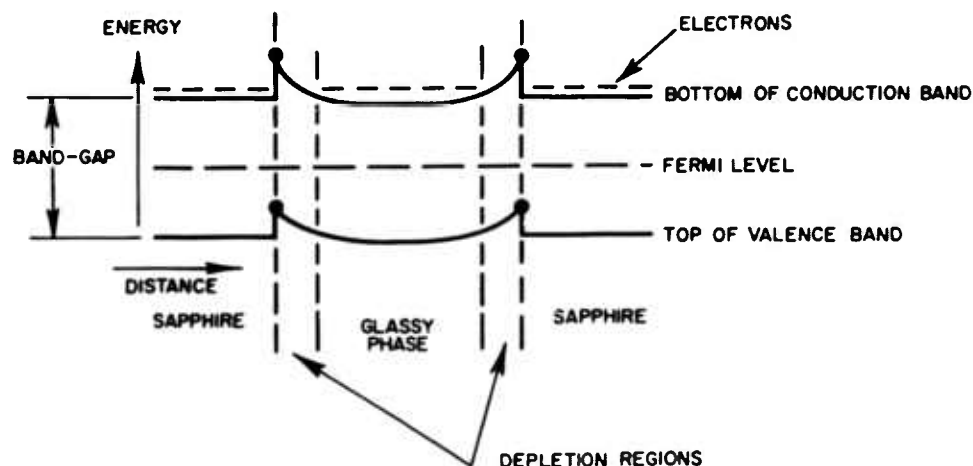
From the results in Fig. 19 it can be seen that the original hypothesis that conduction through the glassy phase is dominant is evidently valid, since specimen A has at least three orders of magnitude less conductivity than C or D. This difference in conductivity could be much greater, since the current measurements for specimen A were near the values obtained without a sample in the system. The difference in specimens A and D is the conduction path. In specimen A the carriers must pass across the glassy phase boundary, whereas in specimen D the carriers may travel from one side of the specimen to the other side through the glassy phase. The results on specimen B indicate that a diffusion process occurred. The glassy phase was removed from specimen B by grinding, yet its conductivity is lower than that of specimen C, which is a single crystal of sapphire. The reduced conductivity effect observed with specimen A possibly can be explained by considering the electronic differences between the two regions; the sapphire region and glassy phase region. A possible situation is that in which the band-gap-energy of the glassy phase region is less than the band-gap-energy of the sapphire region. If it is assumed that the electron affinity of the glassy phase region is less than that of the sapphire region, then a



B-4160-23

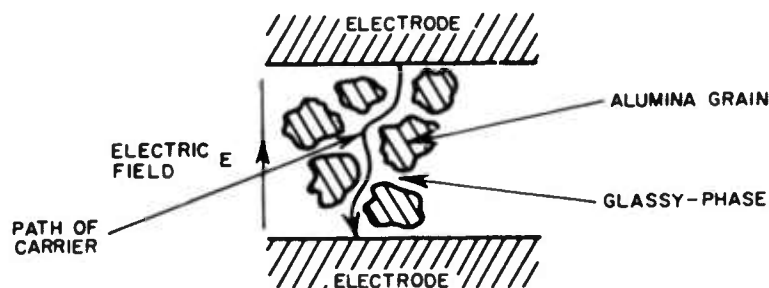
FIG. 19 TEMPERATURE DEPENDENCE OF ELECTRICAL CONDUCTIVITY

model can be constructed which has the desired characteristics. Such a model is shown in Fig. 20. If an electric field is applied from left to right in Fig. 20, carrier transport will be inhibited by the potential barriers formed in the depletion regions. This situation corresponds to specimen A. Figure 21 shows a physical model of the polycrystalline material. In this case the carriers may be transported strictly in the glassy region as shown. This situation possibly corresponds to specimen D.



A-4160-24

FIG. 20 BAND MODEL



A-4160-25

FIG. 21 PHYSICAL MODEL

#### F. Thermoelectric Power

Conductivity versus temperature measurements were made on sapphire specimens; the data were presented in the preceding discussion. These data provided information such as activation energy and conductivity. The electrical properties of sapphire that are of fundamental importance are carrier concentration, type of carrier, and carrier mobility, all as a function of temperature. The method selected to determine these properties was to measure the thermoelectric power of sapphire as a function of temperature and combine this information with the conductivity measurements. The thermoelectric measurements yield the type of carrier and the carrier concentration through the use of a theoretical expression for the thermoelectric power,<sup>18</sup> which is

$$S = \pm \frac{k}{e} \left[ 2 - \ln \left( \frac{n h^3}{2 (2 \pi m^* k T)^{3/2}} \right) \right] \quad (3)$$

where  $S$  is the thermoelectric power,  $k$  is the Boltzmann constant,  $n$  is the carrier concentration (holes or electrons),  $h$  is Planck's constant,  $m^*$  is the effective mass of the carrier, and  $T$  is the temperature. Equation (3) is based on the band theory which considers the carriers free to move about within a conduction band. Equation (3) holds only in the impurity range of a material, that is, where the dominant carrier is from an impurity atom. Once the carrier concentration has been determined, the mobility may be determined from

$$\mu = \frac{\sigma}{n e} \quad (4)$$

where  $\mu$  is the mobility,  $\sigma$  is the conductivity, and  $e$  is the charge of an electron. The type of carrier can easily be determined from the sign of the thermoelectric power.

The experimental apparatus used for the thermoelectric power measurements was similar to the apparatus used for the conductivity measurements described in the third quarterly report. Essentially the apparatus consisted of an air oven in which the sapphire sample was located. A temperature gradient was established along the sapphire specimen by locating

it near one end of the oven. Two chromel-alumel thermocouples were positioned about one inch apart on the sapphire specimen. The thermocouples were held to the specimen by nichrome wires wound about the specimen. Figure 22 shows the experimental arrangement schematically.

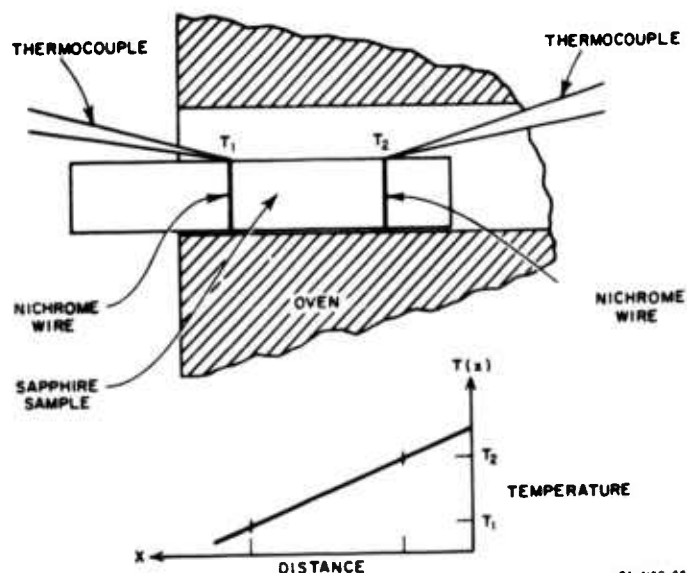


FIG. 22 THERMOELECTRIC APPARATUS

The temperatures  $T_2$  and  $T_1$ , and the thermoelectric voltage developed between  $T_2$  and  $T_1$ , were measured, using a high input impedance electrometer. The thermoelectric voltage was measured between the two chromel leads. The thermoelectric power  $S$  was computed by using

$$S = \frac{V_{TH}}{T_2 - T_1} \quad (5)$$

where  $V_{TH}$  is the measured voltage and  $T_2 - T_1$  is the difference in temperature between the two points, 2 and 1.

The basic difficulties in making thermoelectric power measurements on insulators are (1) stray fields, (2) extraneous thermoelectric voltage, and (3) the high internal impedance of the crystal being measured. The crystal may be considered to be a battery in series with a very high resistance. If the voltage measuring device, in the external circuit,



has an input impedance which is less than the internal impedance of the crystal, the largest part of the thermoelectric voltage will be dropped across the internal impedance of the crystal rather than at the voltmeter. For this reason a high input impedance ( $10^{14}\Omega$ ) electrometer was used to measure the thermoelectric voltage.

Figure 23 shows the measured thermoelectric power for sapphire as a function of temperature. It can be seen that the conduction in the temperature range of  $200^{\circ}\text{C}$  to  $800^{\circ}\text{C}$  is primarily by holes and that the thermoelectric power increases with temperature.

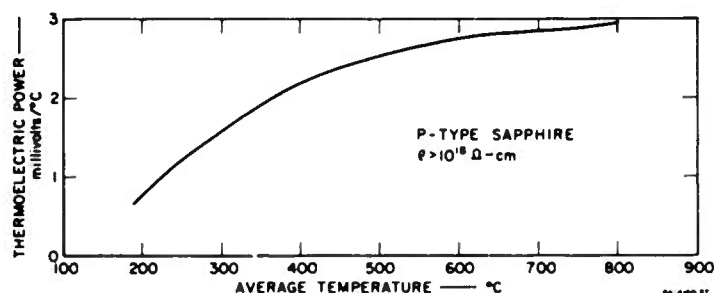


FIG. 23 THERMOELECTRIC POWER-SAPPHIRE

The characteristics of the thermoelectric power curve in Fig. 23 are similar to the curves obtained in measurements on germanium.<sup>19</sup> The similar section in germanium corresponds to an impurity region where the increasing thermoelectric power is due to an increasing carrier concentration. Equation (3) is the equation which is applicable to this region for semiconductors. As was previously mentioned, Eq. (3) considers only lattice scattering and not impurity scattering. Equation (3) appears to be appropriate for sapphire in the  $100$  to  $800^{\circ}\text{C}$  temperature range, since the sapphire crystals have a few tenths of a percent impurities and at a few hundred degrees lattice scattering should dominate over impurity scattering. The conductivity measurements, as were reported, indicated an activation energy of a few electron volts, which would have to correspond to impurity conduction, since the band-gap of  $\text{Al}_2\text{O}_3$  is about 8 electron volts. The magnitude of  $S$  in Fig. 23 is what one may expect, since iron oxide,<sup>20</sup> a similar material, has  $S = 1.0$  in this temperature range.

When the data of Fig. 23 and the conductivity data are combined with Eq. (3) and Eq. (4), we arrive at hole concentrations of about  $10^{10}/\text{cm}^3$  at  $500^\circ\text{C}$  that decrease with increasing temperature, and mobilities of about  $0.002 \text{ cm}^2/\text{volt-sec}$  that increase with increasing temperature.

There are three disturbing factors associated with the thermoelectric data: (1) the carrier concentration decreases with increasing temperature, (2) the mobility increases with increasing temperature, and (3) the mobility is extremely small. In this temperature range the carrier concentration would be expected to increase with increasing temperature. This should be the reason for the increasing thermoelectric power. It may be that the carrier scattering is due primarily to impurity scattering, in which case the thermoelectric power may increase with temperature since the carrier mobility will increase with temperature. For lattice scattering the mobility should decrease with increasing temperature. There is a basic question involved in such measurements on insulators as to what is the significance of a small mobility such as  $0.002 \text{ cm}^2/\text{volt-sec}$ . A mobility of  $0.002 \text{ cm}^2/\text{volt-sec}$  corresponds to a mean free path of about  $10^{-3} \text{ \AA}$ , which is meaningless since the lattice spacing of atoms in a crystal is a few angstroms.

There are several explanations for the results obtained in these experiments, such as (a) that the nondegenerate Fermi-Dirac electron theory does not hold for sapphire, (b) that the conductivity is due to a small polaron process or impurity band conduction, or (c) that the data are in error.

#### G. Mass Transport Experiment

##### 1. Discussion

The purpose of this experiment was to determine the type of charge carrier that is involved in the electrical conductivity of aluminum oxide, that is, whether the electrical carriers are ions or free electrons.

A mass transport experiment was performed in order to investigate this condition. Mass transport experiments have been thoroughly described in various publications.<sup>21</sup> Briefly, the experiment consists of preparing a sample of the material in question in the form of three adjacent discs with metallic electrodes on the end discs. A voltage is applied to the electrodes and the temperature of the stack increased in order to enhance current flow. This condition is maintained for an extended period of time depending upon the magnitude of the current. The three samples have been carefully weighed before the voltage was applied and are weighed again after they have been subjected to the external voltage. If the current is due to ions, a weight change in the three discs is noticeable. From the manner in which the discs' weight changes an idea of type of participating ion may be deduced. The percentage ionic current and electronic current may be obtained from a knowledge of the current as a function of time and the weight change.

## 2. Experiment

Figure 24 shows the stack of sapphire discs with leads attached. The stack consisted of five sapphire discs, flat, highly polished, and carefully cleaned. Three discs were located between platinum foil electrodes with two discs used as end plates to apply an even pressure to the platinum foil electrodes. The discs were 1/2-in. in diameter and 0.020-in. thick. Platinum wires were used as leads to the platinum electrodes. A guard ring was employed in order to obtain accurate current data. The guard ring can be seen in Fig. 24. A fixture to hold the stack was made from sintered aluminum oxide. Figure 25 shows the sample holder with the sapphire stack mounted in the  $\text{Al}_2\text{O}_3$  fixture. A nitrocellulose binder was used to temporarily hold the stack together. The large cubic block in Fig. 25 was placed on top of the stack to maintain a moderate pressure throughout the experiment. The holder containing the sapphire stack was placed in an air oven and the platinum leads were brought out of the oven through 1/2-in.-diameter quartz tubes. The current was measured with an ammeter and monitored with a recorder. The oven was continuously flushed with helium but it is not known to what extent this

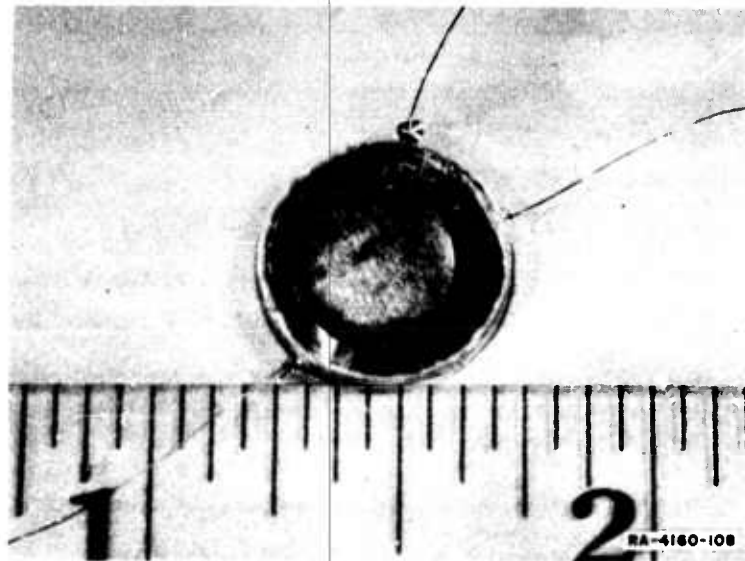


FIG. 24 STACK OF SAPPHIRE DISCS FOR CONDUCTIVITY EXPERIMENT

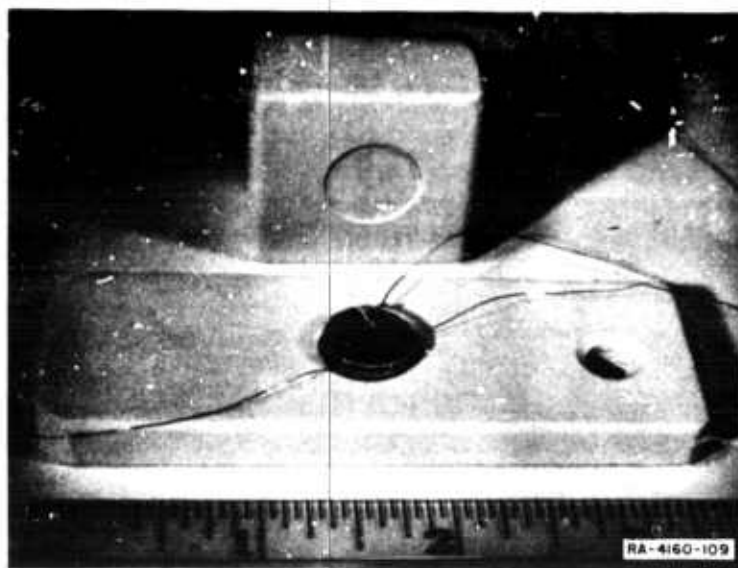


FIG. 25 SAMPLE HOLDER WITH SAPPHIRE STACK MOUNTED IN POSITION

reduced the oxygen partial pressure within the oven. Sapphire discs were heated to 1400°C, without a voltage applied, in order to determine if a weight change would result from evaporation, with the result that no weight change was observed. The discs were weighed with a microbalance capable of measuring  $1 \times 10^{-6}$  g change in weight. All discs, wires, and electrodes were weighed. The weighings were checked with separate weighings on a less sensitive balance ( $10^{-4}$  g sensitivity) and the weighings were repeated several days after the heating in order to detect any change in weight due to absorption of water vapor or oxygen.

Three similar experiments were performed with a reasonable degree of repeatability. The currents involved were about one milliamp and the temperature was 1200°C. The current was maintained for about 9-10 hours. The current as a function of voltage at 1200°C was found to be linear within the voltage range used (100-300 v). A large weight change was observed in the results but was found to be due to the platinum wire which reacted with the quartz tubing and  $\text{Al}_2\text{O}_3$  fixture. The platinum foil was found to be a substantial adhesive between the two adjacent sapphire discs. Apparently the thin platinum foil reacts with the sapphire at 1200°C in air over a long period of time.

The change in mass  $\Delta m$  of one of the discs may be quantitatively described on the basis of a simple model. Let the current  $i$  be entirely ionic and consist of ions leaving one sapphire disc. Then the number of ions leaving the disc per second is  $i/ze$ , where  $z$  is the valence of the ion and  $e$  is the charge of an electron. The mass of a single ion is  $W/N_0$ , where  $W$  is the atomic mass and  $N_0$  is Avogadro's constant =  $6 \times 10^{23} \text{ gm}^{-1} \text{ mole}^{-1}$ ; therefore, the change in mass  $\Delta M$  in time  $T$  is

$$\Delta m = \frac{i}{ze} \frac{WT}{N_0} \quad (6)$$

As a reasonable example, substitute  $i = 10^{-3}$  amp,  $W = 56$  (iron),  $z = 3$  and  $T = 3 \times 10^4$  seconds (8 hours) into Eq. (6). This gives  $\Delta m = 6 \times 10^{-3}$  grams. Since the microbalance will detect  $10^{-6}$  g change in weight, an ionic current of 1% of the total current should be easily detected. The

preceding discussion assumes that all the ions contributing to the current are of one type. If ions of opposite charge were mobile, the net weight change would be reduced. Such a condition would lead to a numerical value of ionic current that would be less than the actual value.

The sensitivity of the microbalance scale of  $10^{-6}$  g was decreased due to the reaction of the platinum wires with the  $\text{Al}_2\text{O}_3$  holder and the quartz tubing. The platinum foil electrodes were separated from the sapphire discs and the discs were weighed separately with a balance of  $10^{-4}$  g sensitivity.

The results of these experiments at  $1200^\circ\text{C}$  show negligible mass transfer. This result indicates that the ionic current is less than 2% of the total current under the assumptions of Eq. (6). The conductivity of the sapphire stack was about the same as that reported by other investigators,<sup>15</sup> about  $10^6$  ohm-cm at  $1200^\circ\text{C}$ . This establishes the current as bulk current and not surface current.

Several mechanisms may be active in a mass transport experiment. The first may consist of blocking ionic conductivity by the use of platinum electrodes. Platinum is relatively inert and may not inject platinum ions into the  $\text{Al}_2\text{O}_3$  crystals. If such a reaction did occur, one platinum electrode would decrease in weight while the opposite electrode would gain or remain constant in weight. A weight change in the platinum electrodes was not observed and such a mechanism will be considered to be negligible.

It is more likely that impurity ions may contribute to the current at  $1200^\circ\text{C}$ , since the highest purity  $\text{Al}_2\text{O}_3$ , at present, contains about  $10^{18}$  impurity atoms per  $\text{cm}^3$ . Such a process might consist, for example, of positive ions moving in one direction due to the electric field while negative ions move in the opposite direction. This would result in a net change of weight that would be much less than the expected change due to the current. It would be somewhat fortuitous for a near equal transfer of charge to occur in order to result in a condition of negligible mass transfer. For this reason this mechanism will be considered improbable.

If just positive or negative impurity ions were mobile, a change in weight would be produced within the  $\text{Al}_2\text{O}_3$  crystals unless oxygen were the ion. The oxygen ion could be replaced by oxygen from the surrounding atmosphere.

From this work it appears that  $\text{Al}_2\text{O}_3$  is an electronic conductor at  $1200^\circ\text{C}$ , to the extent of 98% of the current, and probably electronic down to room temperature, since the conduction process is still an impurity process. This result only applies for atmospheric pressure, since reduced pressures may change the stoichiometry of the  $\text{Al}_2\text{O}_3$  and therefore its transport properties.

#### H. $\text{Al}_2\text{O}_3$ Optical Absorption

Optical absorption data on  $\text{Al}_2\text{O}_3$  are available<sup>22</sup> and have been utilized in estimating the energy band gap. Forbidden energy band gaps of 7.8 e.v.<sup>15</sup> and 8.56 e.v.<sup>23</sup> have been deduced from absorption data and compared with conductivity versus temperature data. The method used to obtain the energy band gaps was to determine the wavelengths that correspond to a specific amount of absorption such as 40 or 50%. The purpose of this work was to obtain the energy band gap by a more rigorous method.

The analytical expressions for optical absorption, as a function of incident photon energy, due to direct and indirect transitions are well known and have been verified experimentally.<sup>24</sup> The absorption coefficient  $\alpha$  for direct transitions varies as the  $1/2$  power of the incident photon energy, while  $\alpha$  varies as the square of the photon energy for indirect transitions. The absorption data are plotted as  $\alpha^{1/2}$  and  $\alpha^2$  versus photon energy, and resulting linear regions indicate direct and/or indirect transitions. Extrapolation of the linear portion of  $\alpha^2$  curve to  $\alpha = 0$  yields  $E_G$ , the energy band gap. Proper interpretation of the  $\alpha^{1/2}$  curve can yield the energy band gap between the conduction band minimum and the valence band maximum and the phonon energy involved in the transition.

Figures 26 through 31 show  $\alpha$ , as taken from reference 22,  $\alpha^2$ , and  $\alpha^{1/2}$  for various temperatures from 20°C to 900°C. A linear region of the  $\alpha^2$  plot can be found in each figure, indicating a direct transition. Figure 31 shows a plot of the intercepts of the linear portions of the  $\alpha^2$  plots with the energy axis. The intercept represents the energy band gap involved in the transition. The plot of  $E_G$  in Figure 31 is extrapolated to  $T = 0^\circ\text{K}$ , giving  $E_G = 7.50$  e.v. at  $T = 0^\circ\text{K}$ . The rate of change of  $E_G$  with  $T$  is obtained from the slope and is  $\Delta E_G / \Delta T = -6.3 \times 10^{-4}$  e.v./°K. The value of  $\Delta E_G / \Delta T$  is reasonable, since many materials have similar values.<sup>15</sup> A value of 7.3 e.v. has been obtained from conductivity versus temperature measurements,<sup>15</sup> which is close to the value obtained from the optical data. Each figure shows a linear portion of the  $\alpha^{1/2}$  plot, which indicates an indirect transition. Unfortunately the  $\alpha$  data do not go high enough in photon energy to show the phonon emission portion of the indirect transition clearly.

It is unfortunate that the data were not taken through 8.0 e.v., since this might have made an important contribution to the determination of the forbidden energy band gap in  $\text{Al}_2\text{O}_3$ . The available data are not conclusive but may be indicative of the true band gap, since the values of  $E_G = 7.5$  e.v. and  $\Delta E_G / \Delta T = -6.3 \times 10^{-4}$  e.v./°K are not unreasonable. It may be that the higher values of activation energy that have been obtained from conductivity experiments correspond to ionic conduction or a polaron mechanism. It is not possible for intrinsic electronic conductivity (band model) to account for the magnitude of conductivity observed in  $\text{Al}_2\text{O}_3$  at high temperatures, since the density of states is not high enough to produce the required number of carriers when the activation energy is about 5 e.v.



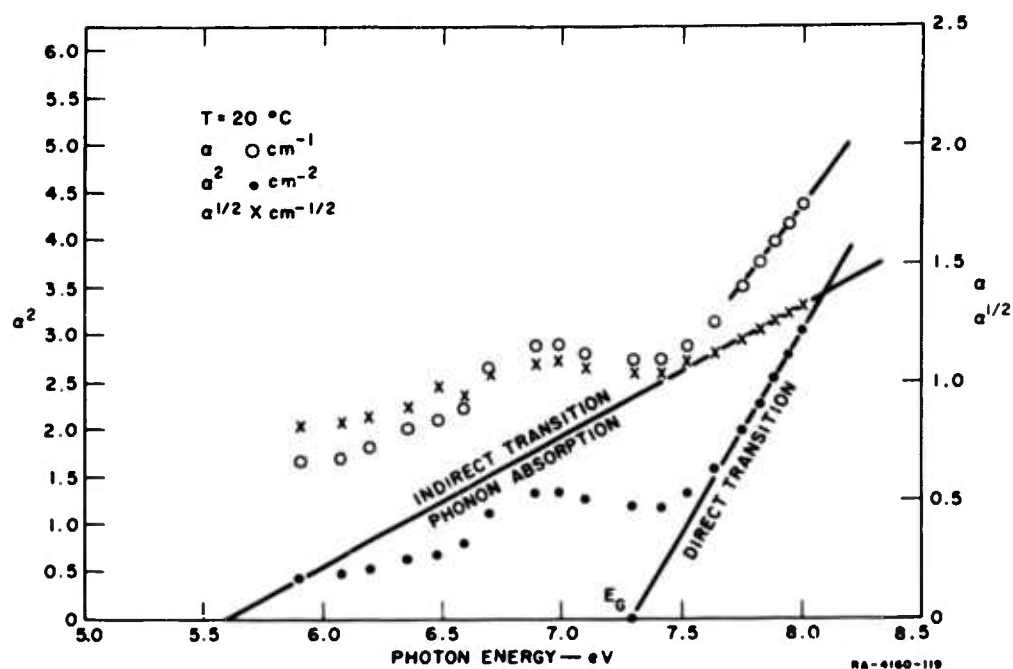


FIG. 26  $\text{Al}_2\text{O}_3$  ABSORPTION  $T = 20^\circ\text{C}$

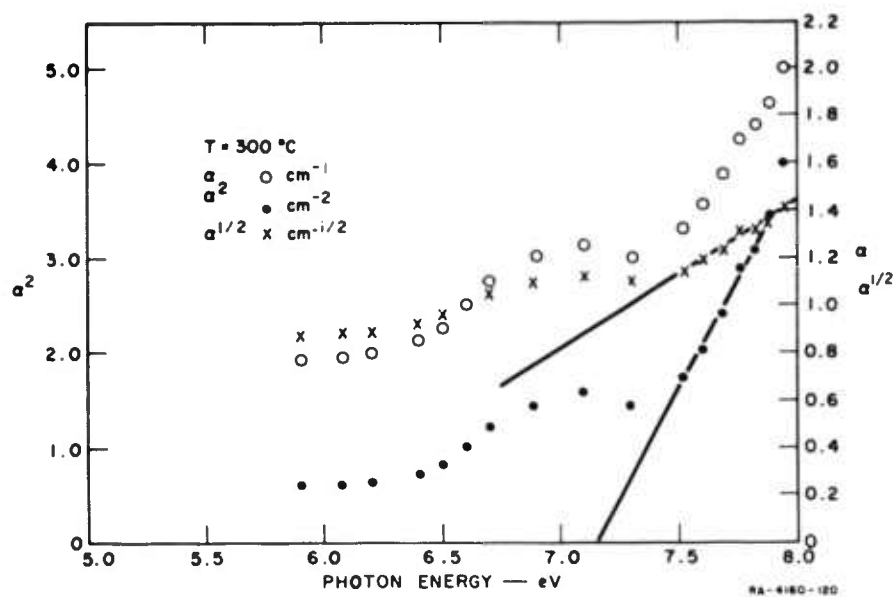


FIG. 27  $\text{Al}_2\text{O}_3$  ABSORPTION  $T = 300^\circ\text{C}$

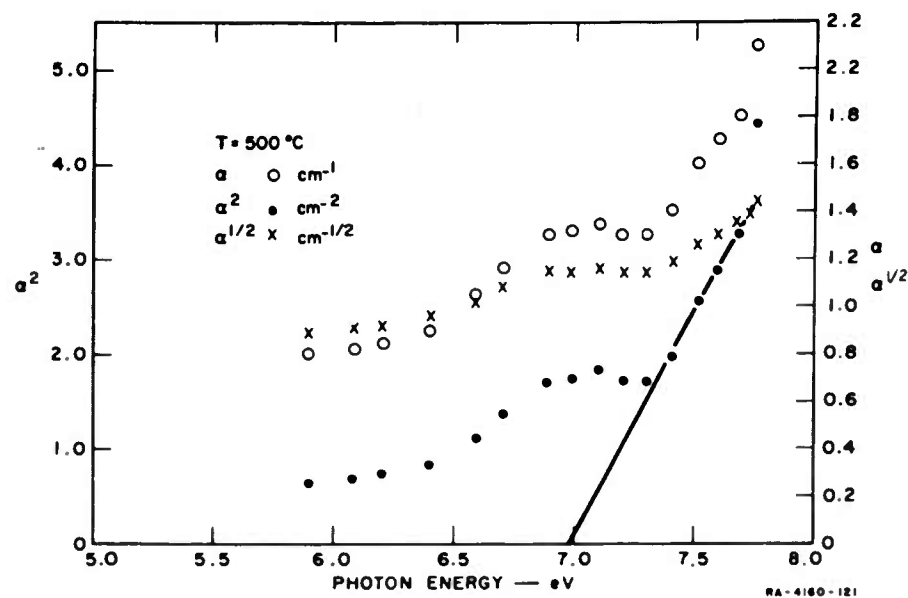


FIG. 28  $\text{Al}_2\text{O}_3$  ABSORPTION  $T = 500^\circ\text{C}$

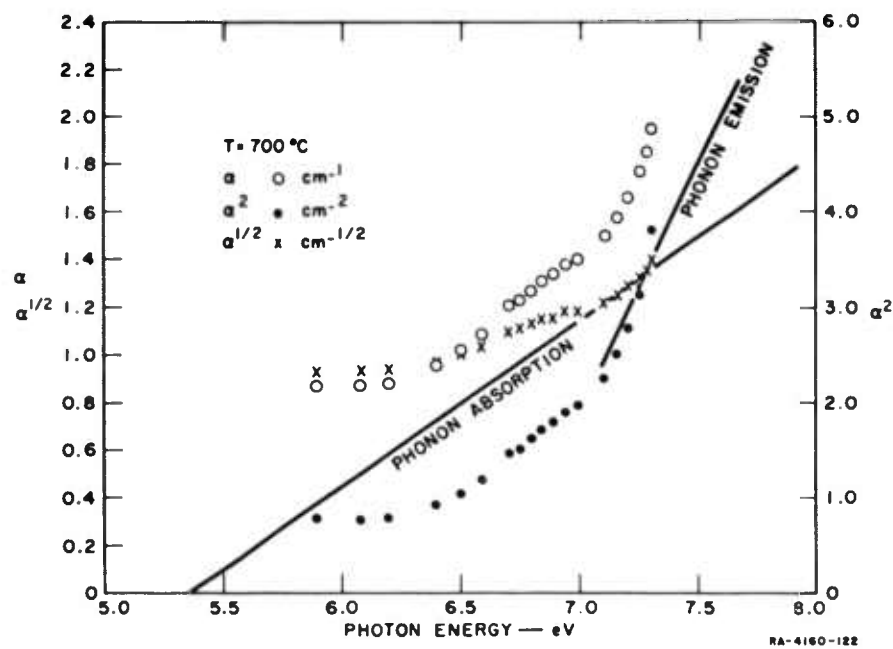


FIG. 29  $\text{Al}_2\text{O}_3$  ABSORPTION  $T = 700^\circ\text{C}$

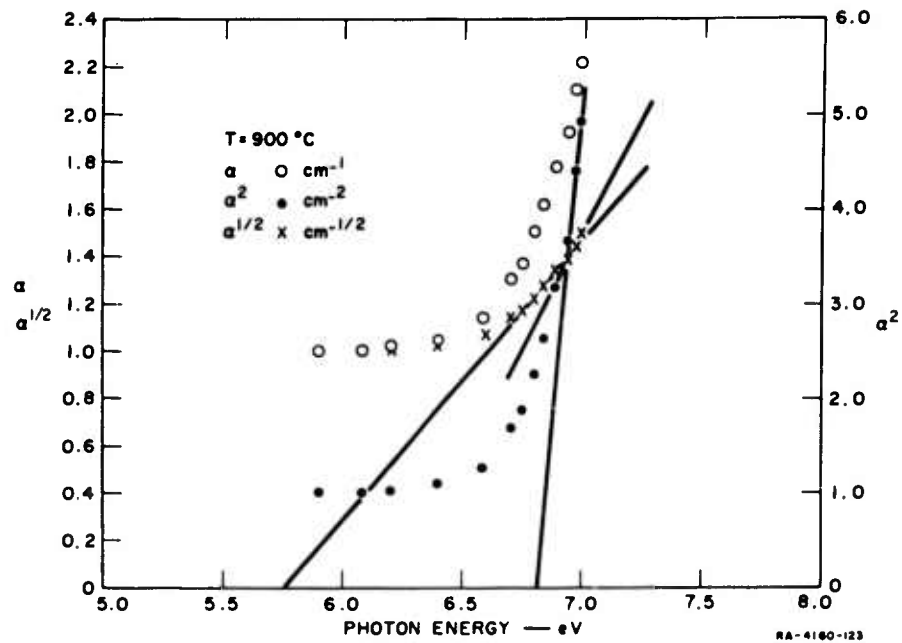


FIG. 30  $\text{Al}_2\text{O}_3$  ABSORPTION  $T = 900^\circ\text{C}$

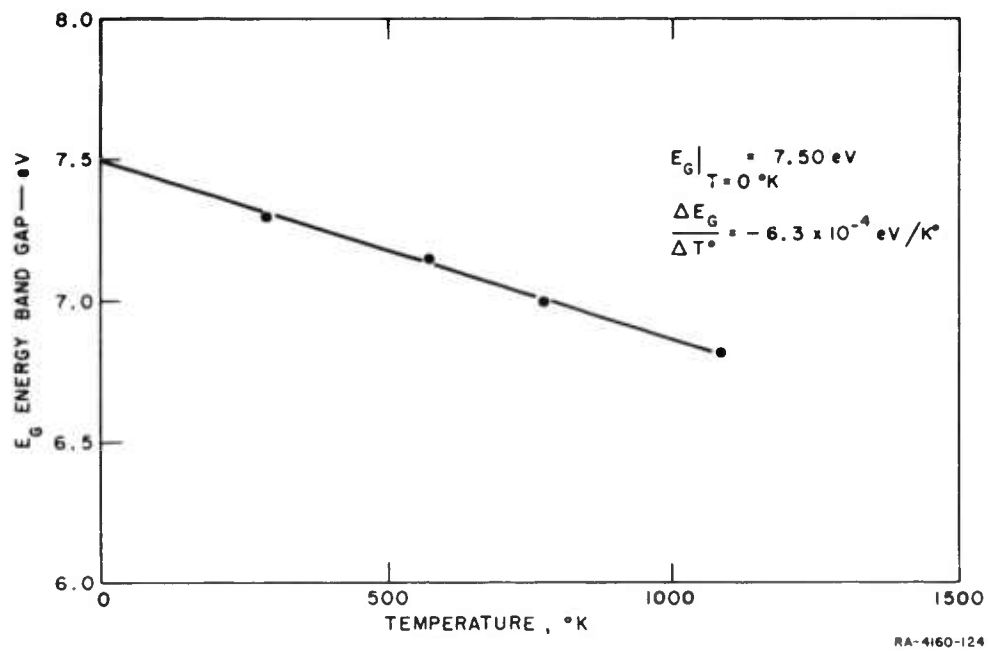


FIG. 31  $\text{Al}_2\text{O}_3$  BAND GAP vs. TEMPERATURE

## I. Electrical Properties of Sapphire

Sufficient data have been accumulated to warrant some preliminary interpretation of the electronic characteristics of sapphire. Accurate conductivity data<sup>26</sup> have been obtained on the extrinsic characteristics of sapphire, along with its thermoelectric power.<sup>27</sup> The purpose of performing conductivity versus temperature measurements and thermoelectric power measurements is to determine the type of carrier, carrier concentration, and carrier mobility. The basic characteristics of the measurements are: (a) an exponential increase in conductivity with increasing temperature; (b) an increasing thermoelectric power with increasing temperature; and (c) p-type conductivity.

Theoretical models must be adopted in order to calculate specific parameters using the experimental data. Three models will be used in this analysis. The three models to be considered are: (a) semiconductor theory; (b) localized level theory; and (c) ionic theory.

### 1. Semiconductor Theory

The classical model for semiconductor theory involves nearly free carriers originating from impurity atoms. The expression for thermoelectric power<sup>28</sup> is:

$$S = \frac{k}{e} \left[ 2 + \ln \left( \frac{N_v}{p} \right) \right] \quad (7)$$

where  $k$  is the Boltzmann constant,  $e$  is the charge of an electron,  $N_v$  is the effective density of states  $2 \left( \frac{2\pi m^x}{h^2} kT \right)^{3/2}$  in the valence band,  $m^x$  is the effective mass of the carrier,  $T$  is the temperature, and  $h$  is Planck's constant. Equation (7) is derived assuming a nondegenerate semiconductor with a mobility which varies as  $1/T^{3/2}$  (lattice scattering only). Knowing  $S$  and  $T$  from an experiment,  $p$ , the concentration of holes, may be calculated. The conductivity  $\sigma$  of a single carrier semiconductor is

$$\sigma = p e \mu \quad (8)$$

where  $\mu$  is the mobility of the holes. Knowing  $p$  from Eq. (7) and  $\sigma$  from experiment,  $\mu$  as a function of temperature may be calculated. The mobility of a semiconductor may be expressed as

$$\mu = \frac{e}{m^*} \frac{\bar{l}}{v} \quad (9)$$

where  $\bar{l}$  is the mean free path of the hole and  $v$  is the thermal velocity of the hole, which is about  $10^7$  cm/sec. If the effective mass  $m^*$  is assumed to be equal to the free electron mass  $m$  then  $\bar{l}$  may be calculated, since  $\mu$  is known. Table I shows the calculated results for several values of temperature.

Table I  
SEMICONDUCTOR THEORY COMPUTATIONS

T (°C)	S $\frac{\text{milli-volts}}{^\circ\text{C}}$	p $\frac{\text{no}}{\text{cm}^3}$	$\mu \frac{\text{cm}^2}{\text{volt-sec}}$	$\bar{l}$ cm
240	1.1	$2.7 \times 10^{15}$	$1.2 \times 10^{-12}$	$7 \times 10^{-21}$
442	2.4	$1.8 \times 10^{10}$	$2.4 \times 10^{-4}$	$2 \times 10^{-12}$
838	3.0	$1.0 \times 10^8$	37.4	$22 \times 10^{-8}$

The computations show the carrier concentration  $p$  to decrease with increasing temperature and the mobility  $\mu$  to increase exponentially with increasing temperature. The decreasing carrier concentration is not expected, since the impurity ionization should increase or remain constant with increasing temperature. The order of magnitude of the carrier concentration is reasonable. At the higher temperatures it is obviously too small. Such small values of  $\mu$  and  $\bar{l}$  violate the uncertainty principle and have little physical meaning. For these reasons the classical semiconductor theory for a nondegenerate material does not seem applicable.

## 2. Localized Levels

The theory of localized levels is related to the more general "Polaron theory." The carriers that contribute to electrical conductivity are assumed to be located at bound energy levels within the material. That is, the wave functions of the adjacent atomic energy levels do not overlap. The carriers may contribute to an electronic current by "hopping" from one site to a neighboring site through thermal activation. Such a model will obviously lead to a low mobility mechanism. Such a theory has been extensively applied to other oxides such as NiO and  $\text{Fe}_2\text{O}_3$ .<sup>23</sup> The aluminum ion in  $\text{Al}_2\text{O}_3$  has emptied its 3s and 3p atomic energy levels of electrons and retains filled 2s and 2p levels. In order to have a hopping process some levels must be empty. The aluminum ion cannot contribute to a hopping process since the 2s and 2p levels are filled. Aluminum oxide does contain Si and Fe impurities at concentrations of about 0.01%, which may introduce partially filled localized levels. Silicon, for instance, could satisfy the valence requirement of 3 and have a partially filled 3s level. Iron could do the same and have a partially filled 3d level. The thermoelectric power expression will not contain a kinetic energy term since the carriers spend most of their time trapped at lattice sites. The thermoelectric power  $S$  may be written as<sup>29</sup>

$$S = \frac{-h}{e} \ln \frac{P}{N_i} \quad (10)$$

Where  $N_i$  is the impurity concentration. Using Eqs. (8) and (10), the same process may be followed as was used in the semiconductor analysis. Table II shows the results. Comparison of Table II with Table I shows close similarity, and therefore, the same invalidating arguments hold for the localized level model.

Table II

## LOCALIZED LEVEL COMPUTATIONS

T (°C)	S $\frac{\text{milli-volts}}{^\circ\text{C}}$	p $\frac{\text{no}}{\text{cm}^3}$	$\mu \frac{\text{cm}^2}{\text{volt-sec}}$	$\bar{l}$ cm
240	1.1	$7.3 \times 10^{13}$	$5.5 \times 10^{-11}$	$3 \times 10^{-19}$
442	2.4	$2.9 \times 10^{11}$	$1.5 \times 10^{-2}$	$9 \times 10^{-11}$
838	3.0	$7.5 \times 10^5$	5000	$3 \times 10^{-5}$

3. Ionic Model

The ionic model assumes that ions move through the crystal lattice via a hopping process. For the extrinsic region of conductivity it is assumed that the concentration of interstitial ions or vacancies remains constant with temperature variations. The conductivity may be written as<sup>30</sup>

$$\sigma = \frac{N^{2/3} (ze)^2 a v}{3 kT} e^{-\epsilon_j / kT} \quad (11)$$

where  $N$  is the number of ion vacancies per unit volume,  $z$  is the ion valence,  $a$  is the jump distance for the ion,  $v$  is the frequency at which an ion vibrates within the lattice, and  $\epsilon_j$  is the activation energy. The required electrical characteristics can be obtained from the ionic model, since the conductivity varies exponentially with temperature and the mobility will be small. From the electrical conductivity data,  $\epsilon_j$  and  $N$  may be calculated, using  $v = 10^{13}/\text{sec}$ ,  $z = 3$ ,  $a = 3 \text{ \AA}$ , which gives  $\epsilon_j = 1.26$  electron-volts and  $N = 7 \times 10^{12} \frac{\text{ions}}{\text{cm}^3}$ . The ion mobility may be calculated from Eq. (8), using  $N$  for  $p$ , which gives  $\mu = 6 \times 10^{-4} \frac{\text{cm}^2}{\text{volt-sec}}$ . The mobility will increase exponentially with temperature. The value of  $\epsilon_j = 1.26$  e.v. is not unreasonable and ion mobilities of  $6 \times 10^{-4} \text{ cm}^2/\text{volt-sec}$  are common.

The preceding discussion was concerned with ionic conductivity in the extrinsic region. An attempt will now be made to estimate the ionic conductivity of  $\text{Al}_2\text{O}_3$  in the intrinsic region. Data for diffusion of aluminum in  $\text{Al}_2\text{O}_3$  are available.<sup>31</sup> These data were obtained by use of the radioactive isotope  $\text{Al}^{26}$  and therefore have no similarity to electrical conductivity measurements. Electrical conductivity measurements in the intrinsic range for  $\text{Al}_2\text{O}_3$  are also available.<sup>14</sup> There are then two different types of experiment that may be compared. The intrinsic ionic conductivity for cation vacancies may be expressed as<sup>30</sup>

$$\sigma = \frac{D N z^2 e^2}{kT} \quad (12)$$

where  $N$  is the number of positive ion sites per unit volume and  $D$  is the diffusion coefficient, which is of the form

$$D = D_0 e^{-\frac{u}{kT}} \quad (13)$$

where  $D_0$  is a constant and  $u$  is an energy term which includes the activation energy of the positive ion and the formation energy of the positive ion vacancy. The electrical data consist of an exponentially rising conductivity with increasing temperature. An activation energy of 5.5 electron-volts is obtained from the electrical conductivity data if electronic conduction is assumed to be dominant. This activation energy corresponds to a band gap energy of 11.0 e.v. The electrical conductivity at  $1687^\circ\text{C}$  is about  $2 \times 10^{-5} \text{ ohm}^{-1} \text{ cm}^{-1}$ . From the diffusion data

$$D = 2.4 \times 10^4 e^{-\frac{5.5}{kT}}.$$

Using Eq. (12) and Eq. (13),  $z = 3$ ,  $N = 4.7 \times 10^{22}/\text{cm}^3$  and  $T = 1687^\circ\text{C}$ , the calculated ionic conductivity is  $\sigma = 1 \times 10^{-5} \text{ ohm}^{-1} \text{ cm}^{-1}$ .

A remarkable agreement exists between the two different experiments; that is, an activation energy of 5.5 e.v. and a conductivity of  $10^{-5} \text{ ohm}^{-1} \text{ cm}^{-1}$  at  $T = 1687^\circ\text{C}$ . The interpretation of the electrical data as being due to electronic conduction may be in error and it is very possible that the conductivity is due partly to ion conduction.



From the previous discussions it can be seen that the experimental data do not agree with semiconductor theory and localized level theory. It has been shown that ionic theory may be applied with reasonable agreement to the electrical data for  $\text{Al}_2\text{O}_3$  in the extrinsic range, and striking agreement in the intrinsic range.

#### 4. Electrical Conductivity

\* High temperature electrical conductivity measurements have been used to investigate the electrical transport properties of  $\text{Al}_2\text{O}_3$ . An important objective of such experiments is to determine the intrinsic activation energy associated with the conduction process. Activation energies of 4.26 e.v.,<sup>23</sup> 2.97 e.v.,<sup>14</sup> and 3.65 e.v.<sup>15</sup> have been reported for single crystal  $\text{Al}_2\text{O}_3$ , in the temperature range of 1000-1600°C. The large variation of activation energies, within the same temperature range, and the magnitude of conductivity associated with the various activation energies present an inconsistent picture of the electrical characteristics of  $\text{Al}_2\text{O}_3$ . The experimental conductivity values, if representative of  $\text{Al}_2\text{O}_3$ , imply realizable densities of electronic states and concentrations of donors or acceptors in order to account for the conductivity in terms of nondegenerate band theory. It would appear that the conductivity, intrinsic or extrinsic, is due to mobile ions or small polarons. The present experiment was undertaken in order to obtain comparative conductivity data on single crystal  $\text{Al}_2\text{O}_3$  in the temperature range of 1000-1600°C.

The experiment was performed in a tubular, platinum-rhodium, air furnace. A two-terminal d.c. method was employed, using a guard ring. The maximum electric field used was  $10^2$  v/cm. All measurements were made on single crystals using platinum foil electrodes. The crystals had flat, polished surfaces. The platinum foil electrodes were pressed against the crystal faces by flat polycrystalline  $\text{Al}_2\text{O}_3$  discs. The force was transmitted to the discs by alumina tubes, which were spring-loaded outside the furnace. External leakage paths apart

---

\* Paper entitled "On the High-Temperature Electrical Conductivity of Alumina." D. Peters, L. Feinstein, C. Peltzer, pages 62-67.

from air conductivity were eliminated, in that the sample electrodes and wires did not make contact with any shunting material. The measured currents could result only from the bulk conductivity of the crystal or from conduction through the air, since the guard ring prevents surface currents from being measured. Figure 32 shows a schematic representation of the experimental apparatus.

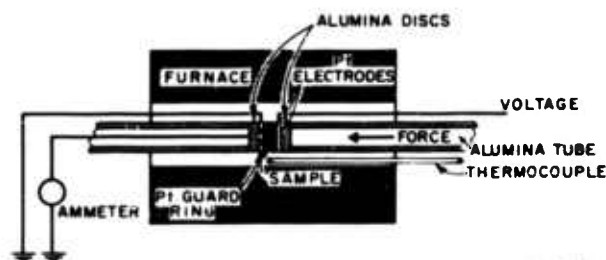


FIG. 32 SCHEMATIC DIAGRAM OF EXPERIMENTAL APPARATUS

A constant voltage was applied to the sample and the current was measured with a microvolt ammeter. The temperature of the sample was measured with a calibrated platinum-rhodium thermocouple. Current readings were made with the oven turned off and the temperature slowly decreasing with time. The samples were obtained from Linde Co., whose spectrographic analysis is given below.

	<u>Sapphire</u>	<u>Ruby</u>
% Cr	0.0001	0.25
Fe	0.01	0.005
Si	0.001	0.006
Ca	0.0001	0.002

Measurements of conductivity versus temperature were made on samples of ruby, sapphire, and rutile in air and in a helium atmosphere. The rutile was used as a check on the measuring system because rutile has a large conductivity<sup>32</sup> relative to  $\text{Al}_2\text{O}_3$ . Figure 33 shows the results of the measurements along with pertinent published data. The actual measured points are shown for sapphire, ruby, and no sample in air and in helium. The solid curves are for the published data.

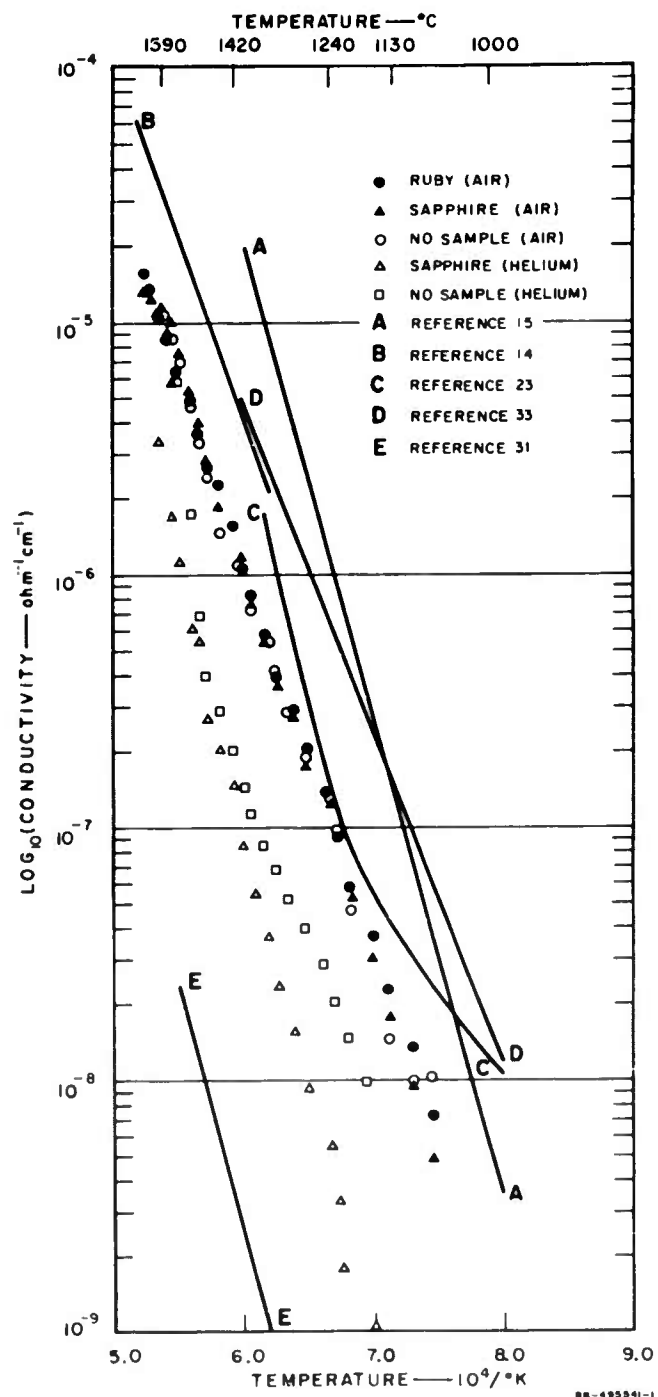


FIG. 33 CONDUCTIVITY vs. TEMPERATURE

It can be seen from Fig. 33 that the three curves for ruby, sapphire, and no sample, in air, are coincident. The conductivity of air then appears to be equal to or greater than the conductivity of sapphire or highly doped ruby. The measurement without a sample was made with an  $\text{Al}_2\text{O}_3$  ring, positioned on the guard ring, between the two electrodes. This arrangement provided a definite spacing for the experiment without a sample. Measurements were made with and without the guard ring, with negligible difference in results. The oven chamber was flushed with helium in an attempt to lower the gas conductivity, since helium has a higher ionization potential than nitrogen or oxygen. Again measurements were made with and without a sample. Coincidence occurred again, approximately as shown in Fig. 33. The helium pressure could not be adequately regulated, so the results are somewhat qualitative. Three curves, A, B, and C, are shown for comparison. All represent measurements made, in air, on single crystal  $\text{Al}_2\text{O}_3$ . The three curves, A, B, and C, are at higher conductivities than the data obtained in this experiment but have similar slopes (activation energies). Evidently the intrinsic conductivity of  $\text{Al}_2\text{O}_3$  lies below the data given for helium. Curve E represents the theoretical conductivity due to cation mobility as determined from diffusion experiments. It may be that  $\text{Al}_2\text{O}_3$  is, intrinsically, an ionic conductor with a conductivity in the range of curve E. It is also possible that  $\text{Al}_2\text{O}_3$  is, intrinsically, an electronic conductor with a conductivity near curve E. The corresponding activation energy could be much smaller than presently expected, which would satisfy the conditions imposed by band theory.

Curve D is the measured conductivity of MgO and suggests that the problem of air conductivity may be significant in all high temperature, high resistivity measurements. It may be possible to measure the intrinsic conductivity of  $\text{Al}_2\text{O}_3$  in vacuum since the air conduction is greatly reduced. Such an experiment is presently being undertaken at this laboratory.

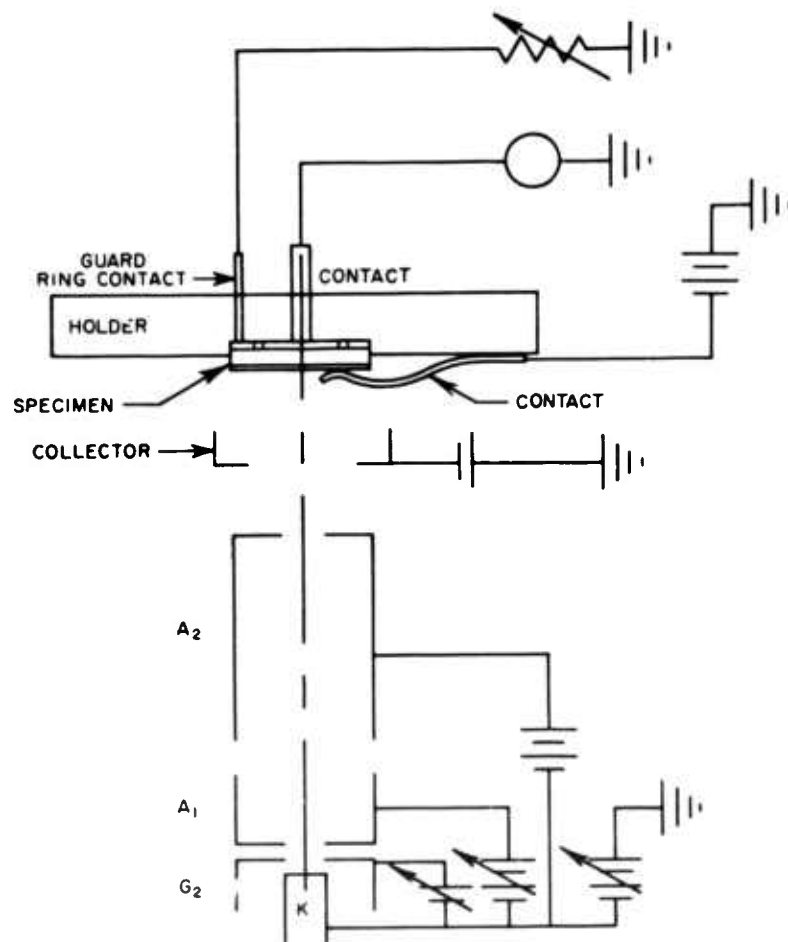
## V Electron Bombardment Studies of Sapphire

The dielectrics that are incorporated as part of the structure of electron beam microwave devices are subject to some degree of particle bombardment regardless of the amount of shielding used to prevent it. These dielectrics may be acting as windows on insulators. Therefore, in the study of dielectrics for microwave devices, it was desirable to investigate the effect of bombardment by electrons or X-rays on the behavior of dielectrics.

This study was initiated and described in Quarterly Reports 3 to 8, inclusive, wherein the electron bombardment of single crystal sapphire was discussed. Figure 34 is a schematic diagram of the test setup, showing the electron gun and specimen to be tested, and Fig. 35 is a photograph of the experimental arrangement, which fits into a vacuum bell jar.

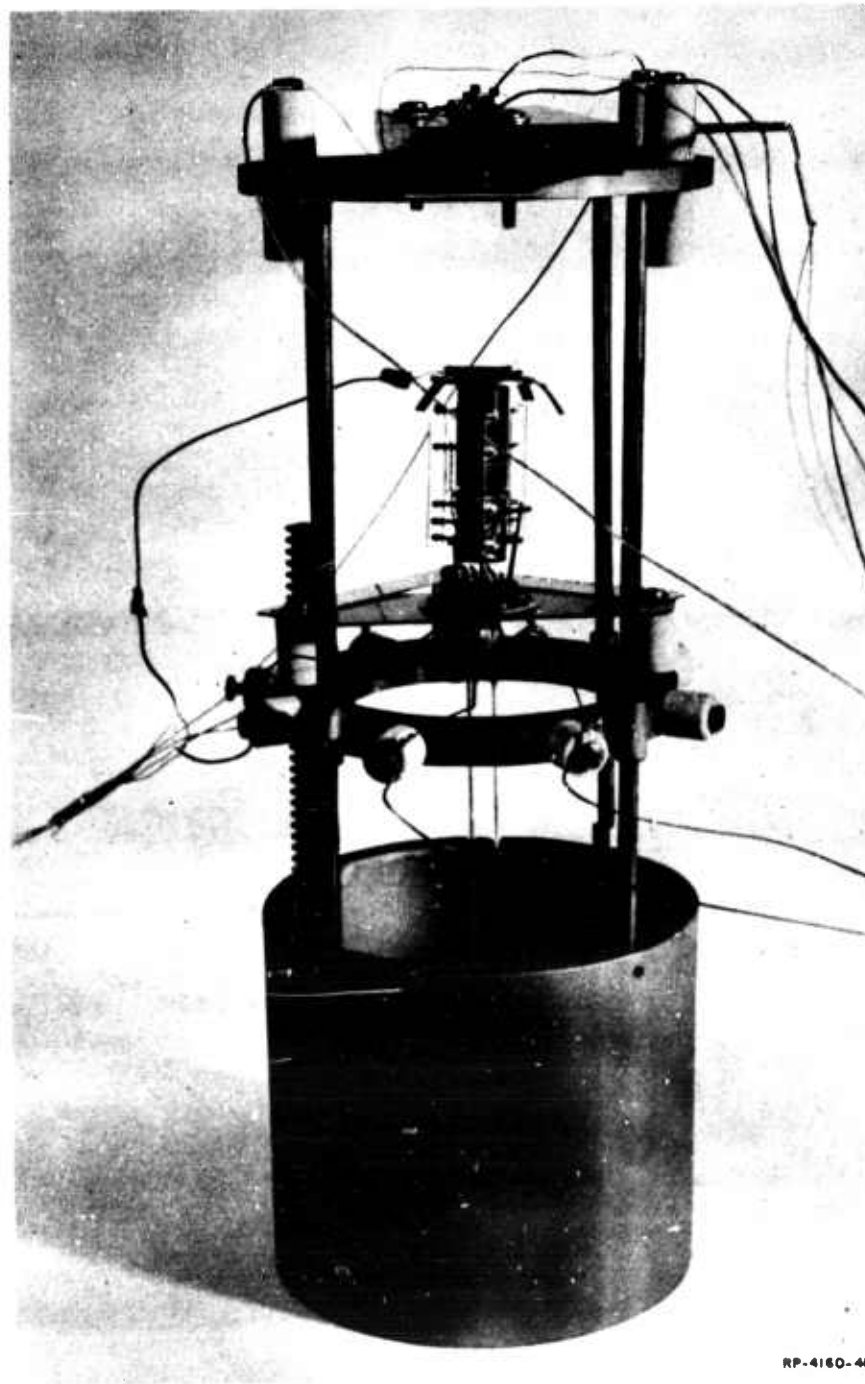
The effect of particle bombardment on the dielectric is to cause the liberation of free carriers, as well as generation of defects, within the bulk of the material. In addition, if the bombarding particles are electrons, there will, in general, be secondary electron emission from the bombarded region, and the bombarding or penetrating electrons can form a layer of negative charge within the specimen. With a field applied across the bombarded specimen, the free carriers will tend to migrate to the surfaces of opposite polarity; however, because of trapping, a number of the carriers will probably form charged regions within the material. The combination of these effects can and often do lead to a material that has an inhomogeneous charge distribution within it. This has been discussed by Kalmann<sup>34</sup> and his coworkers, and Gross,<sup>35</sup> and others.<sup>36-38</sup>

Test specimens were disks of single crystal sapphire with evaporated platinum electrodes on both faces. In the center of the bombarded face a circular section of the platinum approximately 0.100-in. in diameter was stripped off to allow electrons to impinge directly on the sapphire. A negative potential secondary emission suppressor electrode with an aperture approximately 0.060-in. in diameter was placed approx-



A-4160-27

FIG. 34 SCHEMATIC OF INDUCED CONDUCTIVITY TEST



RP-4160-48

FIG. 35 ELECTRON BOMBARDMENT INDUCED CONDUCTIVITY  
TEST SETUP

imately 0.125-in. from the specimen. Specimen thickness was in the order of 0.025-in.

Tests were conducted with electron accelerating voltages ranging up to 10 kV and with bombarding currents ranging from  $10^{-8}$  to  $10^{-5}$  amperes. Voltage across the specimens were varied from 0 to 1000 v and current through the specimens was measured with the electron beam in both steady state and pulsed condition. Figures 36 and 37 represent some of the data for the steady state bombardment.

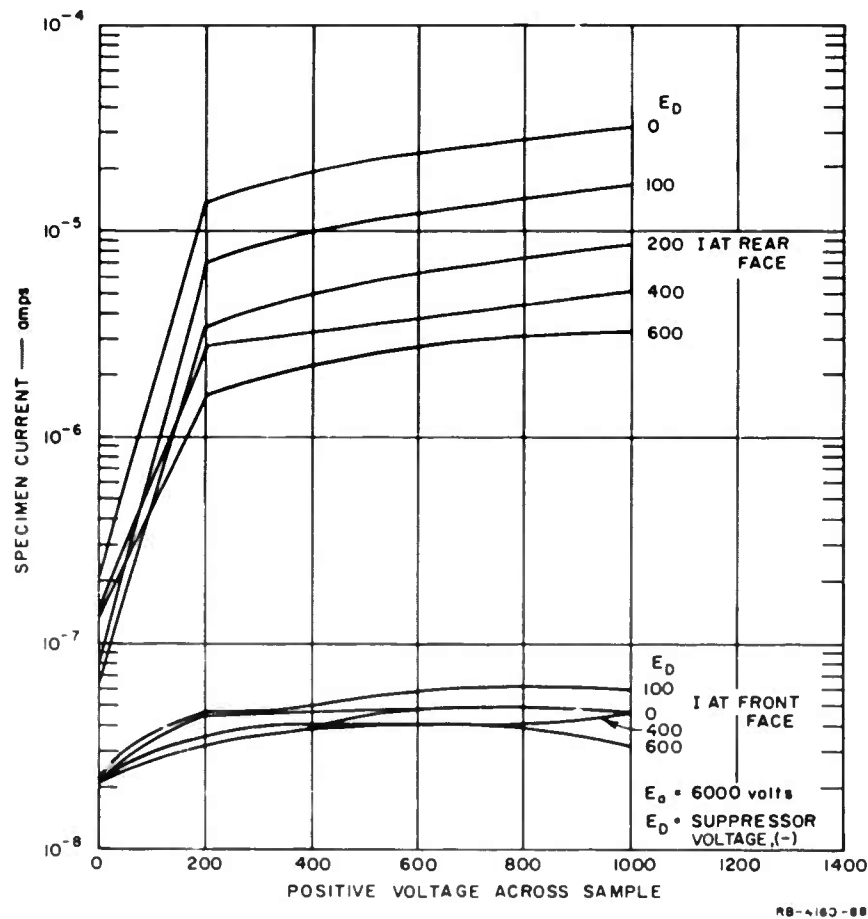
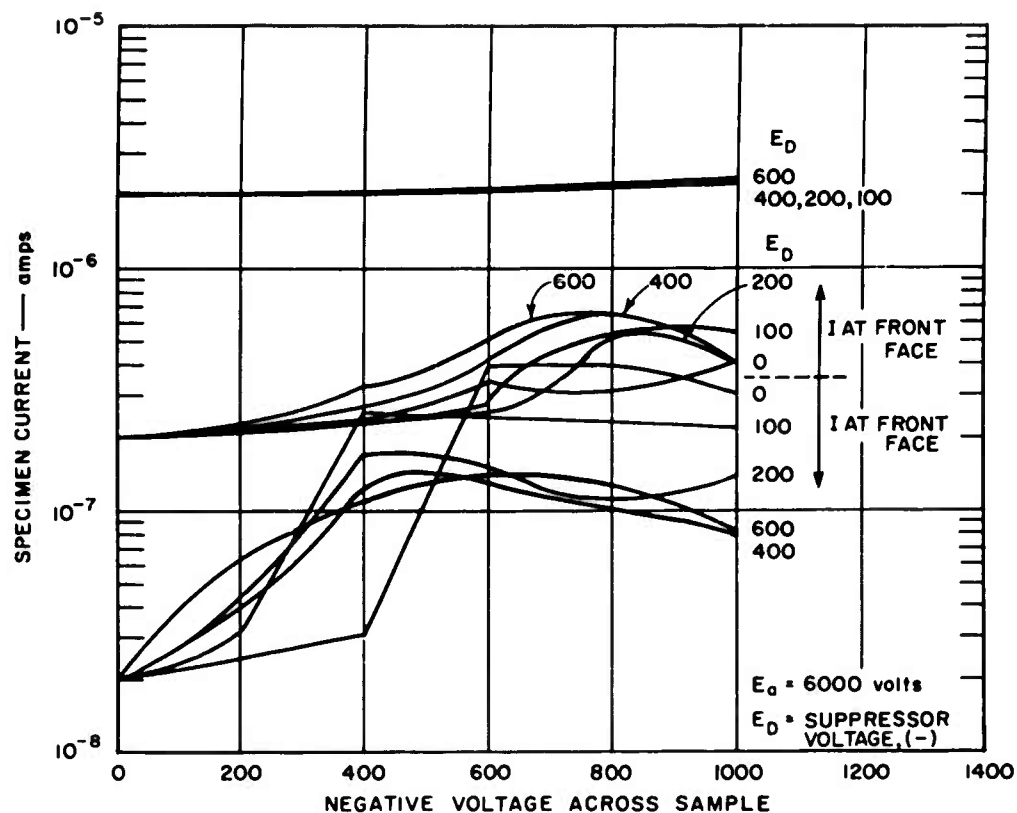


FIG. 36 CURRENT AT FRONT AND REAR FACES OF SAPPHIRE SPECIMEN vs. APPLIED POSITIVE VOLTAGE FOR BOMBARDING CURRENT OF APP.  $10^{-8}$  amp





RB-4180-91

FIG. 37 CURRENT AT FRONT FACE OF SAPPHIRE SPECIMEN vs. APPLIED NEGATIVE VOLTAGE FOR BOMBARDING CURRENTS OF APP.  $10^{-8}$ ,  $10^{-7}$ ,  $10^{-6}$  amp

Figs. 38 and 39 represent data for pulsed bombardment. These data indicate some important points which are important to concepts of dielectrics. It should be noted first that current at front (bombarded) and rear faces are not the same and, second, that as field across the specimen is increased, specimen current does not follow linearly or in accordance with the accepted experimental relations associated with trapped states. In fact the current at some levels of field decreases. For the pulsed case, front and rear currents are the same for low electron beam accelerating voltage, but differ considerably for the high accelerating voltage.

An explanation for this behavior has been described in Report No. 5, and Fig. 40 is a diagram of the proposed charge distribution in the specimen.

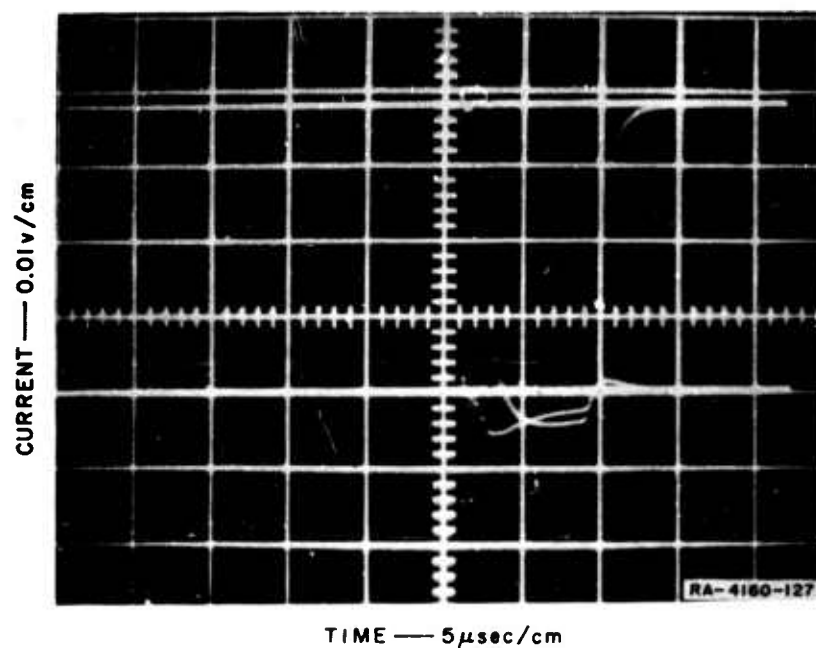


FIG. 38 CURRENT ON FRONT AND REAR FACES UNDER PULSED BOMBARDMENT (Low Bombarding Current), ACCELERATING VOLTAGE 6000 V

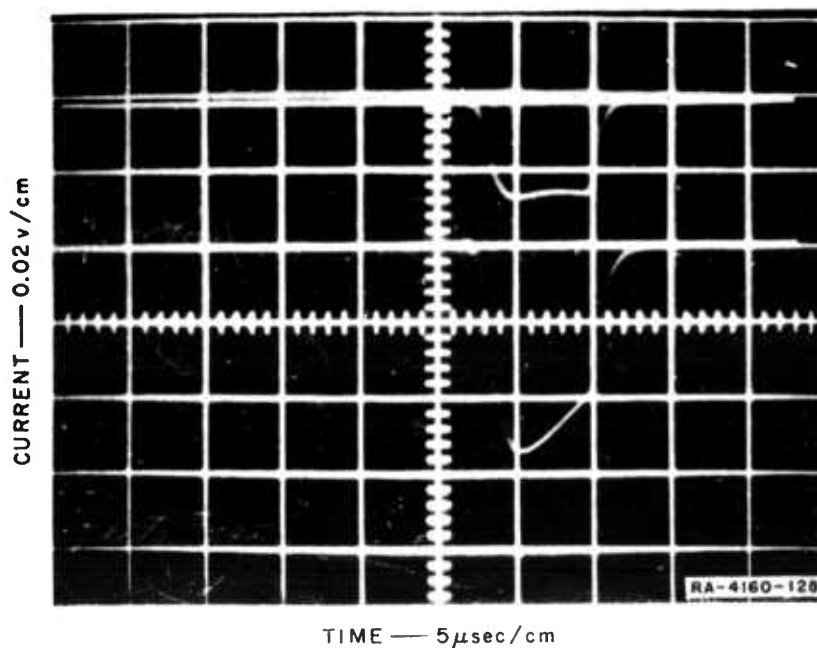


FIG. 39 CURRENT ON FRONT AND REAR FACES UNDER PULSED BOMBARDMENT (High Bombarding Current), ACCELERATING VOLTAGE 6000 V

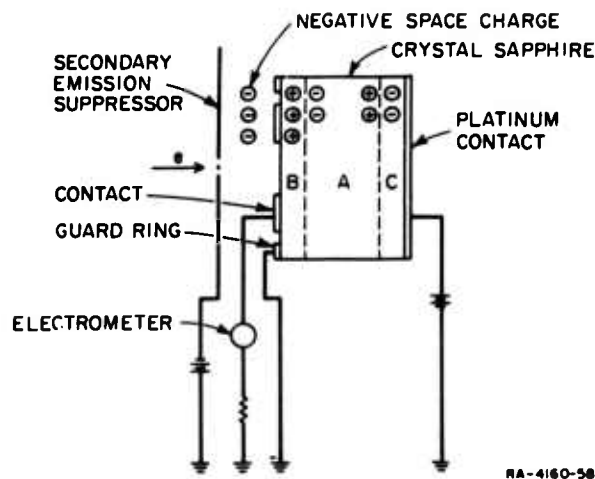


FIG. 40 PROPOSED CHARGE DISTRIBUTION IN SPECIMEN

For positive voltage across the specimen, the bombarding electron current hits the uncoated face of the crystal and causes the following effects: (1) hole-electron pairs are generated, (2) there is secondary emission of electrons, and (3) there is an electron flow to ground through the electrometer, which, following McKay's<sup>36</sup> measurement technique is the bombarding current. As demonstrated by Upatov,<sup>37</sup> a negatively charged electrode in front of a bombarded secondary emitting surface results in that surface's assuming a negative potential and, therefore, to maintain charge neutrality in the crystal, there will be a migration of positive carriers (holes) toward the negatively charged crystal surface. These carriers are provided by the electron-hole pairs formed by the penetrating electrons bombarding the crystal and the pre-existing carriers within it, and the negative (electrons) that make up the secondary emission and the electron currents in the crystal. Then, with no potential applied across the specimen, the region B of positive charge is formed near the bombarded surface and consequently form a polarizing force within the crystal, thereby tending to create a negatively charged region near the back face of the crystal, region C.

With small bombarding currents (secondary emission is small), the polarizing field within the crystal is small, and the retarding effect on current flow due to an applied field is negligible. Therefore, the

electron current increases as field across the specimen increases. With medium bombarding currents the polarizing field due to secondary emission and the external space charge is greater. Consequently there will be a level of internal field which is effectively acting in opposition to the applied field, and this is evidenced by the decrease in electron current with low values of applied field. As this applied field is increased and overcomes the opposing internal field, the electron current follows a response curve similar to that for low values of bombarding current.

This model of the behavior of the insulating crystal under electron bombardment and an applied field is somewhat analogous to the model proposed by Kalmann and Rosenberg<sup>34</sup> in that it suggests polarization due to charge separation under an applied field. However, Kalmann and Rosenberg also postulate localization of the charge carriers in traps which may certainly contribute to the polarization field. For the case where high levels of current are bombarding the specimens, the number of hole-electron pairs is increased, thereby leading to the possibility of an equilibrium condition or saturation of the traps so that there is neither a marked decrease in current with low applied field nor a marked increase in current with the increasing values of applied field.

For negative voltage across the specimen, again there is an induced polarization within the crystal specimen, and this polarization is dependent on the external space charge, the number of free carriers generated, and the traps within the specimen. However, there is in addition the effect of the external negative charge which may not be completely compensated at all times.

For the case of low bombarding currents, the bombarded surface of the specimen is at a negative potential, as for all cases of bombardment with a negative electrode in front of the specimen. However, the number of free pairs generated is small, the external negative charge is small, and the induced field within the crystal is now such that holes are easily transferred through the specimen at the low fields. Following the postulate of Kalmann and Rosenberg, polarization fields within the crystal

are dependent on the external field and, in addition, as the externally applied field becomes more positive the negative space charge tends to be displaced nearer to the crystal surface. Both of these effects tend to limit the hole current within the crystal, as is evidenced by the current maxima observed for relatively low values of applied field. As applied field increases, the retarding effects on current reach a saturation value which may be attributed to maximum displacement of the negative space charge and to saturation of traps. This corresponds to the current minimum followed by an increased current as the applied field increases.

With high bombarding currents, the negative space charge external to the crystal surface is increased considerably. Therefore, as the field is applied, the space charge which is shifted more towards the crystal causes a greater attraction for the free holes made available by electron bombardment. This appears to increase the field polarizing effect and results in decreased specimen current until a minimum, as discussed before, is reached. For the intermediate-bombarding-current case, it is difficult to describe precisely the mechanisms that operate. However, the current vs. voltage curves are probably due to combinations of the above mechanisms.

To confirm that internal polarizing fields do exist in the material, steady state electron bombardment was performed with no voltage applied across the specimen, and current meters to ground were placed in contact with both the electron bombarded and nonbombarded surfaces. Electrons having energies of 2000, 4000, 6000, and 8000 electron volts were used to bombard the specimen. The secondary emission suppressor electrode was biased negatively. The following represents a condensation of the data showing current at both faces of the specimen for a range of electron accelerating voltages.

Eacc	$I_b$	$I_f$	$I_b$	$I_f$	$I_b$	$I_f$	$I_b$	$I_f$
2 KV	$4 \times 10^{-9}$	$7 \times 10^{-7}$	$4 \times 10^{-8}$	$5 \times 10^{-6}$	$4 \times 10^{-7}$	$5 \times 10^{-5}$	$4 \times 10^{-6}$	$6 \times 10^{-4}$
4 KV	$4 \times 10^{-9}$	$3 \times 10^{-7}$	$4 \times 10^{-8}$	$3 \times 10^{-6}$	$4 \times 10^{-7}$	$6 \times 10^{-5}$	$4 \times 10^{-6}$	$7 \times 10^{-4}$
6 KV	$4 \times 10^{-9}$	$4 \times 10^{-7}$	$4 \times 10^{-8}$	$4 \times 10^{-6}$	$4 \times 10^{-7}$	$6 \times 10^{-5}$	$4 \times 10^{-6}$	$7 \times 10^{-4}$
8 KV	$4 \times 10^{-9}$	$3 \times 10^{-7}$	$4 \times 10^{-8}$	$2 \times 10^{-6}$	$4 \times 10^{-7}$	$6 \times 10^{-5}$	$4 \times 10^{-6}$	$7 \times 10^{-4}$

Where Eacc is the bombarding electron beam accelerating voltage,  $I_b$  is the current measured at the bombarded face of the specimen and  $I_f$  is the current measured at the nonbombarded face of the specimen. The currents were from specimen to ground. These data represent averages of currents measured with secondary emission suppressor electrode voltage at 0, -200, -400, -600, -800, and -1000 v with respect to the specimen. For each of the measured bombarding currents, the current at the rear face was approximately a factor of 100 greater, regardless of the accelerating voltage.

Both of these observations reinforce our assumption that the effect of the external space charge is to set up polarizing fields within the specimen. In addition, it may be stated that the measurement of rear face currents with no applied fields is due to the polarization resulting from the external space charge, and as the intensity of the initial current increases, this effect also increases.

Figures 38 and 39 are photographs of the currents at the front and rear faces of an 0.005-in.-thick sapphire crystal that was bombarded by a pulsed electron beam. For Fig. 38, the beam voltage was 1000 v, and for Fig. 39 the accelerating voltage was 6000 v.

The range of electrons in aluminum oxide according to Young<sup>39</sup> varies as  $V^{1.35}$ , which for this case gives a ratio of 8.8 to one for the range of bombarding electrons in the crystal, approximately 300 Å and 2700 Å. These data were taken with no voltage applied across the specimen and it is significant that for the lower accelerating voltage the current at the front face is greater than that at the unbombarded surface. For the higher accelerating voltage the reverse is true. The current at the rear face is greater than that at the bombarded surface.

It should be noted that the deflection of the oscilloscope pattern is the same for both faces, indicating that the same type of carrier is emerging from each face (in this case, electrons). There is no ready or obvious explanation for this behavior. However, it again points up the need for a more detailed study of the field and charge distribution on a localized level. A possible explanation lies in inhomogeneous charge distribution caused by long relaxation time within the material. This will be checked by further experiment.

## VI Studies of Defects in Alumina

The influence of defects such as dislocations on the behavior of semiconductors has been discussed and demonstrated amply in the literature. It was therefore decided that it would be appropriate to investigate whether induced high concentrations of defects, such as dislocations, would have a similar effect on a dielectric. There was some evidence in the literature, e.g., Van Buren<sup>40</sup> and Redfield,<sup>41</sup> that defects will have high fields associated with them, and it was postulated that these fields could be a factor in reducing the breakdown strength of the dielectric.

Single crystals of sapphire were selected as the test specimens because they would not have the complicating factor of defects associated with grain boundaries and multiple phases that are found in sintered ceramics. The crystals were bent at 1600°C and then sectioned and etched with phosphoric acid to bring out the etch pits. The effect of bending the crystals was to introduce slip bands that are accompanied by high densities of dislocations.

Figure 41 is a photograph of a bent crystal and Figures 42a and 42b are etched sections of a bent specimen. Figure 43 is a photograph of the breakdown test fixture with a specimen between the electrodes. Tests were conducted at d.c. in a high dielectric oil to prevent surface flashover. It should be noted that the oil had to be changed frequently because of irreversible changes in its characteristics when a breakdown occurred.



FIG. 41 SAPPHIRE CRYSTAL BENT TO  
INTRODUCE SLIP BANDS



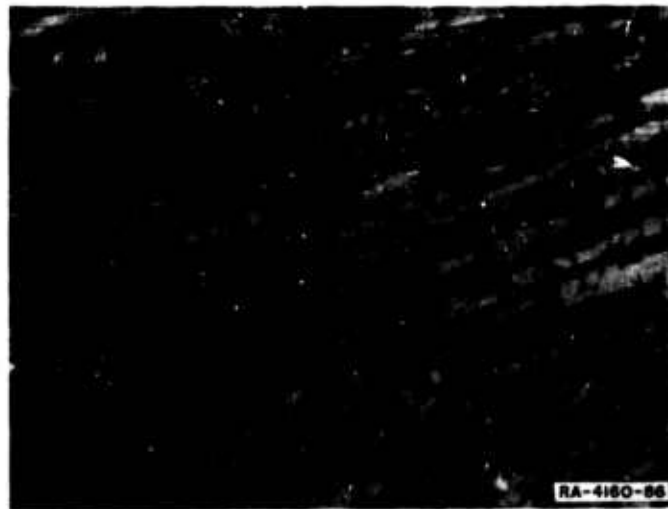


FIG. 42(a) ETCHED SECTION OF BENT SPECIMEN

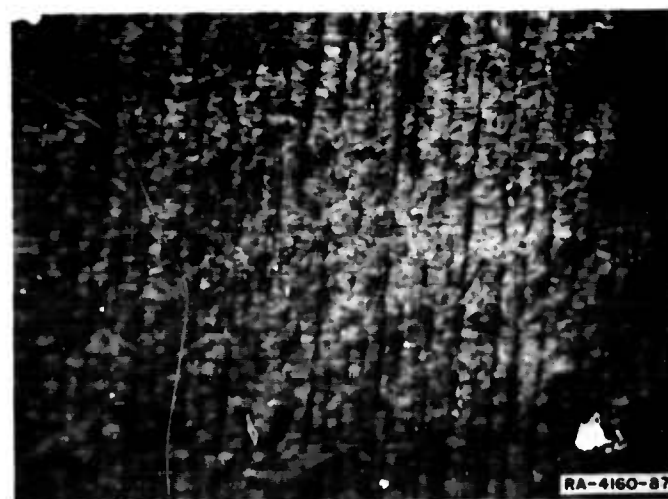
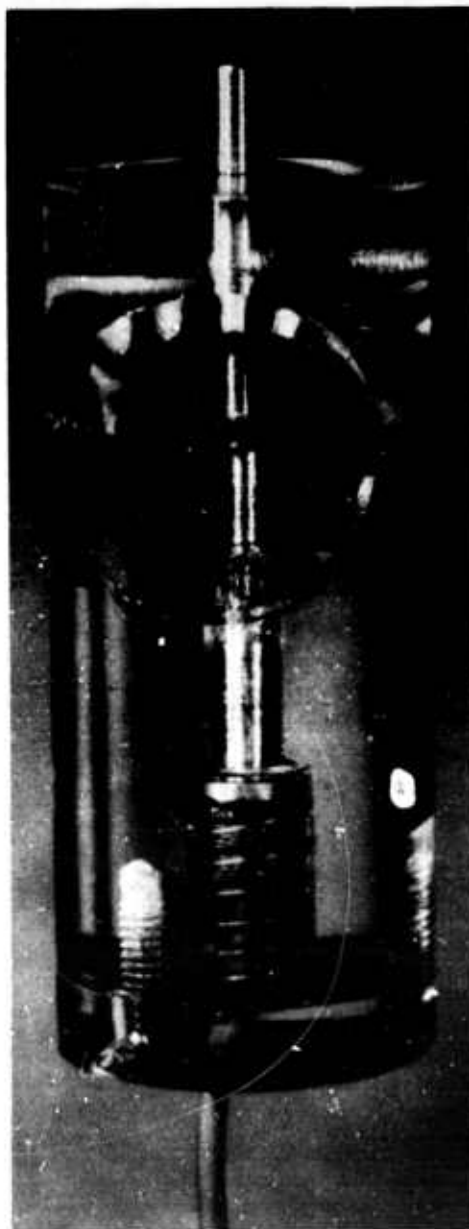


FIG. 42(b) ETCHED SECTION OF BENT SPECIMEN

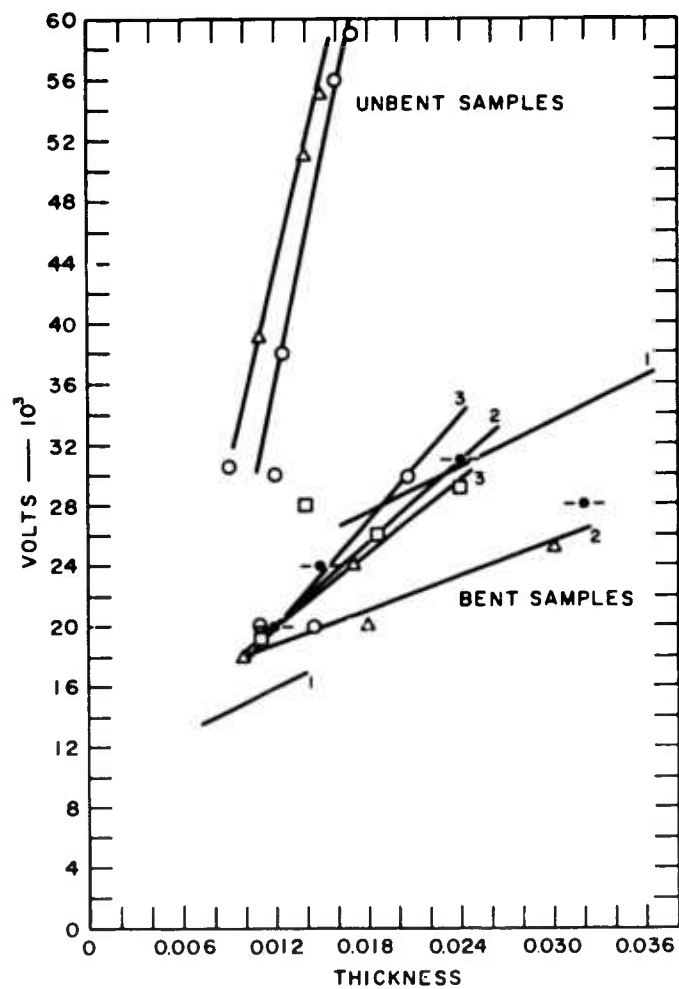


RA-4160-102

FIG. 43 NEW BREAKDOWN TEST FIXTURE

Figures 44 and 45 are plots of the data, which are not yet complete, for the effect of introduction of defects on the breakdown strength. It can be seen that the introduction of the slip bands, and consequently increasing the concentration of dislocations, decreases the breakdown strength appreciably. The second set of data indicate that the heat treatment of specimens can also reduce breakdown strength significantly. At first thought, this latter result appears contradictory; however, if the effect of the heat treatment, which consisted of heating to 1600°C and cooling, was the reduction of dislocation, there is still the possibility of creating a larger number of point defects such as vacancies or interstitials which would have a charge associated with them. This would then lead to localized fields that can reduce breakdown strength.

These data confirm the concept of fields associated with imperfection states and indicate how they may seriously affect breakdown characteristics of the dielectric.



RA-4160-125

FIG. 44 BREAKDOWN DATA FOR BENT AND UNBENT SAPPHIRE SPECIMENS

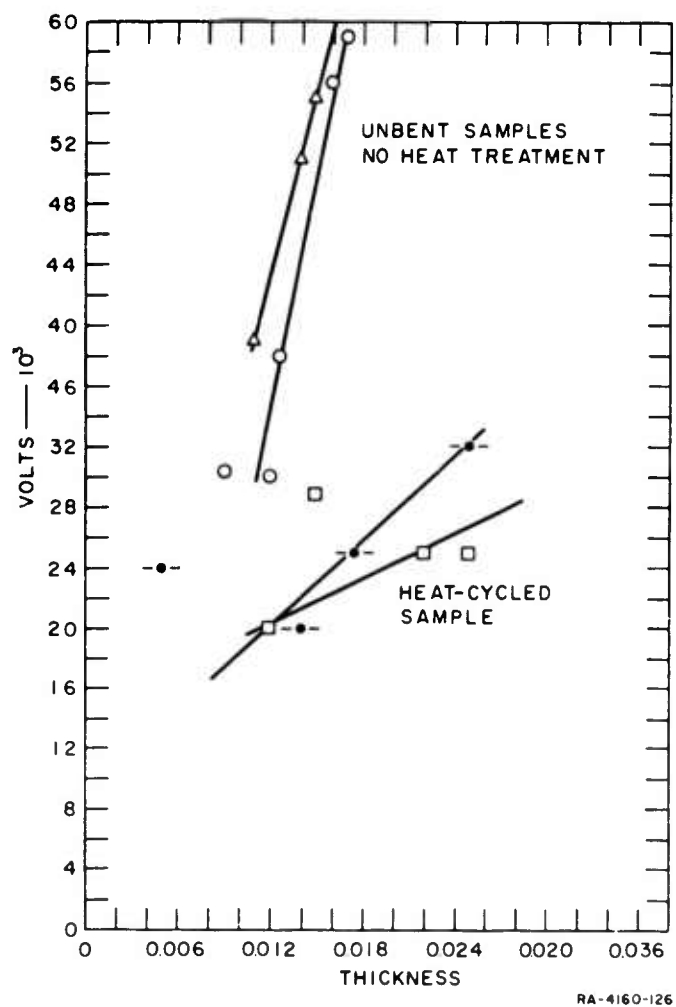


FIG. 45 BREAKDOWN DATA FOR HEAT-CYCLED AND UNCYCLED SAPPHIRE SPECIMENS

## VII Theoretical Treatment

From an analysis of the experimental data on the electrical conductivity and thermoelectric power of  $\text{Al}_2\text{O}_3$  in the medium temperature range (R.T. to  $\sim 800^\circ\text{C}$ ), one can conclude that electrical conduction is here almost exclusively a defect conduction mechanism controlled by the degree of chemical purity and stoichiometry of the sample. Supplementary data on the types and mobilities of the carriers are still necessary and will be obtained in the coming year, but, even with this additional information, in view of the present stage of development of the theories of narrow impurity bands and small polaron transport mechanisms, it is doubtful whether a completely satisfactory description of electrical transport in  $\text{Al}_2\text{O}_3$  can now be achieved. In any event, the detailed structure of the valence and conduction bands of  $\text{Al}_2\text{O}_3$  can be considered as irrelevant to a large extent as far as conduction in actual, even "high purity," crystals are concerned, and attempts at precise calculations of this structure are not urgently needed now. At high temperatures, the experimental evidence gained in this laboratory indicate that most published data are not representative of the conductivity of  $\text{Al}_2\text{O}_3$ , which is probably smaller by several orders of magnitude than the usually quoted values. Such smaller values would be compatible with ionic and electronic impurity conduction mechanisms. Further experimental work is planned to clarify this question.

It is obvious that any realistic theory of breakdown of  $\text{Al}_2\text{O}_3$  cannot be based mainly on consideration of the perfect crystal, but, rather, must take into account first the defect structure of the samples, which is already the dominant factor in normal electrical transport in this material. This point of view is also confirmed by the data obtained on the large reduction of the breakdown strength of alumina samples when high concentrations of line and point defects were introduced by bending and heat treatments.

A third group of experiments on electron bombardment induced conductivity in sapphire have clearly demonstrated the existence of high local internal fields in the presence of external space charges. Several

authors working with different dielectrics (mainly medium gap materials) have reported similar "persistent internal polarization" effects and given evidence of strongly inhomogeneous charge distribution and large internal field gradients. Theoretical considerations also indicate that one can expect fields of the order of  $10^4$ - $10^6$  v/cm as a result of particularly inhomogeneous point and line defect distributions. Several factors can contribute to establishment of such distributions: besides high energy electron bombardment, and resulting external space charges, one can cite temperature and oxygen partial pressure gradients, glassy phase boundaries, etc.

It is obvious that before considering in detail which particular mechanism could lead to breakdown (Zener effect, avalanche---) it is necessary to obtain a description of the internal fields in the material, taking properly into account the defect structure and the external environment. For such purposes it is necessary to know both the types, concentrations, and transport properties of the possible point defects and the dielectric properties of the perfect material over a range of fields up to  $10^6$ - $10^7$  v/cm. At present it appears that sufficiently reliable information on the properties of the point defects will mainly have to be obtained experimentally; on the other hand, it seems worthwhile, possible, and important to calculate directly in various approximations the dielectric tensor of different perfect insulators, but it is essential in such calculations to avoid introducing ad hoc constant ionic polarizabilities, as the aim of such calculations is essentially to establish the limits of linear dielectric response.

#### A. Mixed Ionic and Electronic Conductivity

Excellent presentation of the general aspects of ionic conductivity and allied diffusion processes are available<sup>40</sup> and will not be considered here.

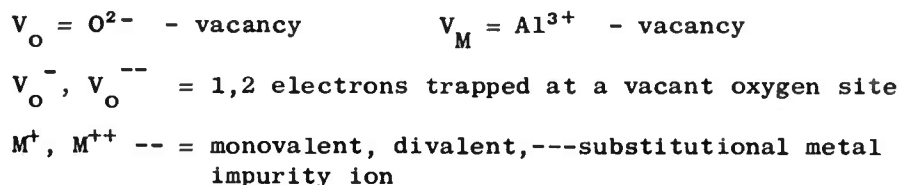
Most authors<sup>42</sup> assume more or less explicitly that only electronic conduction is important in most oxides, at least for temperatures below  $0.9 T_m$  ( $T_m$  being the melting point) but others<sup>43</sup> base their work on just the opposite premises.

Conventional measurements of electrical conductivity cannot give any indication of the magnitude of the components of the different modes of conductivity present in any given circumstances, and such information must be sought from direct measurements of the transport numbers by cell potential and mass transport experiments.

As will be shown in more detail, agreements based on the temperature dependence (activation energies) of the electrical conductivity, although often used, are in no way conclusive evidence for or against any ionic or electronic mode of electrical transport. Even if the amount of ionic conductivity is quite small with respect to the electronic one present, it is still essential to determine its absolute magnitude in view of the role that it can play in breakdown processes.

The tendency of oxides to exhibit electronic conductivity is usually viewed as resulting from their ability to depart easily from stoichiometric conditions. The electronic conductivity of these compounds at low temperatures (for  $\text{Al}_2\text{O}_3$  this could include temperatures well over  $1000^\circ\text{C}$ ) can be considered as an essentially extrinsic property depending on the degree of nonstoichiometry and on the impurity content of the sample.

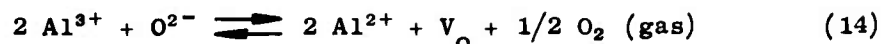
A large number of reactions involving the various ionic defects, impurity ions, and associated electronic carriers are possible in  $\text{Al}_2\text{O}_3$ . We shall only illustrate here some likely situation and restrict ourselves to metal impurity ions and ion vacancies. Our notation is as follows.



It is clear that the occurrence of  $O^-$  - ions and  $Al^{2+}$  - ions is associated with the creation of a hole in the O-2p band and an electron in a Al-3s band respectively. One sees easily that due to the requirement of electrical neutrality (in the bulk), lattice defects arising from departure of stoichiometric conditions are accompanied by corresponding creation of electronic carriers. For example, an excess of metal would

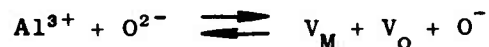


result from the reaction

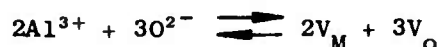


and results in the creation of 2 conduction electrons.

Similarly, an oxygen excess would follow from

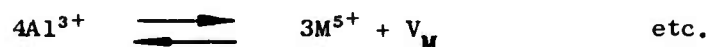
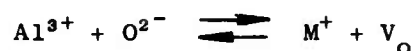


resulting in the creation of one hole, while the formation of the intrinsic Schottky defects occurs without creation of any electronic carriers.

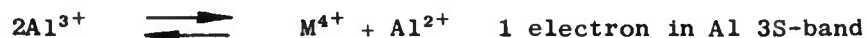


The presence of aliovalent impurities and the neutrality requirement also lead to two types of defects

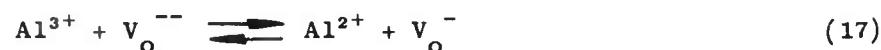
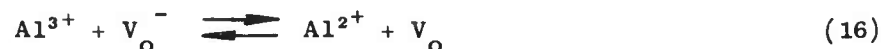
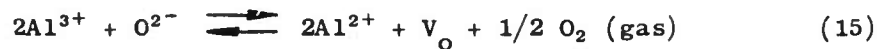
1. Purely ionic defects, i.e., ionic defects without simultaneous creation of electronic carriers



2. Ionic defects and associated electronic carriers



One cannot in general consider such equations separately, and deduce the type of carriers present and the partial pressure dependence of the resulting conductivity. For example, we shall look at the following system of reactions,



Physically, this would lead to an n-type electronic conductor with a metal excess if one neglected ionic conductivity; equations (16) and (17) represent ionization (or trapping) of electrons at vacant oxygen sites. Applying the law of mass action to these reactions, we would obtain the equations

$$[Al^{2+}]^2 [V_O] p_O^{1/2} = k_1 (T) \quad (18)$$

$$[Al^{2+}] [V_O] [V_O^-]^{-1} = k_2 (T) \quad (19)$$

$$[Al^{2+}] [V_O^-] [V_O^{--}]^{-1} = k_3 (T) \quad (20)$$

where the k's are the reaction constants. An additional equation relating the concentrations  $[Al^{2+}]$ ,  $[V_O]$ ,  $[V_O^-]$  is given by the neutrality requirement

$$[Al^{2+}] = [V_O^-] + 2[V_O] \quad (21)$$

If the k's are known, the concentrations of the various ionic and electronic carriers are found by solving the system of Eqs. (18-21). We should note here that we have neglected any hole-producing reaction such as



The reaction constants can, to a certain extent, be estimated on the basis of supplementary assumptions and can sometimes be measured (loss experiments). If one has complete ionization of the  $V_O^-$ ,  $V_O^{--}$  centers, then  $V_O$  and  $Al^{2+}$  are the only remaining defects and one can see that  $[Al^{2+}]$  is proportional to  $p_O^{-1/6}$ . Another limiting case is attained if  $[V_O^-]$  is a dominant defect; then  $[Al^{2+}]$  is proportional to  $p_O^{-1/4}$ .

The magnitude of the transport numbers for this extrinsic conductivity would depend, in these limiting cases, essentially on the ratio of the ionic to the electronic mobility; if, for normal electronic conduction, one can generally assume this ratio to be small, such is not necessarily the case if the electronic conduction is through a small polaron mechanism.

Similar arguments can be developed for an oxygen-excess sample that would exhibit p-type behavior and for impurity reactions. It is clear that the actual situation is extremely involved and that any definite conclusions are still premature. Also one must remember that at any external or internal surface (around glassy inclusions, for example), the neutrality requirement can be relaxed somewhat as it is admissible to form, for instance, double charged layers, so a different system of equations for the defect concentration will be obtained. The preceding considerations also show clearly that arguments based mainly on comparison of observed activation energies for electrical conductivity and diffusion constants are totally inconclusive.

At high temperatures, both electronic and ionic conductivity can depend on the same defect formation energy; their activation energies would differ only by the difference between the ionic migration energy and the carrier ionization energy and eventual mobility activation energy. There are no ways of distinguishing between the two cases at the present on the basis of energy considerations alone. The experimental error in the measurement of diffusion constants is generally rather large and the situation is further complicated by all questions related to the association of various defects, ambipolar diffusion (breakdown of Einstein relation), etc.

#### B. Electronic Energy Levels

A rough estimate of the electronic energy levels (Fig. 46) in  $\alpha\text{-Al}_2\text{O}_3$  can be made on the basis of the well-known qualitative features of the excited state of ionic crystals and quantitative data taken from the Born cycle and spectroscopic measurements.<sup>44,45</sup> A prerequisite for such a sketch is the knowledge of the crystal electrostatic potential at each nonequivalent ion site. As these were not available, they have first been obtained for the usual idealized  $\alpha\text{-Al}_2\text{O}_3$  structure, i.e., a crystal in which the  $\text{O}^{2-}$ -ions occupy a perfect h.c.p. lattice and the  $\text{Al}^{3+}$ -ions the centers of two-thirds of the octahedral voids. The charge carriers are viewed as resulting from various reactions and the corresponding energies of formation are estimated as follows.

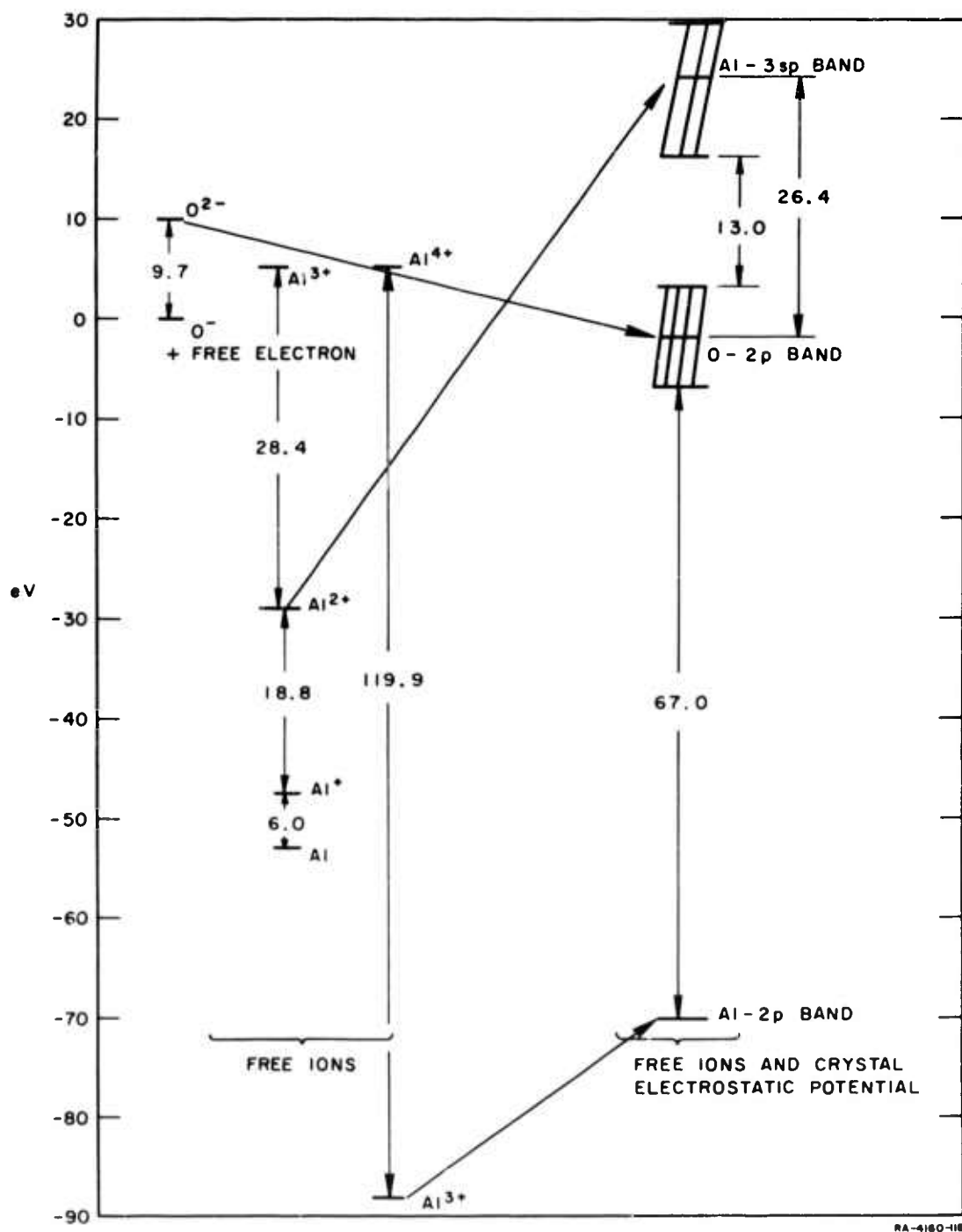


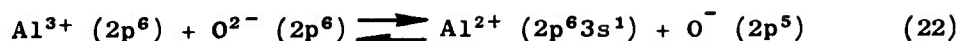
FIG. 46 ELECTRONIC ENERGY LEVELS FOR  $\alpha\text{-Al}_2\text{O}_3$

1. The reaction is considered as taking place between free ions.
2. The resulting energy of formation is corrected by the proper crystal potential energy, the energy of positive charges at  $\text{Al}^{3+}$  sites being raised by 52.8 v, that of negative charges at  $\text{O}^{2-}$  sites being lowered by 11.7 v.
3. A further correction can be made for localized states by taking crudely into account the dielectric (polarization) nature of the medium.

The relative energy levels obtained in this way refer to unbroadened excited state levels and no account is being taken of the crystal local deformation and polarization and of departure from the purely ionic character of the chemical bond. An estimate of the width of the valence and conduction band is possible here. By analogy with other ionic oxides and halides, one can estimate the width of the valence band in  $\alpha\text{-Al}_2\text{O}_3$ , i.e., the 0-2 p band, to be of the order of 10 eV. A tight binding calculation of this band width is possible but of little interest. The width of the conduction band, Al (3sp), can be taken to be similar to that of the Al-metal conduction band as the spacing between the metal ions is similar in both cases; this would give a conduction band approximately 15 eV wide for  $\alpha\text{-Al}_2\text{O}_3$ . These numbers are of course only orders of magnitude but are sufficient for our present purposes.

When one considers localized (in configuration space) excited states, a dielectric constant correction is natural, but a question arises as to which dielectric constant to use, namely the static one (as Morin<sup>18</sup> does), the optical one, or some effective  $\epsilon$ . It is not possible to answer such a question in the elementary framework of the above model for this involves the magnitude of the electron-phonon interaction, the subsequent degree of localization of the "phonon," etc. Furthermore, a similar question arises as to which "effective" charge should be used to take into account the nature of the actual chemical bond, but one can hope that the energies of formation for different reactions will be similarly affected so that a comparison between these will have a greater validity than their

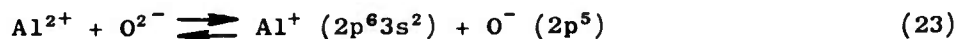
absolute magnitude. Consider the reaction



corresponding to the creation of a completely dissociated electron-hole pair. After displacing the  $\text{O}^{--}$  and  $\text{Al}^{3+}$  levels to take into account the crystal electrostatic potential, one sees that the difference in energy of these two levels, which is the energy of reaction (22), is 26.4 eV. Correcting roughly for band broadening, one would obtain a band gap of the order of 13 eV, but this is certainly an upper bound inasmuch as most neglected effects would result in a notably lower energy of reaction for (22).

Note that, if we consider (22) as giving rise to dissociated but localized electron-hole pairs and corrected for polarization, we could obtain, using the optical and static dielectric constants of  $\text{Al}_2\text{O}_3$ , 8 eV and 2.9 eV, respectively, as energies of formation of such carriers.

Similarly, the reaction



would lead to energies of formation for localized carriers of 6.0 eV and 2.3 eV. In the same way, from reactions involving substitutional metal ions and various other defects, one obtains a spectrum of energies of formation for localized carriers ranging from 1 eV up to several eV's. Because of the crudeness of these estimates and also because the migration energies that also enter into the experimental activation energies are not known, a direct identification with the transport data is difficult. But this at least shows clearly the origin of the variety of activation energies that have been reported for conductivity of various samples of single and polycrystal  $\alpha\text{-Al}_2\text{O}_3$ .

### C. Internal Fields in Dielectrics

In studying transport phenomena in dielectric materials, it is necessary to know the electrostatic potential everywhere in the solid. For a perfect crystal it is sufficient to consider a single unit cell in view of the translation symmetry. For inhomogeneous crystals, one must consider both deviation from the perfect crystal electrostatic potential pattern within a unit cell and its variation from cell to cell; the first aspect is important in determining the local electron energy levels and their occupancy, the second in evaluating the acceleration of the various carriers under the combined influence of the externally applied field and the internally created ones. The time and space dependence of the currents depend, of course, on both aspects and also on the existing scattering mechanisms. From the experimental data obtained here for  $\text{Al}_2\text{O}_3$  and elsewhere for other dielectric materials, one must conclude that under environmental conditions similar to those of a tube window (e.g. external space charge, electron and electromagnetic bombardment, etc.), very inhomogeneous distribution of ionic and electronic defects will exist, and their importance in understanding breakdown phenomena has already been stressed. Some calculations of such inhomogeneous charge distributions have been published for highly idealized models<sup>46-49</sup> but they should be regarded as having little more than a qualitative value due to the nature of the assumptions made; an essential part of the present program is still to obtain experimentally, and eventually theoretically, a better description of the time and position dependence of defect distributions in alumina under various external conditions. Here we consider only the problem of obtaining the potential at various sites in the unit cell for the perfect crystal and a method to follow in the case of a given defect distribution. Some remarks on the screening mechanism (polarization) will be made. The following considerations are purely classical but they have a wider validity if the charge distributions considered are properly interpreted as electron probability ones, obtainable in principle from the total wave functions of the system.

In the theory of dielectric crystals, the atomic or ionic charge distributions that should be considered as of finite extent and deformable in an internal and/or external field are usually treated in the "point approximation," i.e., replaced by point charges, point dipoles, etc., located at the atomic sites.<sup>50</sup> If one works in this approximation, it is necessary to introduce polarizabilities of the point distribution defined as proportionality factors between induced multipole components and the inducing potential field components. By definition, the polarizabilities depend solely on the internal structure of the charge distributions and are introduced to take into account their deformability under applied fields; they are generally taken as scalars for simplicity. We can divide a crystal into identical cells, centered at the lattice points, nonoverlapping, filling out the whole space by translation, and such that all the atomic sites are interior points. We shall denote by  $\vec{R}_n$  the translation lattice vectors, by  $\Omega_n$  the cell centered at  $\vec{R}_n$ ; the crystal charge distribution  $\rho(\vec{x})$  can be written as a sum

$$\rho(\vec{x}) = \sum_{(n)} \rho_n(\vec{x} - \vec{R}_n) = \sum_{(n)} \rho_n(\vec{y})$$

where  $\vec{y}$  is restricted to the cell  $\Omega_n$ , i.e.,

$$\begin{aligned} \rho_n(\vec{y}) &= \rho(\vec{y}) & \text{if } \vec{y} \text{ is in } \Omega_n \\ &= 0 & \text{if } \vec{y} \text{ is outside } \Omega_n \end{aligned}$$

By symmetry, one must have

$$\rho_n(\vec{y}) = \rho_m(\vec{y}) \quad \text{for all } n, m$$

and by charge neutrality in the perfect crystal

$$\oint_{\Omega_n} \rho_n(\vec{y}) d\vec{y} = 0$$

Furthermore, if the unit cell has a center of inversion, the cell dipole moment must be zero.



The "point approximation" consists generally in replacing the finite extent distribution  $\vec{\rho}_n$  by point multipole expansions centered at each atomic site. Of course, one can only introduce as many distinct point expansions as there are nonequivalent sites (2 for  $\text{Al}_2\text{O}_3$ ) and any such point expansion must be compatible with the site symmetry in the crystal. One has then

$$\rho_n(\vec{y}) = \sum_{\lambda} \sum_{n,\lambda} (\vec{y} - \vec{r}_{\lambda}) = \sum_{\lambda} \rho_{n,\lambda}(\vec{z})$$

where  $\lambda$  is the atomic site index in the unit cell with

$$\vec{r}_{\lambda} = \sum_i \lambda_i \vec{a}_i \quad 0 \leq \lambda_i < 1 \quad i = 1, 2, 3$$

the  $\vec{a}_i$ 's being the basis vectors of the lattice. (The geometry of  $\text{Al}_2\text{O}_3$  has been discussed in the progress reports). If we make a spherical harmonic expansion of the potential at any site

$$V_{\lambda}(\vec{r}) = \sum_{\ell, m} V_{\ell, m}^{(\lambda)} r^{\ell} y_{\ell}(\theta, \varphi) \quad \ell \geq 0$$

the constants  $V_{\ell, m}^{(\lambda)}$  will be obtained as lattice sums over the whole crystal that can be evaluated in the usual ways.

The polarizabilities at the site  $(\lambda)$  are defined by

$$Q_{\ell, m}^{(\lambda)} = -\alpha_{\ell, m}^{(\lambda)} V_{\ell, m}^{(\lambda)} \quad \ell > 0$$

where  $Q_{\ell, m}^{(\lambda)}$  is the induced multipole moment at  $(\lambda)$  due to the  $(\ell, m)$  potential field component at that site.

$$Q_{\ell, m}^{(\lambda)} = \frac{4\pi}{2\ell+1} \int \rho(\vec{r}) r^{\ell} y_{\ell, m}(\theta, \varphi) d\vec{z}$$

If the unperturbed charge distribution at  $(\lambda)$  is spherically symmetric, i.e., equivalent to a point charge (no permanent dipole, etc), then

$\alpha_{\ell, m}^{(\lambda)}$  does not depend on  $m$ .

If the polarizabilities are known, one can obtain in a self-consistent way the charge distribution  $\rho(\vec{x})$  and the potential  $V(\vec{x})$  for the perfect crystal. Of course, the multipole expansions will be in practice cut-off for some finite  $l$ .

The most difficult problem in this approach is to obtain a consistent set of polarizabilities. They should be calculated quantum mechanically from the deformation of the finite extent charge distribution  $\rho_n(\vec{y})$  under an applied field. We cannot over-emphasize that free ion polarizabilities, in general, will be unacceptable; the site charge distributions should not be taken too literally as ion electronic clouds in the sense of the elementary ionic crystal theory but simply as one, in no way, unique representation of the finite deformable charge distribution of a cell. Instead of expanding  $\rho_n(\vec{x})$  about each atomic site, one could more simply expand it about each lattice point, i.e., about a single center in each cell, and a different set of polarizabilities would have to be used. This alternative approach could actually be more useful in some cases, especially if the crystal geometry is such that no free ion core distribution remains recognizable in the crystal. As mentioned earlier, the point approximation will not be satisfactory for determining the contribution of the cell containing the field point, which must be handled separately. The essence of this approach is to reduce, for both the perfect and the imperfect crystal, the problem to that of a single cell with known boundary conditions. The charge distribution in that cell can then be investigated separately. The problem is presently being studied along the statistical approach.

The resulting boundary value problem for  $V(\vec{y})$  or  $\rho(\vec{y})$  will be non-linear and we cannot predict at the present how far this line of approach can be pursued. There are several elementary ways of obtaining crude approximate  $\alpha$ 's but the reason for trying to solve, in some consistent approximation, at least the quantum mechanical problem is that this is the only way to obtain the limitations of the simple linear law postulated for the  $\alpha$ 's. As in insulators at low temperatures, the screening of charged defect distributions is essentially due to this polarization of

the crystal in view of the quasi absence of free carriers; such limitations are essential in any attempt to characterize the electric behavior of a dielectric. The solution of the boundary value problem would allow a determination of the  $\alpha$ 's in terms of the cell structure and the boundary conditions. One also obtains the crystal potential for the one-electron Schrödinger equation and so in principle at least we could obtain a local electronic band structure in the approximation of the statistical model.

Many of the areas of modern quantum mechanics covered at the Summer Quantum Institute at the University of Uppsala, which was attended by one of the investigators on this project, are applicable to this study of the polarization and field on a localized basis. The use of projection operators, to define the relations leading to the eigenvalues and eigenvectors of the system under consideration, allows a statement of the quantum mechanical problem on a more physically real basis, and equally important, on a systematic basis wherein the operator is defined in terms of the physics of the system under study. It provides an important tool for expanding the dimensionality of the system under study so that the correspondence between configuration space and phase or momentum space has more significance in setting up the statement of the problem under consideration and allows a greater latitude in the approach to the solution of the problem by removing it from the domain of solution of partial differential equations.

In addition, the use of refined perturbation and partitioning techniques provides an important tool for establishing approximate solutions for both the steady state and time dependent problems. This part of the approach to quantum calculations is extremely important because of the very nature of quantum theory itself, in which exact solutions are found for only the very simplest of problems. However, by use of perturbation and particularly partitioning, the bounds on the eigenvalues may be estimated to a greater degree of accuracy and reliability.

The concept of the evolution operator for time dependent perturbations provides a method of systematic treatment so that estimates of

the state of a system as a function of time may be derived either from initial conditions or from the state at a known time. The evolution operator combined with partitioning methods again allows better, or more precise, definition of the bounds of the approximate solution to the particular problem.

The important tool of the density matrix, which is an extension of the operator method, was also covered. This concept brings the bridge between the statistical mechanics and quantum theory into a useful form so that it has the potential of use in the study of a number of complex problems not easily approached by classical methods. Thus the wave function itself per se is not necessarily defined, but rather the particular operator and associated observables are incorporated as the working tools for the problem. The restrictions and, more important, the methods of application of this technique to solid state problems are being investigated at present.

In essence the density matrix is a matrix representation of the integral expression for the average or expectation value of an observable or property of a system. It may be considered as a substitute for the use of the wave function representing the observable and it is particularly adaptable to many particle systems that would be extremely cumbersome to handle by the wave function methods. It is believed that this technique offers the possibility of aiming at a physically consistent and valid concept of the definition of many of the parameters as yet not well defined in solid state physics and, in particular, material science.

When the microscopic concepts discussed above have produced a method of defining the parameters of the inhomogeneous dielectric it will then be appropriate to use these parameters in conjunction with the data from the experiment to formulate the macroscopic equations for transport in the dielectric medium. These equations are<sup>\*</sup>:

---

See Quarterly Report No. 8, page 18 of this series.

$$\frac{\partial p}{\partial t} = -k_1 p n + g_{vt} - r_{tv} + f_p - \operatorname{div} \frac{J_p}{e} \quad (24)$$

$$\frac{\partial n}{\partial t} = -k_1 p n + g_{tc} - r_{ct} + f_n + \operatorname{div} \frac{J_n}{e} \quad (25)$$

$$\frac{\partial P}{\partial t} = +g_{tc} - r_{ct} - \operatorname{div} \frac{J_P}{e} \quad (26)$$

$$\frac{dN}{dt} = +g_{vt} - r_{tv} + \operatorname{div} \frac{J_N}{e} \quad (27)$$

$$\frac{\partial n_t}{\partial t} = r_{ct} - g_{tc} + g_{vt} - r_{tv} \quad (28)$$

$$J_p = e\mu_p p E - eD_p \operatorname{grad} p \quad (29)$$

$$J_n = e\mu_n n E + eD_n \operatorname{grad} n \quad (30)$$

$$J_P = e\mu_P P E - eD_P \operatorname{grad} P \quad (31)$$

$$J_N = e\mu_N N E + eD_N \operatorname{grad} N \quad (32)$$

$$J = J_e + J_p + J_P + J_N \quad (33)$$

$$\operatorname{div} E = \frac{4\pi e}{\epsilon} (p + P - n - N) \quad (34)$$

where  $p$  = hole density

$n$  = electron density

$P$  = positive ion density

$N$  = negative ion density

$k_1$  = recombination coefficient

$g_{vt}$  = rate of excitation of trapped holes

$g_{tc}$  = rate of excitation of trapped electrons

$r_{tv}$  = rate of trapping of holes

$r_{ct}$  = rate of trapping of electrons

$J_p$  = hole current density  
 $J_n$  = electron current density  
 $J_p$  = positive ion current density  
 $J_N$  = negative ion current density  
 $E$  = field  
 $\mu$  = mobility  
 $D$  = diffusivity (not necessarily isotropic)  
 $\epsilon$  = dielectric constant  
 $f$  = excitation rate due to particle bombardment

The above equations may be considered as the general phenomenological equations for conduction in an excited dielectric with traps and recombination sites; they include the effects of the ionic contribution to the current and the field. Equations (24) and (25) are the continuity equations for free holes and electrons, and it should be noted that the excitation rate terms  $f$  are not necessarily of the same magnitude. For photon or X-ray excitation,  $f_p$  and  $f_n$  would be equal, but, for electron bombardment,  $f_n$  could be greater than  $f_p$  due to the injection of electrons into the dielectric by the electron bombardment.

Under the influence of the bombardment, which is not necessarily homogeneous over the face of the dielectric, a charge is established on and in the specimen. The magnitude of potential associated with the surface or sub-surface charge could be equal to or greater than the potential of the source of the electrons. In addition, there will be, near the dielectric surface, a negative space charge due to secondary emission electrons. This space charge will be time-varying if the electron bombardment is time-varying. The surface potential on the dielectric is, therefore, not uniform and is time-dependent. In addition, because of the inhomogeneous electron bombardment, the generation of carriers is not homogeneous over the dielectric. Therefore, for the bombardment case the problem is three dimensional, and carrier density is actually to be written, e.g.,  $n(x,y,z,t)$ .

Equations (26) and (27) are the continuity equations for ions that may contribute to the total charge in the dielectric and consequently to the field within it. Ions, though of a lower mobility than electrons, and holes will be influenced by the high potential on the surface of the dielectric and also by the fact that there is a differential oxygen pressure across the dielectric. Migration of ions may be slow but its contribution must be evaluated before it is neglected.

Equation (28) is the continuity equation for electrons in traps. Equations (29), (30), (31), (32), and (33) represent the expressions for the current density which include drift currents and diffusion currents. Equation (34) is Poisson's equation for the charge in the dielectric.

The study of the above relations as indicated from both the microscopic and macroscopic concepts should allow a better evaluation of the contribution to breakdown of the discrete and inhomogeneously distributed charges and associated fields within a dielectric. When this evaluation is arrived at, it should be of such a form that the more classic concepts of breakdown as developed by Frohlich and Van Hippel, etc. will have more meaning for a real material.

The above discussion, while emphasizing the theoretical nature of the problem of breakdown, also indicates that the problem of defining the criteria for breakdown is not a go-or-no-go question. It is more than likely that the actual breakdown process is due to a fluctuation in the energy state of the system about an average energy that is the lower limit above which conditions for breakdown are met. This concept, we believe, is implicit in the problem and derives from the existence of inhomogeneous fields, variation in the environment surrounding the dielectric, and variations of external field applied to the dielectric. Therefore, breakdown must be ultimately examined as a stochastic process and will at later stages be studied from this concept.

It should be emphasized that there is still a need for further experimental studies to provide the input to the theoretical analysis. On this basis, the transport, breakdown, defect, and bombardment studies are

to be continued, but with emphasis now directed toward polycrystalline materials that are actually used in microwave devices. To this end, materials of controlled purity will be prepared in a vacuum, pressure, sintering facility constructed at the Institute, and their parameters will be studied.



## OVERALL CONCLUSIONS

The following conclusions can be drawn from the work to date.

### 1. Breakdown of Ceramics due to Ionization of Gas in Voids

Experiments have been conducted at 3000 m.c. on specially prepared specimens. Fields considerably higher than those actually developed across ceramic windows for power tubes operating at this frequency were developed across specimens with no breakdown. This has led to the conclusion that ionization of gas in voids will not lead to breakdown of microwave windows at present or near future power levels at s band. It is believed on the basis of postulated mechanisms that tubes operating at x band will also not be affected.

### 2. Barrier Effect

- (a) It has been demonstrated that electrical conductivity across a barrier formed by sintering two dielectrics (e.g., a glass and aluminum oxide single crystal) is considerably less than that of the individual components. Measurements up to 800°C indicate a reduction of three orders of magnitude.
- (b) It has been further demonstrated that in polycrystalline aluminum oxide having a glassy phase the most probable electrical conduction path is along or through the glassy phase.

### 3. High Temperature Conductivity of Aluminum Oxide

It has been demonstrated that the reported conductivities of single crystal aluminum oxide in the region of 1600°C are actually the conductivities due to the environment and not that of the bulk crystal (e.g., conductivity of air and possibly emission from the metal contacts).

### 4. Effects of Defects on Breakdown

It has been demonstrated that defects introduced into single crystals of aluminum oxide by bending and heat treatment reduce the breakdown strength of this material. It is postulated on the basis of the evidence that point defects rather than line defects are the significant factors in the reduction of breakdown strength.

## 5. Effect of Electron Bombardment on Sapphire

Experimental evidence indicates that electron bombardment of a dielectric (e.g., alumina) with a potential across it produces regions of separated charges within the material. These result in high internal fields within the material (persistent internal polarization) that can contribute significantly to breakdown.

## 6. Accurate Data on some Properties of Sapphire

The conductivity and thermoelectric power at relatively low temperatures for single crystal aluminum oxide have been found. These are from  $10^{-11}$  to  $10^{-9}$  ohm $^{-1}$  cm $^{-1}$  for the range of from 600°C to 800°C for the electrical conductivity and from 1 to 3 mv per degree C from 200°C to 800°C for the thermoelectric power. For the electrical conductivity, an activation or ionization energy of 2.4 e.v. was found indicating the probability of an impurity conduction mechanism.

## 7. Growth of Aluminum Oxide

Five different methods of growing alpha aluminum oxide films in vacuum have been demonstrated and verified by electron diffraction.

- (a) Oxidation of evaporated aluminum
- (b) Thermal evaporation of aluminum oxide
- (c) Reactive deposition on a heated substrate



## 8. Theory of Breakdown of Solid Dielectrics

As a result of the experimental and theoretical work on this contract, the strong influence of inhomogeneous charge and field distribution on the failure of dielectrics has been recognized. These factors have not been given sufficient weight in classical theories and efforts are being made to develop a proper description of their origin (e.g., defects, particle bombardment) and contribution to dielectric failure.

## RECOMMENDATIONS FOR FUTURE WORK

In the light of the progress to date the emphasis in the next phase of work will be on establishing criteria for determining the ability of dielectrics to perform properly in microwave devices. To achieve this goal, the following work will be prosecuted.

1. Transport properties of single crystal and polycrystalline aluminum oxide will be studied
2. Polycrystalline aluminum oxide with controlled composition will be prepared for study
3. Influence of imperfections on breakdown in polycrystalline and single crystal aluminas will be studied
4. Analysis directed towards defining a dielectric tensor will be continued. This will be the basis for developing a model for determining the influence of inhomogeneous charge distribution in a dielectric on its breakdown.


**KEY TECHNICAL PERSONNEL**  
(for period 30 June 1964 to 30 Sept. 1964)

L. Feinstein, Project Leader, 220 hours

J. Bordeaux, Physical Chemist, 400 hours

D. Peters, Research Engineer, 400 hours

C. Peltzer, Solid State Physicist, 200 hours

  
Lester Feinstein, Chairman  
Electronic Materials Department

## REFERENCES

1. Piryatinskii, A. Z. On the Question of Electrical Disturbances in Industrial Dielectrics. J. Tech. Phys. (USSR) 22, 1556 (1952).
2. Volakobinskii, N. Some Questions About the Testing of Heterogeneous Dielectrics. J. Tech. Phys. (USSR) 25, 78 (1955).  
The Effect of Air Inclusions Upon the Dielectric Strength and Losses of Insulating Materials. Soviet Physics Tech. Phys. p. 547 (1956).
3. Skanavi, G. I. and V. I. Sarafanov. Electrical Properties of Titanates of Metals of Group II of the Table of D. I. Medeleev with High Frequency Voltages. J. Experimental-Theoretical Phys. (USSR) 27, 595 (1954).
4. Balygin, I. E. and P. S. Mikhailov. Regarding Ionization in Pores of Ceramic Dielectrics. Soviet Physics Tech. Phys. 3 (8), 1554 (1958).
5. Brown, S. C. High Frequency Gas-Discharge Breakdown Proceedings of IRE, p. 1493 (1951).  
Basic Data of Plasma Physics, John Wiley and Sons, N.Y., 1959.
6. Rose, D. J. and S. C. Brown. Microwave Gas Discharge in Air, Nitrogen and Oxygen. J. App. Phys. 28 (5), 561 (1957).
7. Gould, L. and L. W. Roberts. Breakdown of Air at Microwave Frequencies. J. App. Phys. 27 (10), 1162 (1956).
8. Francis, G. Ionization Phenomena in Gases, Butterworths, London, 1960.
9. Cobine, J. D. Gaseous Conductors, Dover, N.Y., 1958.
10. Spence, E. Electronic Semiconductors, McGraw-Hill, N.Y., 1958.
11. Fröhlich, H. Proc. Royal Soc. A188, 521 (1947).
12. Marcuvitz, N. Wave Guide Handbook, MIT Rad. Lab. Series No. 10, p.178, McGraw-Hill, N.Y., 1947.
13. Ginzton, E. L. Microwave Measurements, McGraw-Hill, N.Y., 1957.
14. Pappis, J. and W. D. Kingery. Electrical Properties of Single-Crystal and Polycrystalline Alumina at High Temperatures, J. Am. Ceram. Soc., 44, No. 9, 459 (1961).
15. Florio, J. V. Dielectric Properties of Alumina at High Temperatures, J. Am. Ceram. Soc., 43, No. 5, 262 (1960).
16. Dekker, A. J. Solid State Physics, Prentice-Hall Inc., p. 312.
17. As indicated by data from Linde.

18. Johnson, V. A. and K. Lark-Horovitz. Theory of Thermoelectric Power in Semiconductors with Applications to Germanium, Phys. Rev. 92, No. 2, p. 226 (1953).
19. Middleton, A. E. and W. W. Scanlon. Measurement of the Thermoelectric Power of Germanium at Temperatures Above 78°C, Phys. Rev. 92, No. 2, p. 219 (1953).
20. Morin, F. J. Electrical Properties of  $\text{Fe}_2\text{O}_3$  and  $\text{Fe}_2\text{O}_3$  Containing Titanium, Phys. Rev. 83, No. 5, p. 1005 (1951).
21. Dekker, A. J. Solid State Physics, Prentice Hall, p. 175, 1961.
22. Gilles, A. Absorption A Haute Temperature De Quelques Materiaux Optiques Dans L'Ultraviolet De Schumann, K. Ph. Radium, Series 8, 13, 247 (1952).
23. Harrop, P. J. and R. H. Creamer. The High Temperature Electrical Conductivity of Single-Crystal Alumina. Brit. J. App. Phys. 14, 335, No. 6 (1963).
24. Bube, R. H. Photoconductivity of Solids, John Wiley and Sons, Inc., N.Y., p. 220 (1960).
25. Reference No. 15, p. 237.
26. Research on Dielectrics for Microwave Electron Devices, Report No. 3, Third Quarterly Progress Report, p. 24 (1963).
27. Research on Dielectrics for Microwave Electron Devices, Report No. 5, Fifth Quarterly Progress Report, p. 15 (1963).
28. Smith, R. A. Semiconductors, Cambridge Press, p. 172, 1959.
29. Morin, F. J. Oxides of the 3rd Transition Metals, B.S.T.J., p. 1047 (July 1958).
30. Dekker, A. J. Solid State Physics, Prentice Hall, p. 177, 1961.
31. Paladino, A. E. and W. D. Kingery. Aluminum Ion Diffusion in Aluminum Oxide, J. Chem. Phys. 37, No. 5, 957 (1962).
32. Cronmeyer, D. C. Phys. Rev., 87, 876, No. 5 (1952).
33. Mitoff, S. P. Electrical Conductivity of Single Crystals of  $\text{MgO}$ , J. Chem. Phys., 31, No. 5, 1261 (1959).
34. Kalmann, H. and E. B. Rosenberg. Persistent Internal Polarization, Phys. Rev. 97, No. 6, 1596 (1955).
35. Gross, B. Irradiation Effects in Plexiglass, J. Polymer Sci. XXVII, p. 135 (1958); Irradiation Effects in Borosilicate Glass, Phys. Rev., 107, No. 2, 368 (1957).

36. McKay, K. G., "Electron Bombardment Conductivity in Diamond," Phys. Rev. 74, 11, 1606, (1948); Phys. Rev. 77, 6, 816 (1950).
37. Upatov, V. Ia, "Radio Engineering and Electronics," USSR, 2, 2, 91 (1957); 4, 3, 237 (1959).
38. Gergely, G. Y. Space Charge Effects in Ambipolar Diffusion of Carriers Induced by Electron Bombardment in Photoconducting Insulator Crystals, J. Phys. Chem. Solids, 21, 105, 1/2 (1961).
39. Young, J. R. J. App. Phys., 28, 524 (1957).
40. Van Buren, H. G. Imperfections In Crystals, Ninth Holland Publishing Co., Amsterdam, 1960.
41. Redfield, D. Phys. Rev., 130, 914 (1963).
42. Lidiard, A. B. Handbuch der Physik XX, 246 (1958); Yost, W. Diffusion, Academic Press Inc., N.Y., 1952.
43. Davies, M. O. J. Chem. Phys., 38, 2047 (1963).
44. Seitz, F. Modern Theory of Solids, McGraw-Hill, 1940.
45. Atomic Energy Levels, NBS Circular No. 467.
46. MacDonald, J. R. Static Space-Charge Effects in the Diffuse Layer, J. Chem. Phys., 22, No. 8, 1317 (1964).
47. MacDonald, J. R. Static Space-Charge and Capacitance for Two-Blocking Electrodes, J. Chem. Phys., 30, No. 3, 806 (1959).
48. MacDonald, J. R. Exact Solution of the Debye-Hückel Equations for a Polarized Electrode, J. Chem. Phys., 22, No. 8, 1314 (1954).
49. MacDonald, J. R. Static Space-Charge and Capacitance for a Single Blocking Electrode, J. Chem. Phys., 29, No. 6, 1346 (1958).
50. Fröhlich, H. Theory of Dielectrics, Clarendon Press, Oxford, England, 1950.

# DISTRIBUTION LIST

ORGANIZATION	NO. OF COPIES	ORGANIZATION	NO. OF COPIES
Commander, Defense Documentation Center ATTN: TISIA Cameron Station, Bldg. 5 Alexandria, Va. 22314	20	Commanding General, U. S. Army Materiel Command ATTN: R&D Directorate Washington, D. C. 20315	2
Advisory Group on Electron Devices 346 Broadway, 8th Floor New York, N.Y. 10013	3	U. S. Army Materiel Command ATTN: AMCRD-RS-PE (Mr. Harold Blodgett) Washington, D. C. 20315	1
NASA Representative Scientific/Technical Information Facility P. O. Box 5700 Bethesda, Md. 20014	1	Director, Materiel Readiness Directorate Hq, U. S. Army Electronics Command ATTN: AMSEL-MR Fort Monmouth, New Jersey 07703	1
Office of the Assistant Secretary of Defense (Research and Engineering) ATTN: Technical Library Room 3E1065, The Pentagon Washington, D. C. 20301	1	Director, USAEL ATTN: AMSEL-RD-DR Fort Monmouth, New Jersey 07703	1
Chief of Research and Development Department of the Army Washington 25, D. C.	2	Director, USAEL ATTN: AMSEL-RD-P Fort Monmouth, New Jersey 07703	1
Commanding Officer, U. S. Army Combat Developments Command ATTN: CDCMR-E Fort Belvoir, Va.	1	Director U. S. Army Electronics Laboratories ATTN: AMSEL-RD-ADO-RHA (Record Copy) Fort Monmouth, New Jersey 07703	1
Commanding General U. S. Army Combat Developments Command Communications-Electronics Agency Fort Huachuca, Ariz. 85613	1	Director U. S. Army Electronics Laboratories ATTN: AMSEL-RD-PRT (File Copy) Fort Monmouth, New Jersey 07703	1
Commanding Officer U. S. Army Engineer Research and Development Laboratories ATTN: STINFO Branch Fort Belvoir, Va.	2	Director, U.S. Army Electronics Laboratories ATTN: AMSEL-RD-PR (Contracts) AMSEL-RD-PR (Tech Staff) AMSEL-RD-PRG (Mr. Zinn) AMSEL-RD-PRM (Mr. Hersh) Fort Monmouth, N. J. 07703	1 1 1 1
Commanding Officer Harry Diamond Laboratories Connecticut Ave. & Van Ness St., N. W. Washington, D. C. 20438	1	Director U. S. Army Electronics Laboratories ATTN: Technical Documents Center (AMSEL-RD-ADT) Fort Monmouth, N. J. 07703	1
Commanding Officer U. S. Army Nuclear Defense Laboratory ATTN: Library Edgewood Arsenal, Md. 21010	2	Commanding Officer U. S. Army Electronics Research & Development Activity ATTN: AMSEL-RD-WS-A White Sands, N. Mexico 88002	1
Commander, U. S. Army Research Office (Durham) Box CM-Duke Station Durham, N. C.	1	Commanding Officer U. S. Army Electronics Research Unit P. O. Box 205 Mountain View, Calif. 94040	1
Chief, U. S. Army Security Agency ATTN: ACofS, G4 (Technical Library) Arlington Hall Station Arlington 12, Va.	2	Commanding General U. S. Army Electronics Command ATTN: AMSEL-PP-E-P/TED-2b 225 So. 18th Street Philadelphia, Penna. 19103	1
Deputy President, U. S. Army Security Agency Board Arlington Hall Station Arlington 12, Va.	1		



## DISTRIBUTION LIST

ORGANIZATION	NO. OF COPIES	ORGANIZATION	NO. OF COPIES
USAEI Liaison Officer Rome Air Development Center ATTN: RAOL Griffiss Air Force Base, N. Y. 13442	1	Director of Defense Research & Engineering, OSD ATTN: Mr. James M. Bridges Washington, D. C. 20301	1
Director U. S. Naval Research Laboratory ATTN: Code 2027 Washington, D. C. 20390	1	Commanding General, U. S. Army Materiel Command, Attn: AMCRD-RP-E Washington, D. C. 20315	1
Chief, Bureau of Ships ATTN: Code 681A-1 Washington 25, D.C.	1	Chief, Army Research Office Washington, 25, D. C.	1
Commanding Officer & Director U. S. Navy Electronics Laboratory ATTN: Library San Diego 52, Calif.	1	Commanding General, U. S. Army Electronics Command ATTN: AMSEL-RE Fort Monmouth, New Jersey 07703	1
Marine Corps Liaison Office U. S. Army Electronics Laboratories ATTN: AMSEL-RD-LNR Fort Monmouth, N. J. 07703	1	Director U. S. Army Electronics Laboratories ATTN: AMSEL-RD-SR (Dir Radar Div) ATTN: AMSEL-RD-SC (Dir CM Div) ATTN: AMSEL-RD-PE (Dir EP&M Div) ATTN: AMSEL-RD-N (Dir Comm Dept) ATTN: AMSEL-RD-PEM ATTN: AMSEL-RD-DR (ARPA Coordinator) Fort Monmouth, New Jersey 07703	1 1 1 1 1 1
Rome Air Development Center ATTN: RAALD Griffiss Air Force Base, N. Y. 13442	1	Chief of Naval Operations Department of the Navy ATTN: OP-7 Washington 25, D. C.	1
Electronic Systems Division (AFSC) Scientific & Technical Information Division (ESTI) L. G. Hanscom Field Bedford, Mass. 01731	2	Chief of Naval Research Department of the Navy ATTN: 461 ATTN: 427 Washington 25, D. C.	1 1 1
Air Force Cambridge Research Laboratories ATTN: CRXL-R L. G. Hanscom Field Bedford, Mass. 01731	2	Director, U. S. Naval Research Laboratory ATTN: Dr. S. T. Smith, Code 5240 ATTN: Mr. R. C. Guthrie, Code 5300 Washington, D. C. 20390	1 1
Air Force Cambridge Research Laboratories 1 ATTN: CRZC L. G. Hanscom Field Bedford, Mass. 01731	1	Chief, Bureau of Ships Department of the Navy ATTN: Code 680 and 670B ATTN: Code 335 and 261B Washington 25, D. C.	1 1
Systems Engineering Group (SEPRR) Wright-Patterson Air Force Base, Ohio 45433	1	Commander, New York Naval Shipyard Naval Material Laboratory ATTN: Code 920 Brooklyn 1, N. Y.	1
Hq. Aeronautical Systems Division ATTN: ASRNE Wright-Patterson AFB, Ohio 45433	1	Chief, Bureau of Naval Weapons Department of the Navy ATTN: RRRE and PNEN-3 ATTN: RAAV-4423 and RMWC Washington, D. C. 20360	1 1
AFSC Scientific/Technical Liaison Office 1 U. S. Army Electronics Laboratories ATTN: AMSEL-RD-LNA Fort Monmouth, N. J. 07703	1	Headquarters, USAF ATTN: AFRST-EL/CS Room 4D335 Pentagon Washington, D. C. 20330	1
AFSC Scientific/Technical Liaison Office 1 U. S. Naval Air Development Center Johnsville, Pa.	1	Commander, Electronic Systems Division Air Force Systems Command ATTN: ESRDE Bedford, Mass. 01731	1
General Electric Company Tube Dept., Bldg 269 Schenectady, N. Y. ATTN: Dr. R. Bondley	1		

## DISTRIBUTION LIST

ORGANIZATION	NO. OF COPIES	ORGANIZATION	NO. OF COPIES
Commander, Rome Air Development Center ATTN: RALTT and RALTP ATTN: RALS and RAIC Griffiss Air Force Base, N. Y. 13442	1 1	Kane Engineering Laboratories 845 Commercial Street Palo Alto, Calif. ATTN: Mr. John Kane	1
Commander EOAR ATTN: Lt. Col. O. R. Hill The Shell Bldg 47 Rue Cantersteen Brussels, Belgium	1	Director, Lincoln Laboratory P. O. Box 73 Lexington 73, Mass. ATTN: Dr. G. L. Guernsey	1
Commander, Air Force Systems Command ATTN: Mr. S. Tepper, RTHC R&T Division Bolling AFB, Washington, D. C. 20332	1	Litton Industries 960 Industrial Road San Carlos, Calif. ATTN: Dr. J. F. Hull and A. Promer	1
Aerospace Corporation Los Angeles, 45, Calif. ATTN: Dr. I. Getting	1	Mitre Corporation Bedford, Mass. ATTN: Dr. R. F. Naka, Bldg 2A-251	1
Applied Physics Laboratory Howard County, Maryland ATTN: Mr. William Dobbins Via: Bureau of Naval Weapons Representative Silver Springs, Maryland	1	Rand Corporation The Los Angeles Air Procurement District 1700 Main Street Santa Monica, Calif. ATTN: Administrative Contracting Officer	1
Battelle Memorial Institute 505 King Avenue Columbus 1, Ohio 43201 ATTN: Defender Library	1	RCA Aerospace Communication and Controls Division P. O. Box 588 Burlington, Mass. ATTN: Mr. N. L. Laschever	1
Bell Telephone Labs, Inc. Whippany, N. J. 07981 ATTN: Mr. R. C. Newhouse	1	Radio Corporation of America Lancaster, Pa. ATTN: Mr. E. E. Spitzer	1
Zeus Project Liaison Officer Bell Telephone Labs Whippany, N. J. 07981 ATTN: Lt. Col. Lee G. Jones	1	David Sarnoff Research Center RCA Laboratories Princeton, N. J. ATTN: Dr. L. S. Nergaaid	1
Cornell Aeronautical Labs, Inc. 4455 Genessee St. Buffalo 21, N. Y. ATTN: Mr. R. C. Beitz	1	Raytheon Company Waltham, Mass. 02154 ATTN: Mr. William C. Brown	1
Eitel-McCullough, Inc. 301 Industrial Way San Carlos, Calif ATTN: Dr. George Caryotekis and Mr. Earl Shelton	1	SFD Laboratories 800 Rahway Avenue Union, N. J. ATTN: Dr. J. Feinstein	1
General Electric Company Traveling Wave Tube Products Section 601 California Avenue Palo Alto, Calif. ATTN: Mr. S. E. Webber	1	Sperry Electronic Tube Division Sperry Rand Corporation Gainesville, Fla. 32601 ATTN: Dr. A. D. Sutherland ATTN: Dr. V. R. Learned	1 1
General Electric Company Power Tube Department 1 River Road Schenectady, N.Y. ATTN: Mr. E. D. McArthur Knolls Research Lab	1	Project M Stanford University Stanford, Calif ATTN: Mr. J. Jasberg	1
Hughes Aircraft Company Culver City, Calif. ATTN: Dr. L. M. Field Microwave Tubes Division	1	Stanford University Microwave Laboratory Stanford, Calif. ATTN: Prof. M. Chodorow	1
		Sylvania Electric Products, Inc. 500 Evelyn Avenue Mountain View, Calif. ATTN: Dr. Rudy Hutter	1

# DISTRIBUTION LIST

ORGANIZATION	NO. OF COPIES	ORGANIZATION	NO. OF COPIES
Sylvania Electric Products, Inc. East 3rd Street Williamsport, Pa. ATTN: Dr. John Whitmore	1	Mr. Walter H. Kohl P. O. Box 426 Los Altos, Calif. 94023	1
Varian Associates 611 Hanaen Way Palo Alto, Calif. ATTN: Dr. T. Moreno and Dr. A. Staprans ATTN: Dr. E. W. Herold	1 1	Microwave Associates, Inc. South Ave., Burlington, Mass. ATTN: Dr. Grand St. John	1
Watkins-Johnson Company 3333 Hillview Avenue Palo Alto, Calif. ATTN: Dr. Rolf Peter	1	Northrup Nortronics 100 Morae St. Norwood, Mass. 02062 ATTN: Mr. R. H. Schoemann	1
Electron Tube Division Westinghouse Electric Corporation P. O. Box 746, Baltimore 3, Md. ATTN: Mr. G R. Kilgore	1	Semicon Associates, Inc. Box 832 Lexington, Ky. 40501 ATTN: Mr. J. H. O'Neill	1
Director, Advanced Research Projects Agency Office of Secretary of Defense ATTN: Lt. Col. Benjamin I. Hill Washington, D. C. 20301	1	Sperry Electronic Tube Div., Sperry Rand Corp. Gainesville, Fla. 32601 ATTN: Mr. L. A. Tentarelli	1
Director, USAEL ATTN: AMSEL-RD-PEM (Mr. S. Divits) AMSEL-RD-PFM (Mr. H. Mette) AMSEL-RD-PFM (Dr. L. Wandinger) Fort Monmouth, New Jersey 07703	1 1 1	Westinghouse Electric Corporation Friendship International Airport ATTN: Technical Information Center Box 1693 Baltimore, Md. 21203	1
Chief, Bureau of Ships, Dept of the Navy ATTN: Code 681A-1 Washington 25, D. C.	1		
American Lava Corp., Steatite Div. Chattanooga, Tenn. 37405 ATTN: Mr. R. D. Dillender	1		
Beryllium Corp. Box 1462 Reading, Pa. ATTN: Mr. Jack Blum	1		
Consolidated Ceramics & Metalizing Corp. Flemington, N. J. 08822 ATTN: Mr. J. E. Comeforo	1		
Coors Porcelain Co.. Golden, Colorado ATTN: Mr. L. E. Ferreira	1		
Eitel-McCullough, Inc. 301 Industrial Way San Carlos, Calif. ATTN: Mr. D. Priest ATTN: Dr. L. Reed	1 1		
Field Emission Corp. 611 Third Street McMinnville, Oregon 97128 ATTN: Dr. F. M. Charbonnier	1		

This contract is supervised by the Techniques Branch, Electron Tubes Division, ECD, USAEL, Ft. Monmouth, N.J. For further technical information contact Miss Barbara Malley, Project engineer, telephone 201-59-61402.

<p>AD STANFORD RESEARCH INSTITUTE, Menlo Park, California</p> <p>Div. 8/4, 14/2, 25/3, 6</p> <p>RESEARCH ON DIELECTRICS FOR MICROWAVE ELECTRON DEVICES, L. Feinstein, J. Bordeaux, D. Peters, C. Peltzer, Report No. 9, Final Report, 1 July 1962 to 30 September 1964, 113 pages, inc. 46 Illustrations, 2 Tables.</p> <p>Contract DA-36-039 SC-90856. Unclassified Report</p> <p>This report reviews the results of twenty-seven months' study of the transport and breakdown properties of aluminum oxide and of methods of growth of this dielectric from the vapor phase in an evacuated system.</p> <p>An ultrahigh vacuum system capable of reaching pressures of <math>10^{-8}</math>-<math>10^{-10}</math> torr has been completed. The growth of aluminum oxide films ranging in thickness from 1000 Å to 5000 Å by five different methods was achieved in an integim vacuum system operating in the <math>10^{-6}</math> to <math>10^{-7}</math> torr range.</p>	<p>UNCLASSIFIED</p> <ol style="list-style-type: none"> <li>1. Dielectrics</li> <li>2. High Vacuum</li> <li>3. Solid State</li> <li>4. Insulators</li> <li>5. Microwave Windows</li> </ol> <ol style="list-style-type: none"> <li>I. Project DEFENDER</li> <li>II. Research on Dielectrics for Microwave Devices</li> <li>III. L. Feinstein</li> <li>IV. J. Bordeaux</li> <li>V. D. Peters</li> <li>VI. C. Peltzer</li> <li>VII. USAEL, Fort Monmouth, N.J.</li> </ol>
<p>AD STANFORD RESEARCH INSTITUTE, Menlo Park, California</p> <p>Div. 8/4, 14/2, 25/3, 6</p> <p>RESEARCH ON DIELECTRICS FOR MICROWAVE ELECTRON DEVICES, L. Feinstein, J. Bordeaux, D. Peters, C. Peltzer, Report No. 9, Final Report, 1 July 1962 to 30 September 1964, 113 pages, inc. 46 Illustrations, 2 Tables.</p> <p>Contract DA-36-039 SC-90856. Unclassified Report</p> <p>This report reviews the results of twenty-seven months' study of the transport and breakdown properties of aluminum oxide and of methods of growth of this dielectric from the vapor phase in an evacuated system.</p> <p>An ultrahigh vacuum system capable of reaching pressures of <math>10^{-8}</math>-<math>10^{-10}</math> torr has been completed. The growth of aluminum oxide films ranging in thickness from 1000 Å to 5000 Å by five different methods was achieved in an integim vacuum system operating in the <math>10^{-6}</math> to <math>10^{-7}</math> torr range.</p>	<p>UNCLASSIFIED</p> <ol style="list-style-type: none"> <li>1. Dielectrics</li> <li>2. High Vacuum</li> <li>3. Solid State</li> <li>4. Insulators</li> <li>5. Microwave Windows</li> </ol> <ol style="list-style-type: none"> <li>I. Project DEFENDER</li> <li>II. Research on Dielectrics for Microwave Devices</li> <li>III. L. Feinstein</li> <li>IV. J. Bordeaux</li> <li>V. D. Peters</li> <li>VI. C. Peltzer</li> <li>VII. USAEL, Fort Monmouth, N.J.</li> </ol>

<p>Alpha aluminum oxide films were grown by thermal evaporation in the ultrahigh vacuum system.</p> <p>Data from experiments on transport in single crystal sapphire indicate that electron or hole conduction is primarily due to the effect of impurities or defects, and therefore, indicates either an impurity band or hopping process or a polaron conduction mechanism. The degree of ionic conductivity is still uncertain, particularly at high temperatures (1600°C). The effect of the glassy phase which exists in commercial polycrystalline aluminas is to form a barrier to conduction across the boundary between the aluminum oxide crystals and the glassy phase.</p> <p>The data from electron bombardment and breakdown studies indicate that particle bombardment, in addition to creating defects if particle energy is sufficiently high, can also lead to formation of separated charge regions in the material. These regions can act as sources of internal fields within the dielectric. Defects within the material introduced by bending sapphire single crystals have a pronounced effect on decreasing the breakdown strength of specimens.</p>	<p>VIII.</p> <p>UNCLASSIFIED</p> <p>DA-36-039</p> <p>SC-90856</p>
<p>Alpha aluminum oxide films were grown by thermal evaporation in the ultrahigh vacuum system.</p> <p>Data from experiments on transport in single crystal sapphire indicate that electron or hole conduction is primarily due to the effect of impurities or defects, and therefore, indicates either an impurity band or hopping process or a polaron conduction mechanism. The degree of ionic conductivity is still uncertain, particularly at high temperatures (1600°C). The effect of the glassy phase which exists in commercial polycrystalline aluminas is to form a barrier to conduction across the boundary between the aluminum oxide crystals and the glassy phase.</p> <p>The data from electron bombardment and breakdown studies indicate that particle bombardment, in addition to creating defects if particle energy is sufficiently high, can also lead to formation of separated charge regions in the material. These regions can act as sources of internal fields within the dielectric. Defects within the material introduced by bending sapphire single crystals have a pronounced effect on decreasing the breakdown strength of specimens.</p>	<p>VIII.</p> <p>UNCLASSIFIED</p> <p>DA-36-039</p> <p>SC-90856</p>
<p>Alpha aluminum oxide films were grown by thermal evaporation in the ultrahigh vacuum system.</p> <p>Data from experiments on transport in single crystal sapphire indicate that electron or hole conduction is primarily due to the effect of impurities or defects, and therefore, indicates either an impurity band or hopping process or a polaron conduction mechanism. The degree of ionic conductivity is still uncertain, particularly at high temperatures (1600°C). The effect of the glassy phase which exists in commercial polycrystalline aluminas is to form a barrier to conduction across the boundary between the aluminum oxide crystals and the glassy phase.</p> <p>The data from electron bombardment and breakdown studies indicate that particle bombardment, in addition to creating defects if particle energy is sufficiently high, can also lead to formation of separated charge regions in the material. These regions can act as sources of internal fields within the dielectric. Defects within the material introduced by bending sapphire single crystals have a pronounced effect on decreasing the breakdown strength of specimens.</p>	<p>VIII.</p> <p>UNCLASSIFIED</p> <p>DA-36-039</p> <p>SC-90856</p>
<p>Alpha aluminum oxide films were grown by thermal evaporation in the ultrahigh vacuum system.</p> <p>Data from experiments on transport in single crystal sapphire indicate that electron or hole conduction is primarily due to the effect of impurities or defects, and therefore, indicates either an impurity band or hopping process or a polaron conduction mechanism. The degree of ionic conductivity is still uncertain, particularly at high temperatures (1600°C). The effect of the glassy phase which exists in commercial polycrystalline aluminas is to form a barrier to conduction across the boundary between the aluminum oxide crystals and the glassy phase.</p> <p>The data from electron bombardment and breakdown studies indicate that particle bombardment, in addition to creating defects if particle energy is sufficiently high, can also lead to formation of separated charge regions in the material. These regions can act as sources of internal fields within the dielectric. Defects within the material introduced by bending sapphire single crystals have a pronounced effect on decreasing the breakdown strength of specimens.</p>	<p>VIII.</p> <p>UNCLASSIFIED</p> <p>DA-36-039</p> <p>SC-90856</p>

<p>Analytic studies indicate the need for developing a method of describing the relation between imperfection states in a dielectric and the inhomogeneous internal fields within the material. These fields must be accounted for in the description of the factors which control breakdown in dielectrics.</p> <p>The study on the effect of ionization of gas in alumina ceramics has been completed. Experiments conducted indicated that microwave fields in the order of 132,000 volts per cm peak and 4,000 volts per cm average at 3,000 mc do not cause breakdown in aluminum oxide ceramics with 0.020-inch diameter voids.</p>	UNCLASSIFIED	<p>Analytic studies indicate the need for developing a method of describing the relation between imperfection states in a dielectric and the inhomogeneous internal fields within the material. These fields must be accounted for in the description of the factors which control breakdown in dielectrics.</p> <p>The study on the effect of ionization of gas in alumina ceramics has been completed. Experiments conducted indicated that microwave fields in the order of 132,000 volts per cm peak and 4,000 volts per cm average at 3,000 mc do not cause breakdown in aluminum oxide ceramics with 0.020-inch diameter voids.</p>	UNCLASSIFIED
<p>Analytic studies indicate the need for developing a method of describing the relation between imperfection states in a dielectric and the inhomogeneous internal fields within the material. These fields must be accounted for in the description of the factors which control breakdown in dielectrics.</p> <p>The study on the effect of ionization of gas in alumina ceramics has been completed. Experiments conducted indicated that microwave fields in the order of 132,000 volts per cm peak and 4,000 volts per cm average at 3,000 mc do not cause breakdown in aluminum oxide ceramics with 0.020-inch diameter voids.</p>	UNCLASSIFIED	<p>Analytic studies indicate the need for developing a method of describing the relation between imperfection states in a dielectric and the inhomogeneous internal fields within the material. These fields must be accounted for in the description of the factors which control breakdown in dielectrics.</p> <p>The study on the effect of ionization of gas in alumina ceramics has been completed. Experiments conducted indicated that microwave fields in the order of 132,000 volts per cm peak and 4,000 volts per cm average at 3,000 mc do not cause breakdown in aluminum oxide ceramics with 0.020-inch diameter voids.</p>	UNCLASSIFIED

<p>AD STANFORD RESEARCH INSTITUTE, Menlo Park, California</p> <p>Div. 8/4, 14/2, 25/3,6</p> <p>RESEARCH ON DIELECTRICS FOR MICROWAVE ELECTRON DEVICES, L. Feinstein, J. Bordeaux, D. Peters, C. Peltzer, Report No. 9, Final Report, 1 July 1962 to 30 September 1964, 113 pages, inc. 46 Illustrations, 2 Tables.</p> <p>Contract DA-36-039 SC-90856. Unclassified Report</p> <p>This report reviews the results of twenty-seven months study of the transport and breakdown properties of aluminum oxide and of methods of growth of this dielectric from the vapor phase in an evacuated system.</p> <p>An ultrahigh vacuum system capable of reaching pressures of <math>10^{-9}</math>-<math>10^{-10}</math> torr has been completed. The growth of aluminum oxide films ranging in thickness from 1000 Å to 5000 Å by five differ- ent methods was achieved in an interrim vacuum system operating in the <math>10^{-6}</math> to <math>10^{-7}</math> torr range.</p>	<p>UNCLASSIFIED</p> <ol style="list-style-type: none"> <li>1. Dielectrics</li> <li>2. High Vacuum</li> <li>3. Solid State</li> <li>4. Insulators</li> <li>5. Microwave Windows</li> </ol> <ol style="list-style-type: none"> <li>I. Project DEFENDER</li> <li>II. Research on Dielec- trics for Microwave Devices</li> <li>III. L. Feinstein</li> <li>IV. J. Bordeaux</li> <li>V. D. Peters</li> <li>VI. C. Peltzer</li> <li>VII. USARL, Fort Monmouth, N.J.</li> </ol>	<p>AD STANFORD RESEARCH INSTITUTE, Menlo Park, California</p> <p>Div. 8/4, 14/2, 25/3,6</p> <p>RESEARCH ON DIELECTRICS FOR MICROWAVE ELECTRON DEVICES, L. Feinstein, J. Bordeaux, D. Peters, C. Peltzer, Report No. 9, Final Report, 1 July 1962 to 30 September 1964, 113 pages, inc. 46 Illustrations, 2 Tables.</p> <p>Contract DA-36-039 SC-90856. Unclassified Report</p> <p>This report reviews the results of twenty-seven months study of the transport and breakdown properties of aluminum oxide and of methods of growth of this dielectric from the vapor phase in an evacuated system.</p> <p>An ultrahigh vacuum system capable of reaching pressures of <math>10^{-9}</math>-<math>10^{-10}</math> torr has been completed. The growth of aluminum oxide films ranging in thickness from 1000 Å to 5000 Å by five differ- ent methods was achieved in an interrim vacuum system operating in the <math>10^{-6}</math> to <math>10^{-7}</math> torr range.</p>	<p>UNCLASSIFIED</p> <ol style="list-style-type: none"> <li>1. Dielectrics</li> <li>2. High Vacuum</li> <li>3. Solid State</li> <li>4. Insulators</li> <li>5. Microwave Windows</li> </ol> <ol style="list-style-type: none"> <li>I. Project DEFENDER</li> <li>II. Research on Dielec- trics for Microwave Devices</li> <li>III. L. Feinstein</li> <li>IV. J. Bordeaux</li> <li>V. D. Peters</li> <li>VI. C. Peltzer</li> <li>VII. USARL, Fort Monmouth, N.J.</li> </ol>	<p>AD STANFORD RESEARCH INSTITUTE, Menlo Park, California</p> <p>Div. 8/4, 14/2, 25/3,6</p> <p>RESEARCH ON DIELECTRICS FOR MICROWAVE ELECTRON DEVICES, L. Feinstein, J. Bordeaux, D. Peters, C. Peltzer, Report No. 9, Final Report, 1 July 1962 to 30 September 1964, 113 pages, inc. 46 Illustrations, 2 Tables.</p> <p>Contract DA-36-039 SC-90856. Unclassified Report</p> <p>This report reviews the results of twenty-seven months study of the transport and breakdown properties of aluminum oxide and of methods of growth of this dielectric from the vapor phase in an evacuated system.</p> <p>An ultrahigh vacuum system capable of reaching pressures of <math>10^{-9}</math>-<math>10^{-10}</math> torr has been completed. The growth of aluminum oxide films ranging in thickness from 1000 Å to 5000 Å by five differ- ent methods was achieved in an interrim vacuum system operating in the <math>10^{-6}</math> to <math>10^{-7}</math> torr range.</p>	<p>UNCLASSIFIED</p> <ol style="list-style-type: none"> <li>1. Dielectrics</li> <li>2. High Vacuum</li> <li>3. Solid State</li> <li>4. Insulators</li> <li>5. Microwave Windows</li> </ol> <ol style="list-style-type: none"> <li>I. Project DEFENDER</li> <li>II. Research on Dielec- trics for Microwave Devices</li> <li>III. L. Feinstein</li> <li>IV. J. Bordeaux</li> <li>V. D. Peters</li> <li>VI. C. Peltzer</li> <li>VII. USARL, Fort Monmouth, N.J.</li> </ol>
<p>AD STANFORD RESEARCH INSTITUTE, Menlo Park, California</p> <p>Div. 8/4, 14/2, 25/3,6</p> <p>RESEARCH ON DIELECTRICS FOR MICROWAVE ELECTRON DEVICES, L. Feinstein, J. Bordeaux, D. Peters, C. Peltzer, Report No. 9, Final Report, 1 July 1962 to 30 September 1964, 113 pages, inc. 46 Illustrations, 2 Tables.</p> <p>Contract DA-36-039 SC-90856. Unclassified Report</p> <p>This report reviews the results of twenty-seven months study of the transport and breakdown properties of aluminum oxide and of methods of growth of this dielectric from the vapor phase in an evacuated system.</p> <p>An ultrahigh vacuum system capable of reaching pressures of <math>10^{-9}</math>-<math>10^{-10}</math> torr has been completed. The growth of aluminum oxide films ranging in thickness from 1000 Å to 5000 Å by five differ- ent methods was achieved in an interrim vacuum system operating in the <math>10^{-6}</math> to <math>10^{-7}</math> torr range.</p>	<p>UNCLASSIFIED</p> <ol style="list-style-type: none"> <li>1. Dielectrics</li> <li>2. High Vacuum</li> <li>3. Solid State</li> <li>4. Insulators</li> <li>5. Microwave Windows</li> </ol> <ol style="list-style-type: none"> <li>I. Project DEFENDER</li> <li>II. Research on Dielec- trics for Microwave Devices</li> <li>III. L. Feinstein</li> <li>IV. J. Bordeaux</li> <li>V. D. Peters</li> <li>VI. C. Peltzer</li> <li>VII. USARL, Fort Monmouth, N.J.</li> </ol>	<p>AD STANFORD RESEARCH INSTITUTE, Menlo Park, California</p> <p>Div. 8/4, 14/2, 25/3,6</p> <p>RESEARCH ON DIELECTRICS FOR MICROWAVE ELECTRON DEVICES, L. Feinstein, J. Bordeaux, D. Peters, C. Peltzer, Report No. 9, Final Report, 1 July 1962 to 30 September 1964, 113 pages, inc. 46 Illustrations, 2 Tables.</p> <p>Contract DA-36-039 SC-90856. Unclassified Report</p> <p>This report reviews the results of twenty-seven months study of the transport and breakdown properties of aluminum oxide and of methods of growth of this dielectric from the vapor phase in an evacuated system.</p> <p>An ultrahigh vacuum system capable of reaching pressures of <math>10^{-9}</math>-<math>10^{-10}</math> torr has been completed. The growth of aluminum oxide films ranging in thickness from 1000 Å to 5000 Å by five differ- ent methods was achieved in an interrim vacuum system operating in the <math>10^{-6}</math> to <math>10^{-7}</math> torr range.</p>	<p>UNCLASSIFIED</p> <ol style="list-style-type: none"> <li>1. Dielectrics</li> <li>2. High Vacuum</li> <li>3. Solid State</li> <li>4. Insulators</li> <li>5. Microwave Windows</li> </ol> <ol style="list-style-type: none"> <li>I. Project DEFENDER</li> <li>II. Research on Dielec- trics for Microwave Devices</li> <li>III. L. Feinstein</li> <li>IV. J. Bordeaux</li> <li>V. D. Peters</li> <li>VI. C. Peltzer</li> <li>VII. USARL, Fort Monmouth, N.J.</li> </ol>	<p>AD STANFORD RESEARCH INSTITUTE, Menlo Park, California</p> <p>Div. 8/4, 14/2, 25/3,6</p> <p>RESEARCH ON DIELECTRICS FOR MICROWAVE ELECTRON DEVICES, L. Feinstein, J. Bordeaux, D. Peters, C. Peltzer, Report No. 9, Final Report, 1 July 1962 to 30 September 1964, 113 pages, inc. 46 Illustrations, 2 Tables.</p> <p>Contract DA-36-039 SC-90856. Unclassified Report</p> <p>This report reviews the results of twenty-seven months study of the transport and breakdown properties of aluminum oxide and of methods of growth of this dielectric from the vapor phase in an evacuated system.</p> <p>An ultrahigh vacuum system capable of reaching pressures of <math>10^{-9}</math>-<math>10^{-10}</math> torr has been completed. The growth of aluminum oxide films ranging in thickness from 1000 Å to 5000 Å by five differ- ent methods was achieved in an interrim vacuum system operating in the <math>10^{-6}</math> to <math>10^{-7}</math> torr range.</p>	<p>UNCLASSIFIED</p> <ol style="list-style-type: none"> <li>1. Dielectrics</li> <li>2. High Vacuum</li> <li>3. Solid State</li> <li>4. Insulators</li> <li>5. Microwave Windows</li> </ol> <ol style="list-style-type: none"> <li>I. Project DEFENDER</li> <li>II. Research on Dielec- trics for Microwave Devices</li> <li>III. L. Feinstein</li> <li>IV. J. Bordeaux</li> <li>V. D. Peters</li> <li>VI. C. Peltzer</li> <li>VII. USARL, Fort Monmouth, N.J.</li> </ol>



<p>Alpha aluminum oxide films were grown by thermal evaporation in the ultrahigh vacuum system.</p> <p>Data from experiments on transport in single crystal sapphire indicate that electron or hole conduction is primarily due to the effect of impurities or defects, and therefore, indicates either an impurity band or hopping process or a polaron conduction mechanism. The degree of ionic conductivity is still uncertain, particularly at high temperatures (1600°C). The effect of the glassy phase which exists in commercial polycrystalline alumina is to form a barrier to conduction across the boundary between the aluminum oxide crystals and the glassy phase.</p> <p>The data from electron bombardment and breakdown studies indicate that particle bombardment, in addition to creating defects if particle energy is sufficiently high, can also lead to formation of separated charge regions in the material. These regions can act as sources of internal fields within the dielectric. Defects within the material introduced by bending sapphire single crystals have a pronounced effect on decreasing the breakdown strength of specimens.</p>	<p>VIII.</p> <p>UNCLASSIFIED</p> <p>DA-36-039</p> <p>SC-90856</p>
<p>Alpha aluminum oxide films were grown by thermal evaporation in the ultrahigh vacuum system.</p> <p>Data from experiments on transport in single crystal sapphire indicate that electron or hole conduction is primarily due to the effect of impurities or defects, and therefore, indicates either an impurity band or hopping process or a polaron conduction mechanism. The degree of ionic conductivity is still uncertain, particularly at high temperatures (1600°C). The effect of the glassy phase which exists in commercial polycrystalline alumina is to form a barrier to conduction across the boundary between the aluminum oxide crystals and the glassy phase.</p> <p>The data from electron bombardment and breakdown studies indicate that particle bombardment, in addition to creating defects if particle energy is sufficiently high, can also lead to formation of separated charge regions in the material. These regions can act as sources of internal fields within the dielectric. Defects within the material introduced by bending sapphire single crystals have a pronounced effect on decreasing the breakdown strength of specimens.</p>	<p>VIII.</p> <p>UNCLASSIFIED</p> <p>DA-36-039</p> <p>SC-90856</p>
<p>Alpha aluminum oxide films were grown by thermal evaporation in the ultrahigh vacuum system.</p> <p>Data from experiments on transport in single crystal sapphire indicate that electron or hole conduction is primarily due to the effect of impurities or defects, and therefore, indicates either an impurity band or hopping process or a polaron conduction mechanism. The degree of ionic conductivity is still uncertain, particularly at high temperatures (1600°C). The effect of the glassy phase which exists in commercial polycrystalline alumina is to form a barrier to conduction across the boundary between the aluminum oxide crystals and the glassy phase.</p> <p>The data from electron bombardment and breakdown studies indicate that particle bombardment, in addition to creating defects if particle energy is sufficiently high, can also lead to formation of separated charge regions in the material. These regions can act as sources of internal fields within the dielectric. Defects within the material introduced by bending sapphire single crystals have a pronounced effect on decreasing the breakdown strength of specimens.</p>	<p>VIII.</p> <p>UNCLASSIFIED</p> <p>DA-36-039</p> <p>SC-90856</p>



<p>Analytic studies indicate the need for developing a method of describing the relation between imperfection states in a dielectric and the inhomogeneous internal fields within the material. These fields must be accounted for in the description of the factors which control breakdown in dielectrics.</p> <p>The study on the effect of ionization of gas in alumina ceramics has been completed. Experiments conducted indicated that microwave fields in the order of 132,000 volts per cm peak and 4,000 volts per cm average at 3,000 mc do not cause breakdown in aluminum oxide ceramics with 0.020-inch diameter voids.</p>	<p>Analytic studies indicate the need for developing a method of describing the relation between imperfection states in a dielectric and the inhomogeneous internal fields within the material. These fields must be accounted for in the description of the factors which control breakdown in dielectrics.</p> <p>The study on the effect of ionization of gas in alumina ceramics has been completed. Experiments conducted indicated that microwave fields in the order of 132,000 volts per cm peak and 4,000 volts per cm average at 3,000 mc do not cause breakdown in aluminum oxide ceramics with 0.020-inch diameter voids.</p>	<p>Analytic studies indicate the need for developing a method of describing the relation between imperfection states in a dielectric and the inhomogeneous internal fields within the material. These fields must be accounted for in the description of the factors which control breakdown in dielectrics.</p> <p>The study on the effect of ionization of gas in alumina ceramics has been completed. Experiments conducted indicated that microwave fields in the order of 132,000 volts per cm peak and 4,000 volts per cm average at 3,000 mc do not cause breakdown in aluminum oxide ceramics with 0.020-inch diameter voids.</p>	<p>UNCLASSIFIED</p>
<p>Analytic studies indicate the need for developing a method of describing the relation between imperfection states in a dielectric and the inhomogeneous internal fields within the material. These fields must be accounted for in the description of the factors which control breakdown in dielectrics.</p> <p>The study on the effect of ionization of gas in alumina ceramics has been completed. Experiments conducted indicated that microwave fields in the order of 132,000 volts per cm peak and 4,000 volts per cm average at 3,000 mc do not cause breakdown in aluminum oxide ceramics with 0.020-inch diameter voids.</p>	<p>Analytic studies indicate the need for developing a method of describing the relation between imperfection states in a dielectric and the inhomogeneous internal fields within the material. These fields must be accounted for in the description of the factors which control breakdown in dielectrics.</p> <p>The study on the effect of ionization of gas in alumina ceramics has been completed. Experiments conducted indicated that microwave fields in the order of 132,000 volts per cm peak and 4,000 volts per cm average at 3,000 mc do not cause breakdown in aluminum oxide ceramics with 0.020-inch diameter voids.</p>	<p>Analytic studies indicate the need for developing a method of describing the relation between imperfection states in a dielectric and the inhomogeneous internal fields within the material. These fields must be accounted for in the description of the factors which control breakdown in dielectrics.</p> <p>The study on the effect of ionization of gas in alumina ceramics has been completed. Experiments conducted indicated that microwave fields in the order of 132,000 volts per cm peak and 4,000 volts per cm average at 3,000 mc do not cause breakdown in aluminum oxide ceramics with 0.020-inch diameter voids.</p>	<p>UNCLASSIFIED</p>

**STANFORD  
RESEARCH  
INSTITUTE**

**MENLO PARK  
CALIFORNIA**

## **Regional Offices and Laboratories**

### **Southern California Laboratories**

820 Mission Street  
South Pasadena, California 91031

### **Washington Office**

808-17th Street, N.W.  
Washington, D.C. 20006

### **New York Office**

270 Park Avenue, Room 1770  
New York, New York 10017

### **Detroit Office**

1025 East Maple Road  
Birmingham, Michigan 48011

### **European Office**

Pelikanstrasse 37  
Zurich 1, Switzerland

### **Japan Office**

Nomura Security Building, 6th Floor  
1-1 Nihonbashidori, Chuo-ku  
Tokyo, Japan

## **Retained Representatives**

### **Toronto, Ontario, Canada**

Cyril A. Ing  
67 Yonge Street, Room 710  
Toronto 1, Ontario, Canada

### **Milan, Italy**

Lorenzo Franceschini  
Via Macedonio Melloni, 49  
Milan, Italy

**UNCLASSIFIED**

**UNCLASSIFIED**